A STUDY OF WELD-INTERFACE PHENOMENA AND ASSOCIATED CRACK INITIATION IN A LOW-ALLOY STEEL

by

Edward S. Szekeres

Rensselaer Polytechnic Institute
Troy, New York

February 1968

A STUDY OF WELD-INTERFACE PHENOMENA AND ASSOCIATED CRACK INITIATION IN A LOW-ALLOY STEEL

by

Edward S. Szekeres

A Thesis Submitted to the Faculty of the
Department of Materials Engineering
in Partial Fulfillment of the
Requirement for the Degree of
DOCTOR OF PHILOSOPHY
Major Subject: Metallurgy

Approved by the following
Examining Committee:

W. F. Savage, Chairman

J. J. McCarthy

W. J. Childs

E. F. Nippes

F. V. Lenel

R. H. Trathen

Rensselaer Polytechnic Institute
Troy, New York

February 1968

TABLE OF CONTENTS

Page

LIST OF TABLES..... v

LIST OF FIGURES..... vi

ABSTRACT.....xiv

INTRODUCTION AND HISTORICAL REVIEW..... 1

Certain Characteristics of Fusion Welds..... 1

Metallographic Examination of Welds..... 4

The Origin of Substructure in Weld Metal..... 8

Historical Background of HY-80 Steel..... 17

Welding of HY-80 Steel..... 18

Cracking in Weldments of HY-80 Steel..... 22

Analysis of the Problem..... 29

OBJECTIVES..... 33

MATERIALS AND EXPERIMENTAL PROCEDURES..... 34

Material..... 34

Metallographic Examination of the Base Metal..... 37

Metallographic Examination of the Weld Fusion Boundary.. 39

Electron Beam Microanalysis Across the Fusion Boundary.. 40

Varestraint Tests of the Weld Metal..... 41

Cold Cracking Tests..... 45

Examination of a Transverse Section From a Cruciform

Test Specimen..... 52

Page

RESULTS AND DISCUSSION..... 56

Metallographic Examination of the Base Metal..... 56

Transformation Products..... 56

Nonmetallic Inclusions..... 56

Banding..... 66

Metallographic Studies of the Fusion Boundary..... 66

Evaluation of Etching Procedures..... 68

Recognition of an Unmixed Zone..... 74

Electron Beam Microanalysis of the Fusion Boundary..... 78

Suggested Revisions in Terminology..... 88

Mechanisms of Partial Melting..... 93

Constitutional Liquation of Elongated Sulfide Inclusions..... 93

Liquation of Small Spherical Regions.....104

Grain Boundary Wetting.....106

Super-Solidus Grain Boundary Melting.....112

Other Defects Due to Sulfide Inclusions.....117

Microvoid Formation at the Weld Interface.....117

Sulfide Alignment in the Unmixed Zone.....120

Varestraint Tests of Heterogeneous Weld Metal.....122

Cold Cracking Tests.....130

General Observations.....131

The Role of Hydrogen.....134

Page

The Nucleation of Heat-Affected-Zone Cracks by Sulfide Inclusions.....137

The Influence of Banding on Heat-Affected-Zone Cracking.....144

Cracking Associated With the Fusion Boundary.....147

Nucleation of Cold Cracks in the Partially-Melted Zone.....155

A Mechanism for Crack Nucleation in the Unmixed Zone...158

Cracking in the Cruciform Test.....163

A New Approach to the Understanding of Cold Cracking in Welds.....166

CONCLUSIONS.....173

ACKNOWLEDGMENTS.....178

REFERENCES CITED.....179

LIST OF TABLES

Table		Page
I	Chemical Composition Requirements for HY-80 Steel Plates, Percent	19
II	Mechanical Property Requirements for HY-80 Steel Plates	20
III	Chemical Composition of HY-80 Steels Used in This Investigation	35
IV	Mechanical Properties of HY-80 Steels Used in This Investigation	36
V	Single-Pass-Cruciform-Test Performance of the Heats of HY-80 Steel Used in This Investigation	38
VI	Etching Procedures Used to Reveal the Weld-Metal Base-Metal Junction in Bead Welds in HY-80 Steel	69
VII	Proposed Terminology and Definitions of Discrete Regions in Heterogeneous Welds	94
VIII	Qualitative Results of the Varestraint Tests for Weld Metal Crack-Susceptibility	125
IX	Summary of General Observations of Cold-Cracking-Test Specimens of HY-80 Steel	132

LIST OF FIGURES

Figure		Page
1	Typical Macrograph of a Transverse Section of a Bead Weld Made by the Shielded Metal-Arc Welding Process. Such Macrographs Show Only Gross Features of a Weld. Ammonium Persulfate Etchant, 6X.....	5
2	Example of the Planar Solidification Mode. A. Schematic Illustration. B. Transverse Section of a Gas Tungsten-Arc Weld in an Iron-Nickel Alloy. Etched, 250X. (Photomicrograph courtesy of C. D. Lundin).....	12
3	Example of the Cellular Solidification Mode. A. Schematic Illustration. B. Transverse Section of a Gas Tungsten-Arc Weld in HY-80 Steel. Nital and Sodium Bisulfite Etchant, 250X.....	13
4	Example of Cellular-Dendritic Solidification Mode. A. Schematic Illustration. B. Surface of Gas Tungsten-Arc Weld in a Silicon-Iron Alloy. As-Welded, 300X. (Photomicrograph courtesy of C. D. Lundin).....	14
5	Example of Columnar-Dendritic Solidification Mode. A. Schematic Illustration. B. Surface of a Gas Tungsten-Arc Weld in a Titanium-Manganese Alloy. As-Welded, 15X. (Photomicrograph courtesy of C. D. Lundin).....	15
6	Example of the Equiaxed-Dendritic Solidification Mode. A. Schematic Illustration. B. Surface of the Terminal Crater in a Gas Tungsten-Arc Weld in a Silicon-Iron Alloy. As-Welded, 100X. (Photomicrograph courtesy of C. D. Lundin).....	16
7	Transverse Section of a Frame-to-Hull Tee Joint Revealing Cracks in a Heavy-Gage Composition HY-80 Steel Hull Plate. Ammonium Persulfate Etchant, 4X. (Modification of Figure 14 in Reference 21).....	24

Figure		Page
8	Schematic Illustration of the Varestraint Testing Device. When the Welding Arc Reaches Point A, the Specimen is Forced to Conform to the Radius-Block B and the Arc Continues to Point C Where it is Extinguished.....	42
9	Orientation of the Varestraint-Test Specimens to the As-Received HY-80 Steel Plate.....	44
10	Schematic Illustration of the Top Surface of a Welded-and-Tested Varestraint-Test Specimen Showing the Location of the Metallographic Sample.....	46
11	Orientation of the Cold-Cracking Test Specimens Machined From the As-Received HY-80 Steel Plates.....	48
12	Schematic Illustration Showing the Welding of Cold-Cracking Test Specimens.....	49
13	Detailed Drawing of the Loading Apparatus Used to Stress Specimens in the Cold-Cracking Test.....	51
14	View of the Loading Apparatus, With a Cold-Cracking Test Specimen Inserted, Mounted on the Stage of the Microscope.....	53
15	Details of the Cruciform Test Specimen Used to Evaluate the Weldability of Quenched-and-Tempered Low-Alloy Steel Plate.....	54
16	Microstructure of the As-Received HY-80 Steel Plates in Sections Longitudinal and Transverse to the Final Rolling Direction. Super-Picral Etchant, 100X. A. Heat No. 72P305. B. Heat No. N51755.....	57

Figure		Page
17	The General Appearance of Nonmetallics in Sections of the HY-80 Steel Plates Longitudinal to the Final Rolling Direction. Polished and Unetched, 100X. A. Heat No. 72P305. B. Heat No. N51755.....	58
18	Typical Sulfide Inclusions in Sections of the HY-80 Steel Plates Longitudinal to the Final Rolling Direction. Polished and Unetched, 1000X. A. The Edge of a Long Sulfide in Heat No. 72P305. B. A Relatively Long Sulfide in Heat No. N51755.....	59
19	Typical Globular Inclusions in a Section of Heat No. N51755 Longitudinal to the Final Rolling Direction. Note the Many Duplex Oxide-Sulfide Inclusions. Polished and Unetched, 1000X.....	61
20	The Appearance of Banding in Sections of the HY-80 Steel Plates Longitudinal to the Final Rolling Direction. Nital and Sodium Bisulfite Etchant, 100X. A. Heat No. 72P305. B. Heat No. N51755.....	67
21	Comparison of Two Etching Procedures Used to Reveal the Fusion Boundary on a Transverse Section of a Shielded Metal-Arc Bead-Weld in HY-80 Steel, 250X. A. Location at a Reference Mark Etched With the Two-Stage Nital and Sodium Bisulfite Proceudre. B. The Identical Location Repolished and Etched With Nital Only.....	71
22	Comparison of Two Etching Procedures Used to Reveal the Fusion Boundary on a Transverse Section of a Shielded Metal-Arc Bead-Weld in HY-80 Steel, 250X. A. A Location Etched With Nital. B. The Identical Location Repolished and Etched With Ammonium Persulfate.....	73
23	Substructure at the Weld Interface as Highlighted by Nomarski Interference Contrast.[29] The Location is Identical to that Shown in Figure 21 Except the Image is Inverted. Ammonium Persulfate Etchant, 250X.....	75

Figure		Page
24	A Transverse Section of a Shielded Metal-Arc Bead Weld Showing Evidence of Laminar Flow Within an Unmixed Zone of Molten Weld Metal. Note the Sharp Angle Between the Bands in the Base Metal and Those in the Unmixed Zone. Nital and Sodium Bisulfite Procedure, 100X.....	76
25	Traverses AA' and BB' of the Electron Beam Microanalyser Across the Fusion Boundary of a Bead Weld in a Specimen From Heat No. 72P305. Ammonium Persulfate Etchant, 100X.....	79
26	Traverses CC', DD', and EE' of the Electron Beam Microanalyser Across the Fusion Boundary of a Bead Weld in Heat No. N51755. Ammonium Persulfate Etchant, 100X.....	80
27	The Concentration Profiles for Manganese and Chromium Obtained by Traverse AA' Across the Fusion Boundary of a Bead Weld in Heat No. 72P305.....	81
28	The Concentration Profiles for Manganese and Chromium Obtained by Traverse BB' Across the Fusion Boundary of a Bead Weld in Heat No. 72P305.....	82
29	The Concentration Profiles for Manganese and Chromium Obtained by Traverse CC' Across a Fold in the Weld Metal and Across the Fusion Boundary of a Bead Weld in Heat No. N51755.....	83
30	The Concentration Profiles for Manganese and Chromium Obtained by Traverse DD' Across the Fusion Boundary of a Bead Weld in Heat No. N51755.....	84
31	The Concentration Profiles for Manganese and Chromium Obtained by Traverse EE' Across the Fusion Boundary of a Bead Weld in Heat No. N51755.....	85

Figure		Page
32	A Comparison of the Regions at the Fusion Boundary Obtained With Different Welding Processes. Nital and Sodium Bisulfite Procedure, 250X. A. Weld Made by the Heterogeneous Shielded Metal-Arc Process. B. Weld Made by the Autogenous Gas Tungsten-Arc Process.....	90
33	Schematic Illustration Showing the Regions of a Heterogeneous Weld Recognized in This Investigation and the Proposed Terminology to Identify These Regions.....	95
34	Transverse Section of a Bead Weld in a Specimen from Heat No. 72P305 Showing the Fusion Boundary. Note the Evidence of Various Types of Partial Melting in the Heat-Affected Zone Adjacent to the Fully-Molten Weld Metal. Nital and Sodium Bisulfite Procedure, 100X.....	96
35	Some Examples of Constitutional Liquation of Sulfide Inclusions in the Partially-Melted Zone. Note the Small Globular Precipitates in the Vicinity of the Remnant of the Original Inclusion. Nital and Sodium Bisulfite Procedure, 500X.....	98
36	A Greater Magnification of One of the Examples of Constitutional Liquation in Heat No. 72P305. Nital and Sodium Bisulfite Procedure, 1000X.....	100
37	Examples of Grain Boundary Wetting in the Partially-Melted Region of Bead Welds in HY-80 Steel. Nital and Sodium Bisulfite Procedure. A. Specimen from Heat No. N51755, 250X. B. Specimen from Heat No. 72P305, 500X.....	108
38	Grain Boundary Wetting Resulting from the Intersection of a Prior-Austenite Grain Boundary and a Constitutionally Liquated Region. Note the Alignment of an Inclusion Along the Liquated Boundary. Nital and Sodium Bisulfite Procedure, 1000X.....	111

Figure		Page
39	The Peritectic Portion of the Iron-Carbon Binary Diagram (Data From Reference 52)	114
40	Microvoids Caused by Sulfide Inclusions at the Fusion Boundary of Bead Welds in HY-80 Steel. Nital and Sodium Bisulfite Procedure, 250X. A. Specimen from Heat No. 72P305. B. Specimen from Heat No. N51755	119
41	Examples of the Alignment of Small Sulfide Globules and Films Along Prior Austenite Grain Boundaries in the Unmixed Zone of Bead Welds in Specimens from Heat No. 72P305. Nital and Sodium Bisulfite Procedure, 1000X	121
42	Irregular Weld-Metal Cracking in the Varestraint-Test Specimen From Heat No. 72P305 Strained 2.00 Percent. Ammonium Persulfate Etchant, 10X	124
43	Results of Previous Varestraint Tests on Specimens From Heat Nos. 72P305 and N51755 Welded by the Gas Tungsten-Arc Process (from Reference 55)	126
44	A Transverse Section Showing the Fusion-Boundary Crack in the Varestraint Test Specimen from Heat No. 72P305 Strained 2.00 Percent. Nital and Sodium Bisulfite Procedure, 300X	128
45	Schematic Illustration of the Probable Mechanism Producing the Intermittent Bursts of Hydrogen Observed During Delayed Cracking	136
46	Examples of Sulfide Inclusions Along Cracks in the Heat-Affected Zone of a Cold-Crack-Test Specimen Welded Under High-Hydrogen Conditions. Polished and Unetched, 1000X	138

Figure		Page
47	Example of Crack-Nucleation by a Sulfide Inclusion in a Bead Weld in Heat No. 72P305. Nital Etchant. A. View of an Inclusion in the Heat-Affected Zone, 250X. B. An Over-Enlargement of the Same Inclusion, Approximately 2100X.....	139
48	Examples of True Heat-Affected Zone Cracks Along Light-Etching Bands in the Cold-Cracking-Test Specimen From Heat No. 72P305 Welded Under High-Hydrogen Conditions. Nital and Sodium Bisulfite Procedure, 250X.....	145
49	Examples of True Heat-Affected Zone Cracks in a Cold-Cracking Test Specimen From Heat No. 72P305. The Banding Was Parallel to the Stress Direction. A. A Crack Soon After Nucleation in a Light-Etching Band (the Black Specks are Dirt on the Oil Film). Nital Etchant, 250X. B. A Crack With Propagation Stopped in Dark-Etching Bands. Nital and Sodium Bisulfite Procedure, 500X.....	146
50	An Example of Delayed Cracking Nucleated at the Fusion Boundary in a Cold-Cracking-Test Specimen From Heat No. 72P305. The Black Area at the Upper Left Corner of the Photomicrographs is a Region Pulled Out During Separation of the Welded Specimens. Nital Etchant, 50X.....	149
51	Examples of Delayed Cracking Nucleated at the Fusion Boundary in a Cold-Cracking-Test Specimen From Heat No. 72P305. The Composite Region is at the Top in the Photomicrographs. Nital Etchant, 50 X.....	150
52	Examples of Delayed Cracking in the Weld Metal, at the Fusion Boundary and in the Heat-Affected Zone of a Cold-Cracking-Test Specimen From Heat No. N51755. Nital Etchant, 50X.....	151

Figure		Page
53	Examples of Cold Cracking Primarily Within the Unmixed and Partially-Melted Zones in a Cold-Cracking-Test Specimen From Heat No. 72P305 With the Banding Transverse to the Stress Direction. Welded Under High-Hydrogen Conditions. Nital and Sodium Bisulfite Procedure, 1000X.....	153
54	Hot-Cracks in the Unmixed Zone in a Cold-Cracking-Test Specimen From Heat No. 72P305 With the Banding Transverse to the Stress Direction Welded Under Low-Hydrogen Conditions. Nital and Sodium Bisulfite Procedure, 500X. A. Cracks at Substructure Boundaries. B. A Crack Similar to the Hot-Crack Shown in Figure 44.....	154
55	Examples of Crack-Embryo in the Partially-Melted Zone of a Specimen From Heat No. 72P305 With the Banding Transverse to the Stress Direction Welded Under High-Hydrogen Conditions. Nital and Sodium Bisulfite Procedure, 500X. A. Crack Nucleated at a Liquated Grain Boundary. B. Crack Nucleated at the Matrix-Inclusion Interface of a Sulfide in a Constitutionally Liquated Region.....	156
56	A View of the Unmixed Zone on a Transverse Section of a Bead Weld in a Specimen From Heat No. 72P305. Note the Predominance of Platelets of Low-Temperature Transformation Product Which are not Continuous Across Adjacent Cells. Nital and Sodium Bisulfite Procedure, 500X.....	159
57	Schematic Illustration of the Extent of the Delta-Ferrite Region Under a High Concentration of Elements Promoting Solidification to Austenite and Under a High Concentration of Elements Promoting Solidification to Ferrite....	161
58	Views Along the Macrocrack Under Fillet Weld C on a Transverse Section of a Cruciform Test Specimen of HY-80 Steel. Ammonium Persulfate Etchant, 250X. A. A Digression of the Crack-Path into the Unmixed Zone. B. Crack-Branches into the Unmixed and Partially-Melted Zones.....	165

ABSTRACT

In certain quenched-and-tempered low-alloy steels, the formation of cracks in weldments is an unresolved problem. A typical example is the cracking in weldments of HY-80 steel which is presently the principal material for submarine hulls. The understanding of the mechanisms of cracking in HY-80 steel is far from complete, especially the aspects of crack initiation and the role of sulfur. Some generalizations of the cracking problem are that (1) the cracks usually appear to be associated in some way with the weld fusion boundary, (2) variations in crack susceptibility can exist among heats made to the same specification, and (3) hydrogen plays a very significant role in the cracking.

For this investigation, two heats of HY-80 steel with a well-documented difference in crack susceptibility were obtained. In addition to a metallographic study of the as-received base metal, the features of the fusion boundary of heterogeneous bead welds were studied both metallographically and by means of electron beam microanalysis. Also, aspects of cold cracking in the two heats were investigated using a procedure that allowed direct microscopic observation of crack initiation and propagation in small stressed specimens.

The results of the investigation showed that the fusion boundary of heterogeneous welds is not a simple "fusion line" but rather a region composed of (1) an unmixed zone of weld metal which has a composition essentially that of the base metal and (2) a partially-melted zone in which occur various phenomena such as constitutional liquation of sulfide inclusions and grain boundary wetting. The term weld interface was defined as the demarcation between these two zones. Furthermore, cold cracking in both heats of HY-80 steel was found to be associated with the zones adjacent to the weld interface as well as with the sulfides in the true heat-affected zone.

The primary reason for a difference in the degree of cold cracking between the two heats appeared to be a difference in the size and shape of the sulfides. Also, hydrogen was found to be absolutely necessary for the initiation and propagation of cold cracks. Although a small amount of hot-microcracking was found in the crack-susceptible heat, hot-microcracking did not appear to be a prerequisite for cold cracking.

INTRODUCTION AND HISTORICAL REVIEW

In certain quenched-and-tempered low-alloy steels, the formation of cracks in weldments is an unresolved problem. Furthermore, this problem is unlikely to be resolved without a greater understanding of both the location and the mechanism of crack initiation and the metallurgical response of the base material to the thermal cycle of welding.

A typical example of the cracking problem frequently encountered in structures fabricated from low-alloy steels is the cracking in weldments of HY-80 steel. This investigation, which is concerned with the nature of crack formation, will relate crack initiation and propagation in HY-80 steel to features of fusion welds and metallurgical phenomena which occur as a result of welding. However, it should be emphasized that the observations and conclusions, although based on HY-80 steel, may be equally pertinent to other quenched-and-tempered low-alloy steels.

Certain Characteristics of Fusion Welds

The non-pressure fusion welding processes, which include the several arc-welding processes, can be divided into those processes in which filler metal is introduced into the weld pool during welding and those in which a filler is not introduced. Adopting the terminology suggested by Udin, Funk,

and Wulff,[1)] a homogeneous welding process is defined as one in which the filler metal is essentially the same in composition as the parts being welded. If however, the filler has a composition significantly different from that of the base material or if the members being joined differ significantly from one another in composition, the process is defined as heterogeneous. An autogenous welding process is defined as one in which members with the same chemical composition are welded together without the use of added filler material.

In general, filler metal may be added for one or more of the following reasons:

1. to fill the space between the members being joined,
2. to create a reinforcement,
3. to control or modify the chemical composition of the weld metal.

With regard to the third reason, new elements or additional amounts of certain elements present in the base material may be introduced in order to promote weld-metal soundness and to insure that the cast weld-metal will have properties equal to, or better than, those of the base metal.

In heterogeneous welds, the manner in which the composition changes at the junction of the weld metal and the base metal is a question that has only been dealt with in

in a few special situations, such as the case of stainless steel weld metal deposited on low-alloy or mild-steel base metal. In this case, a narrow diffusion band has often been observed between the weld metal and the base metal. It has been postulated that this diffusion band, which differs in both microstructure and properties from either the weld metal or the base metal, results from diffusion in the solid state after the weld pool has passed.[1,2] Whenever such a diffusion band is present, the true fusion boundary may not be readily discernable.[2]

In heterogeneous welds, where composition differences are not sufficient to form a detectable diffusion band, little information is available concerning the concentration gradients at the fusion boundary. The microscopic demarcation between metal that was liquid and metal that remained solid during the passage of the weld pool is generally assumed to be rather straight-forward. Usually all the material in the so-called heat-affected zone is regarded as remaining solid right up to the boundary of the fully-molten region. However, investigations such as those conducted by Owczarski et al.[3] and Pepe and Savage[4] have shown that metallographic examination at high magnifications reveals significant localized melting within the so-called heat-affected zone near the fusion boundary. It has become apparent, therefore, that the

definition of the fusion boundary is dependent upon both the magnification and the metallographic technique used to examine this region.

Metallographic Examination of Welds. Metallographic examination of welds usually involves the observation, at a chosen magnification, of the polished and etched surfaces of samples cut from the weld. The purposes for such examination are listed in The Welding Handbook[5] as the determination of:

1. the distribution of nonmetallic inclusions,
2. the number of weld passes,
3. the grain structure in the weld and fusion zone,
4. the extent and structure of the heat-affected zone.

Metallographic techniques have become relatively standardized over years of common usage. Except in cases where individual microstructural constituents are to be resolved, metallographic examination is usually conducted at 1 to 20 magnification. A weld photomacrograph, typical of those often found in the literature, is shown in Figure 1 at a magnification of 6X. Note that only gross features such as the dimensions of the single weld bead, the extent of the heat-affected zone, and the location or absence of sizeable defects can be resolved in such photomacrographs.

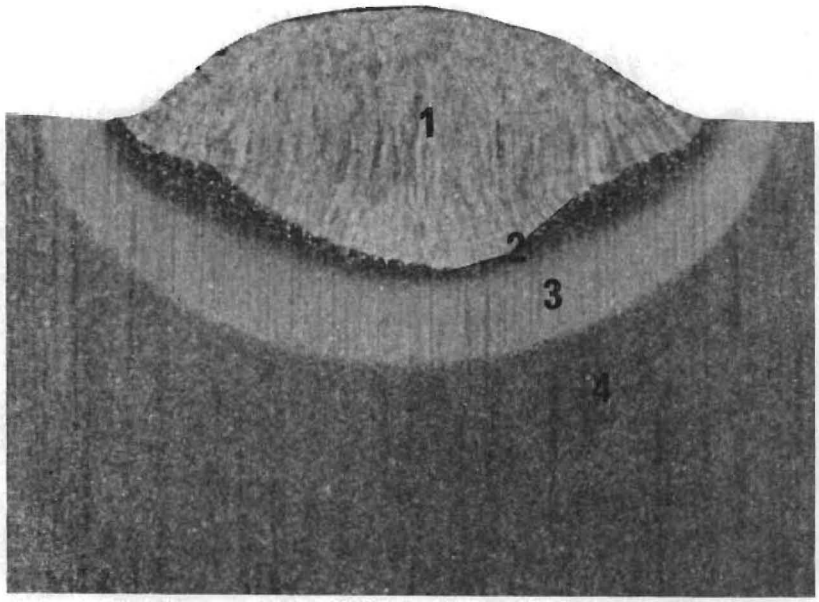

1. Weld Metal
2. Apparent Fusion Line
3. Heat-Affected Zone
4. Unaffected Base Metal

Figure 1 Typical Macrograph of a Transverse Section of a Bead Weld Made by the Shielded Metal-Arc Welding Process. Such Macrographs Show Only Gross Features of a Weld. Ammonium Persulfate Etchant, 6X.

Late in 1960, it became apparent that the standardized metallographic procedures were not revealing some significant features of the microstructure of weldments. For example, in December of 1960, Brown and Adams[6] and Calvo et al.[7] simultaneously published evidence that a solidification substructure was present and metallographically observable in weld metal. In welds, such substructure is manifested either as a regular closely-spaced network of fine corrugations (or dimples) on the as-solidified surface of the weld metal, or as a regular pattern of light- and dark-etching regions within grains on etched sections prepared using appropriate metallographic procedures. The substructure is a direct result of the redistribution of solute atoms, on a microscopic scale, during the solidification of the weld metal, and, therefore, has a significant influence on the properties of the weld metal.

The recognition of a solidification substructure in weld metal meant that the concepts of solidification mechanics introduced by Chalmers and his associates[8] in the early 1950's were applicable to the solidification of fusion welds. Subsequently, Borland,[9] Savage et al.,[10] and Wada[11] have discussed the application of solidification mechanics to fusion welding. A solidification substructure has since been shown to exist in various types of fusion welds made in

numerous alloys. In fact, some form of solidification substructure undoubtedly occurs in all types of fusion welds in every commercially available structural material. The realization of this fact is of considerable importance since the mechanical properties, as well as the soundness of the weld metal, depend, to a large extent, upon the nature of the solidification substructure.

In view of its importance, it is rather surprising that more attention has not been given to the solidification substructure of welds. In a large part, this inattention probably results from the fact that solidification substructures can be revealed clearly only by special metallographic procedures which may be more elaborate than the commonly used macrographic procedures. Since the subgrain boundaries are relatively low-energy boundaries, they are not readily attacked by normal etchants. Consequently, many investigators are not aware of the existence of solidification substructures.

In addition to the metallographic difficulties, a lack of familiarity with the basic concepts of solidification mechanics makes some investigators reluctant to apply these concepts to practical welding problems. Some of the more important solidification concepts will be reviewed briefly below. However, for treatment in depth, reference should be made to several excellent texts on the subject.[8,12,13,14,15)]

The Origin of Substructure in Weld Metal. The introduction, by Rutter and Chalmers[16] in 1953, of the concept of constitutional supercooling was probably the most significant contribution to the development of a theoretical explanation of alloy solidification. The application of this concept successfully accounted for the various solidification substructures observed in cast alloys.

According to the concept of constitutional supercooling, the accumulation of solute atoms in the liquid ahead of an advancing solid-liquid interface can reduce the effective liquidus of the molten phase in front of that interface. Thus, the effective liquidus temperature exhibits a minimum at the interface and exponentially rises to that of the nominal composition at some point in the adjacent bulk liquid.

As a consequence of the depressed liquidus at the interface, it is possible to visualize the existence of a "constitutionally supercooled" region in the liquid ahead of an advancing interface even in the presence of a positive temperature gradient in the liquid. Therefore, if the temperature gradient in the liquid at the interface is gradually diminished, a condition of instability develops when the actual temperature falls below the effective liquidus in the region immediately ahead of the interface. As a result of such instability, the interface tends to assume a characteristic

nonplanar geometry which leads to the development of a particular type of solidification substructure. According to the concepts proposed by Rutter and Chalmers, the mode of solidification experienced is dependent upon the extent of the region of constitutional supercooling.

In order to predict the extent of constitutional supercooling and hence the solidification mode, the use of a "Chalmers number" is suggested. The Chalmers number can be considered analogous to the dimensionless Reynolds number used in fluid mechanics to predict the point at which laminar flow breaks down into turbulent flow.

The Chalmers number is obtained by simply rearranging, into a dimensionless quantity, the terms in the relationship obtained when the slope of the actual temperature gradient in the liquid at the interface is equated to the slope of the exponential liquidus-temperature-curve at the interface. This relationship has been derived in numerous texts and will not be repeated here.[8,12,14]

For a simple binary system solidifying with a constant interface velocity and a steady-state solute spike, the Chalmers number, $\mathcal{C}$, can be defined by the following equation:

$$\mathcal{C} = - \frac{m\, C_o\, R\, (1-k_o)}{G_L\, D\, k_o} \qquad (1)$$

where: m = slope of the liquidus in the binary diagram (^{o}C/wg fraction),

C_o = nominal solute concentration in the liquid (weight fraction),

R = velocity of growth at the planar interface (cm/sec),

k_o = the distribution coefficient for the binary system (dimensionless),

G_L = temperature gradient in the liquid at the solid-liquid interface (^{o}C/cm),

D = the diffusion coefficient of the solute in the liquid (cm^2/sec).

Usually m, k_o, C_o, and D are approximately constant for a given solute, thus equation (1) can be rewritten as:

$$\mathcal{C} = \beta \left(\frac{R}{G_L} \right) \qquad (2)$$

where the solute factor, β, has the units ^{o}C sec per sq cm.

When $\mathcal{C}$ is between zero and unity,* planar growth will occur, since the effective liquidus will be less than the actual temperature in the liquid at all points and a constitutionally supercooled region will not be established. When $\mathcal{C}$ is greater than unity, the planar interface breaks down into a nonplanar growth mode since the actual temperature near the interface will be below the effective liquidus. It should be noted that with the breakdown of the planar interface, the terms defining the Chalmers number no longer strictly apply.

* Consideration is limited to cases of a positive G_L.

The system of classifying solidification modes in welds adopted at Rensselaer recognizes the planar mode and four distinct nonplanar modes. In order of increasing Chalmers number, the nonplanar modes are: cellular, cellular-dendritic, columnar-dendritic, and equiaxed-dendritic. Unfortunately, the range of values of the Chalmers number within which a given nonplanar solidification mode will occur has not been determined. Figure 2A shows a schematic illustration of the planar solidification mode and Figure 2B shows a typical example of a region of planar growth in a weld. Figures 3, 4, 5, and 6 show schematic illustrations as well as typical examples of the cellular, cellular-dendritic, columnar-dendritic, and equiaxed-dendritic modes, respectively. Experience has shown that the most common modes of solidification encountered in welds are cellular and cellular-dendritic.

An important point which should be noted is that with the cellular and cellular-dendritic modes of solidification, a solidifying grain is composed of <u>subgrains</u> which are the basic units of the substructure. In other words, parallel and adjacent cells (or branched cells, in the case of cellular-dendritic growth) are all part of the same grain, as illustrated in Figures 3 and 4, and have almost identical crystallographic orientation. On the other hand, an entire grain may solidify by branched growth from either a single central stalk

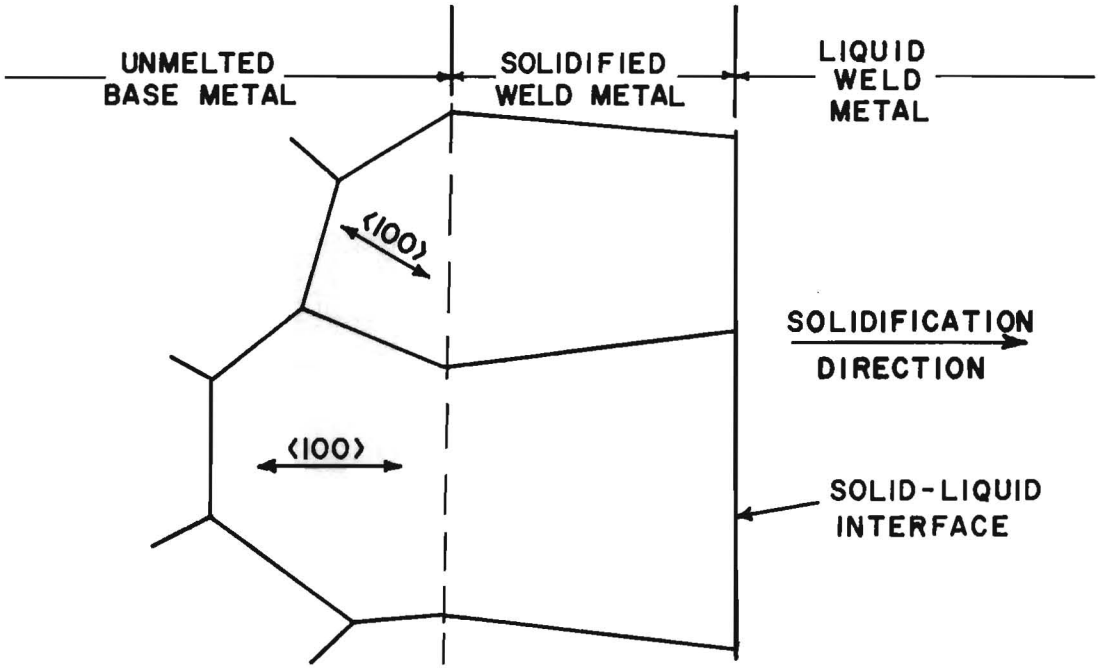

A.

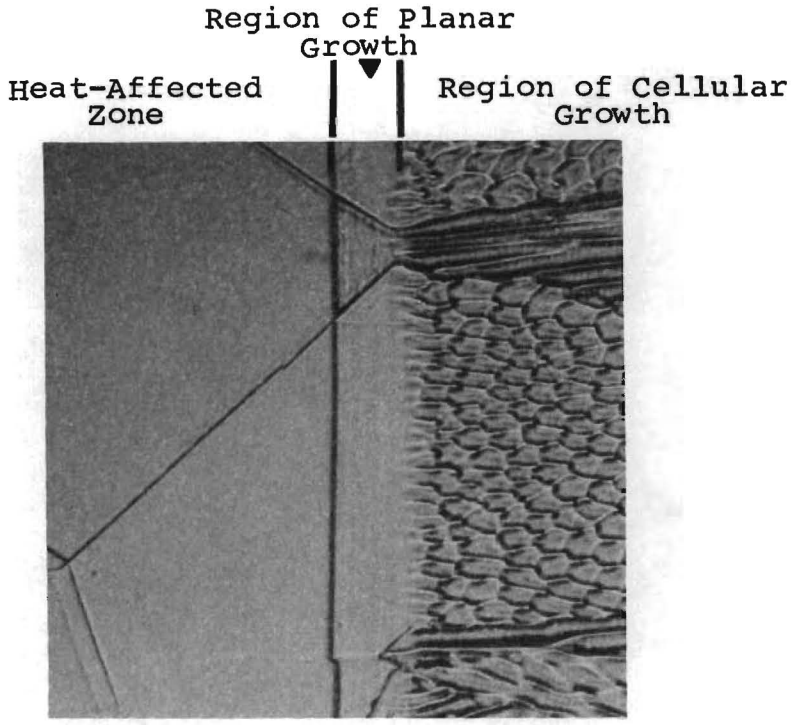

B.

Figure 2 Example of the Planar Solidification Mode. A. Schematic Illustration. B. Transverse Section of a Gas Tungsten-Arc Weld in an Iron-Nickel Alloy. Etched, 250X. (Photomicrograph courtesy of C. D. Lundin).

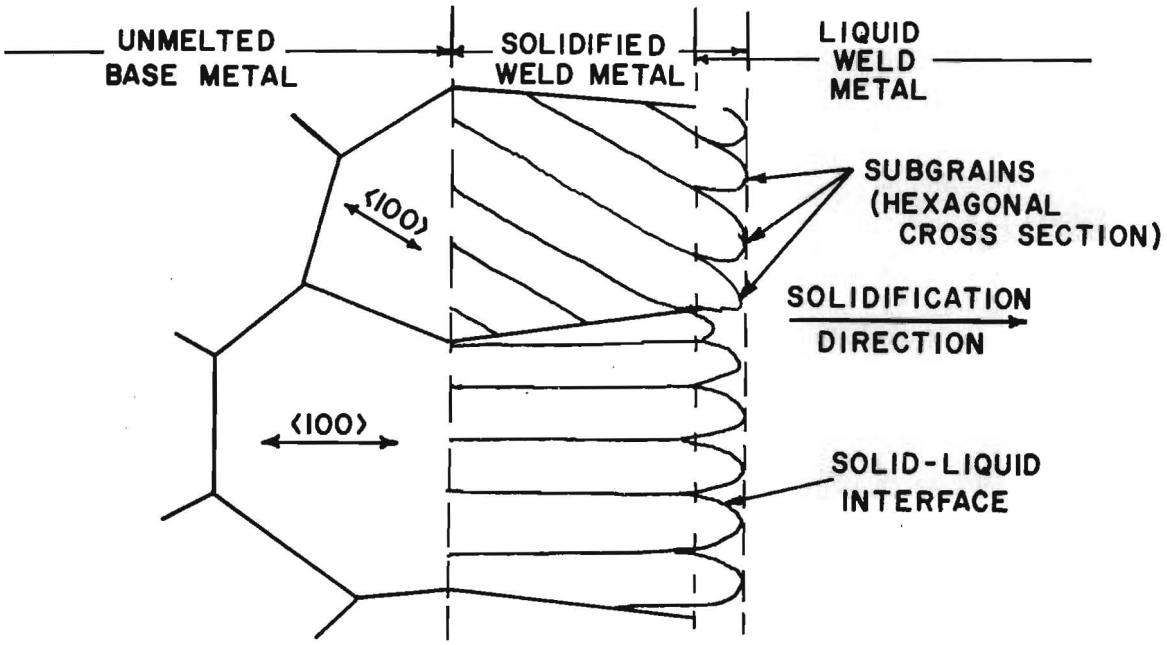

A.

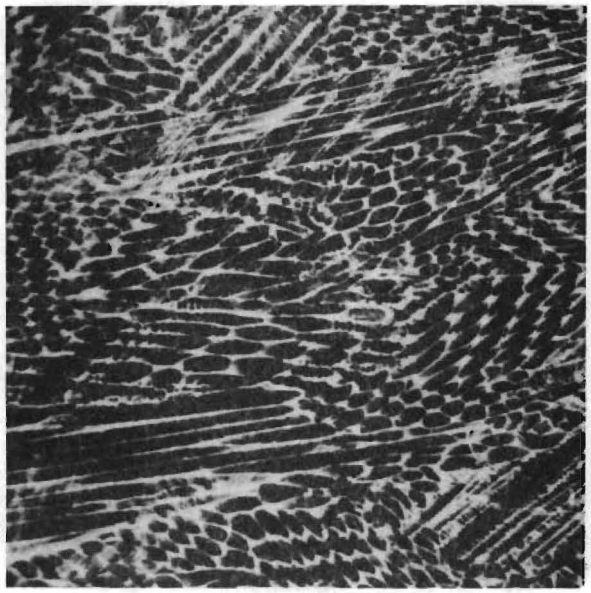

B.

Figure 3 Example of the Cellular Solidification Mode. A. Schematic Illustration. B. Transverse Section of a Gas Tungsten-Arc Weld in HY-80 Steel. Nital and Sodium Bisulfite Etchant, 250X.

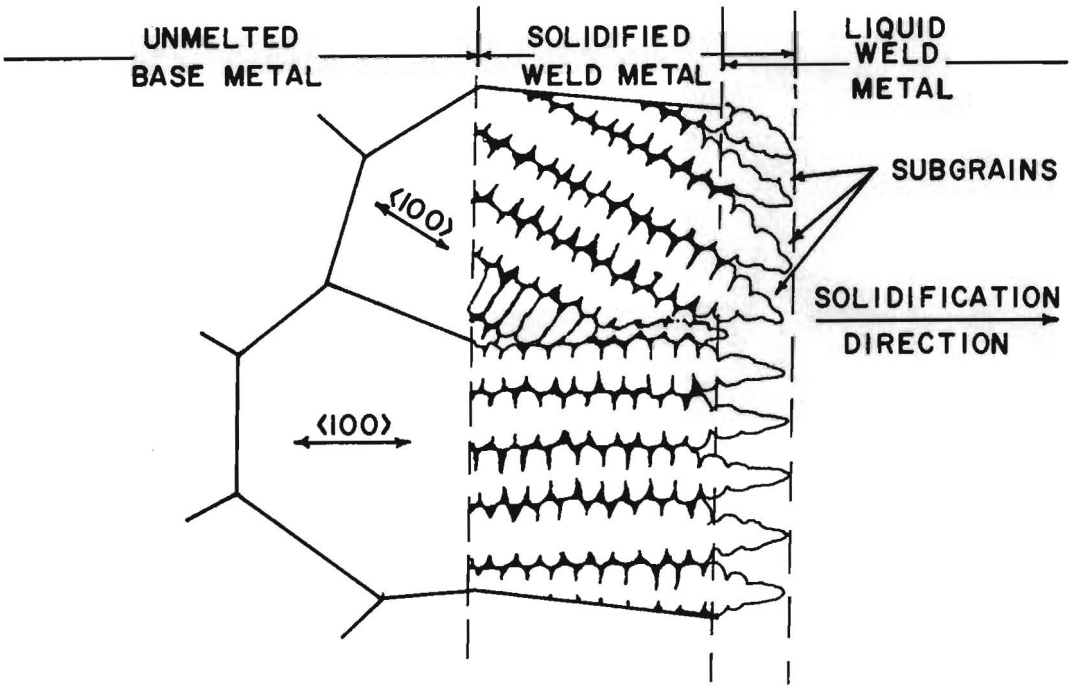

A.

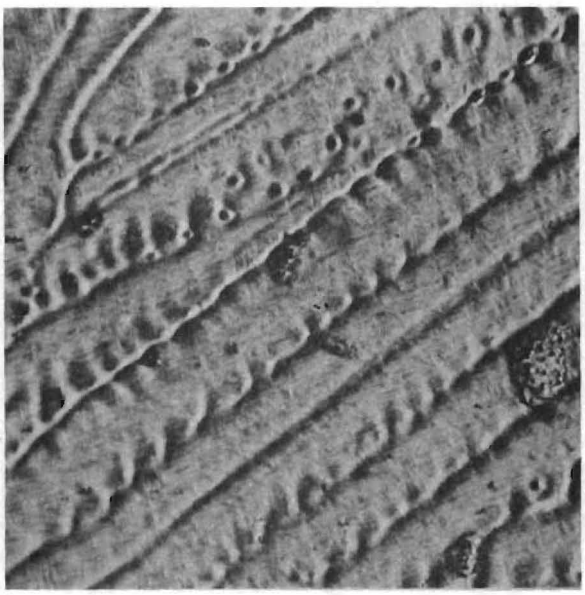

B.

Figure 4 Example of Cellular-Dendritic Solidification Mode. A. Schematic Illustration. B. Surface of Gas Tungsten-Arc-Weld in a Silicon-Iron Alloy. As-Welded, 300X. (Photomicrograph courtesy of C. D. Lundin)

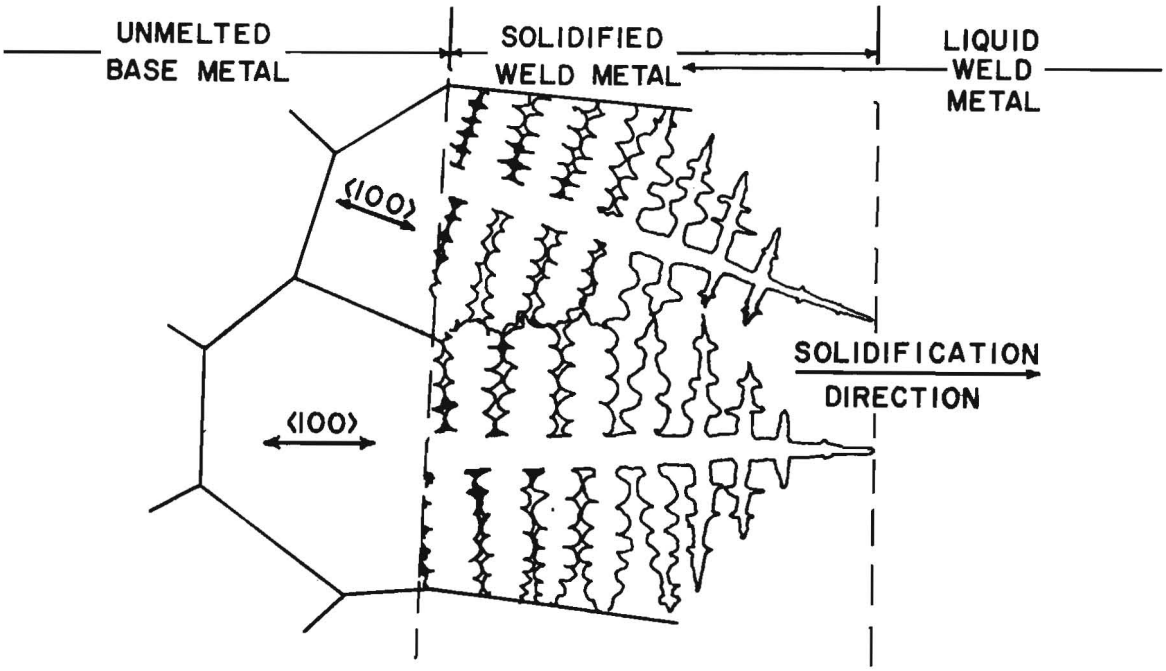

A.

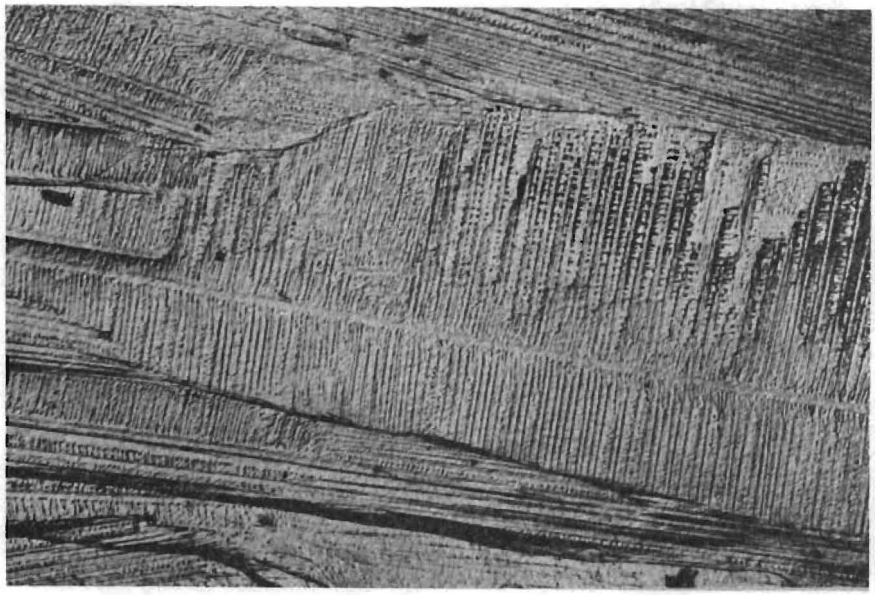

B.

Figure 5 Example of Columnar-Dendritic Solidification Mode. A. Schematic Illustration. B. Surface of a Gas Tungsten-Arc Weld in a Titanium-Manganese Alloy. As-Welded, 15X. (Photomacrograph courtesy of C. D. Lundin)

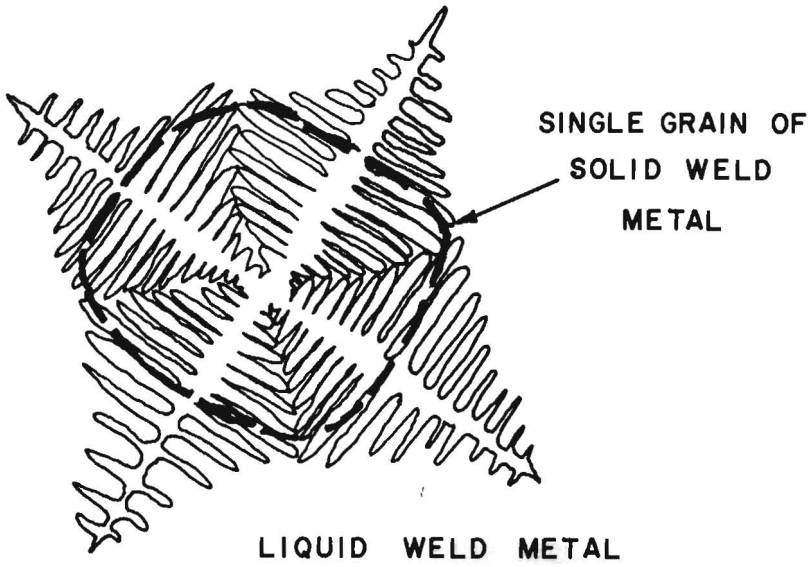

A.

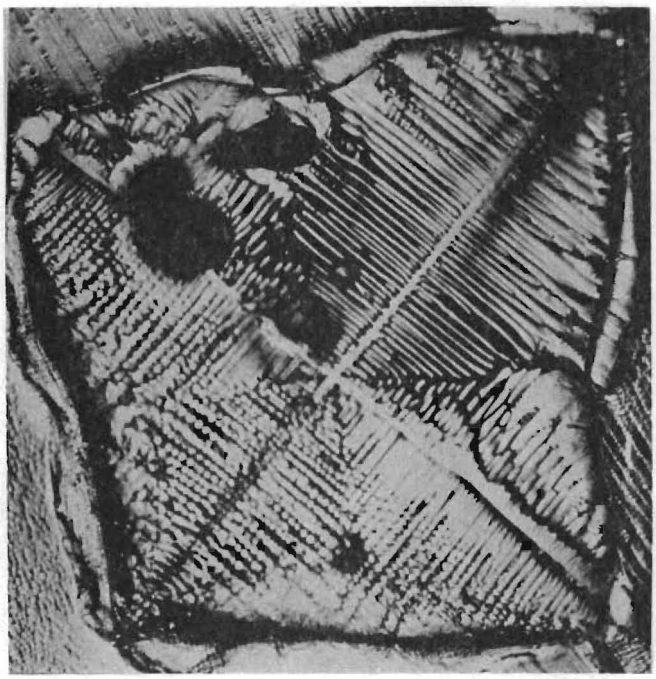

B.

Figure 6 Example of the Equiaxed-Dendritic Solidification Mode. A. Schematic Illustration. B. Surface of the Terminal Crater in a Gas Tungsten-Arc Weld in a Silicon-Iron Alloy. As-Welded, 100X. (Photomicrograph courtesy of C. D. Lundin)

as with the columnar-dendritic mode, or from a single nucleation site, as with the equiaxed-dendritic mode, see Figures 5 and 6.

In addition, it must be recognized that the solidification of welds does not involve the formation and growth of isolated nuclei in the classical sense, except possibly for the case of the equiaxed-dendritic mode which is normally encountered only in the terminal crater of a weld. Instead, the nucleation process in welds invariably occurs by what can best be defined as epitaxial nucleation. In other words, an "ideal substrate" is available for heterogeneous nucleation in the form of the solid grains of base metal at the border of the molten pool.[17,18] Thus, growth can occur with much less supercooling than would be required for establishing separate nucleation events; in fact, the amount of supercooling required becomes vanishingly small. Growth proceeds epitaxially with the atoms from the liquid phase joining and extending the crystal structure of the solid grains which serve as epitaxial nuclei. In addition, this growth is competitive in that grains more favorably oriented grow preferentially at the expense of grains less favorably oriented.

Historical Background of HY-80 Steel

In 1957, HY-80 armor steel was adopted by the United States Navy Department under specification MIL-S-16216.

Since 1957, the use of HY-80 steel has continuously expanded with a major expansion in 1958, when the Bureau of Ships adopted HY-80 steel as the principal material for submarine hulls.

The composition and specified mechanical properties of HY-80 steel are presented in Tables I and II, respectively.[19] Basically, HY-80 steel is a low-carbon alloy steel that possesses an excellent combination of strength, toughness, and ductility as a result of a microstructure of tempered low-carbon martensite. In order to insure that a fully-martensitic structure is obtained by commercial quenching practice, the nickel, chromium, and molybdenum contents are specified in amounts that compensate for the reduction in hardenability resulting from the necessity for maintaining a low carbon content. In normal practice, HY-80 steel plates are water-quenched from 1650 F and tempered at 1200 F.

Welding of HY-80 Steel. When welding HY-80 steel, the retention of adequate strength and toughness in the heat-affected zone is a major concern. During the welding operation, the conduction of heat from the weld pool into the surrounding base metal modifies the original microstructure of the quenched-and-tempered base metal in a complex fashion. Therefore, the welding conditions must be appropriately chosen in order to minimize metallurgical transformations

Table I

Chemical Composition Requirements for HY-80 Steel Plates, Percent

Specification	Plate Thickness, inches	C	Mn	P	S	Si	Ni	Cr	Mo
MIL 16216D (Obsolete)	to 1-3/8	0.22 max	0.10 to 0.40	0.035 max	0.040 max	0.15 to 0.35	2.00 to 2.75	0.90 to 1.40	0.23 to 0.35
	over 1-1/4 ("Heavy Gage")	0.23 max	0.10 to 0.40	0.035 max	0.040 max	0.15 to 0.35	2.50 to 3.25	1.35 to 1.85	0.30 to 0.60
MIL 16216E	to 6	0.18 max*	0.10 to 0.40	0.025 max**	0.025 max**	0.15 to 0.35	2.00 to 3.25	1.00 to 1.85	0.20 to 0.60

* Add 0.02 percent to max carbon for plates 6-inches thick and over.

** The combined phosphorus and sulfur contents shall be no more than 0.045 percent.

Table II

Mechanical Property Requirements of HY-80 Steel Plates[19)]

Tensile Properties

Plate Thickness, inches	Yield Strength (0.2% Offset), psi	Elongation Min. Percent in 2 Inches	Reduction in Area, Minimum Percent	
			Longitudinal	Transverse
less than 5/8	80,000 to 100,000	19	-	-
5/8 and over	80,000 to 95,000	20	55	55

Longitudinal Charpy V-Notch Impact Strength

Plate Thickness, inches	Testing Temperature, F	Specimen Size, mm	Required Min. Avg. of 3 Specimens, ft-lbs
under 1/2	-120	10 x 5	-
1/2 to 2	-120	10 x 10	60
over 2	-120	10 x 10	30

in the heat-affected zone which impair the overall performance of the weldment.

Basically, the thermal-energy input during the welding operation, generally measured in joules per inch, should be controlled so as to produce cooling conditions in the heat-affected zone which are neither too slow nor too fast. Excessively high heat inputs cause the base metal next to the weld to cool slowly enough to permit the formation of high-temperature transformation products such as ferrite and high-temperature bainite. A heat-affected zone containing such products is known to exhibit significantly poorer impact properties than the unaffected base metal and therefore a limitation has been imposed on the maximum energy input.

On the other hand, if too low an energy input is employed, the cooling rate between the M_s and M_f is so rapid that the martensite formed in the heat-affected zone does not have an opportunity to adequately self temper (which also results in poor impact properties). Therefore, to avoid cooling rates too rapid to provide sufficient self-tempering, a minimum energy input may be specified as well.

Ledman, et al.[20] studied the continuous-cooling-transformation behavior of a heat of HY-80 steel which met specification MIL-16216E. They found the M_s temperature to be 715 $\pm$ 15 F and the M_f temperature to be 495 $\pm$ 15 F.

Furthermore, by means of Gleeble tests, they determined that energy inputs of 50,000 joules per inch and over produced a mixture of bainite and martensite in the weld heat-affected zone. In addition, it has been reported elsewhere[21] that the heat-affected zone of bead welds made in HY-80 steel of "heavy gage composition" with a more optimum heat input of 47,000 joules per inch consisted essentially of tempered and untempered martensite. However, with energy inputs much less than 30,000 joules per inch, it is expected that in thick plates the cooling rates below the M_S temperature are too fast to provide adequate self-tempering of the low-carbon martensite.

Cracking in Weldments of HY-80 Steel. With the initial application of HY-80 steel in submarine construction, fabricators encountered cracking difficulties. These difficulties were reported to consist primarily of transverse cracks in the weld metal and longitudinal cracks in the heat-affected zone of fillet welds joining frame members to hull plates. The problem of weld metal cracking was minimized by the development of improved low hydrogen electrodes and by strict control of:

1. the procedures for the care and use of low-hydrogen welding materials,
2. the welding procedures (in order to minimize residual stresses),
3. the welding energy input.[22]

Although the adoption of "low hydrogen" welding practice sharply reduced the incidence of weld-metal cracking, the perplexing problem of cracking in the apparent heat-affected zone of HY-80 steel weldments persisted. For example, in a survey of shipyard experiences, referred to by Masabuchi and Martin,[23] it was stated that the cracking which occurred even when "correct" welding procedures were followed was always associated with the apparent heat-affected zone. Although some cracks were observed which propagated into the weld metal, no example of a crack located entirely within the weld metal was cited in the above survey. Figure 7 shows, for orientation only, typical cracks in the apparent heat-affected zone of a frame-to-hull tee-joint sample removed from a submarine.[21]

Consequently, in the early 1960's, investigators focused their attention on the problem of cracking in the apparent heat-affected zone. Since that time, various theories have been proposed in an attempt to explain the mechanisms of initiation and propagation of cracks in this region and to establish the factors responsible for each.

An early analysis by Griffin[24] suggested that heat-affected-zone cracking in HY-80 steel is similar to "underbead" cracking (also referred to as cold cracking, delayed cracking, and hydrogen-stress cracking). He proposed that during welding,

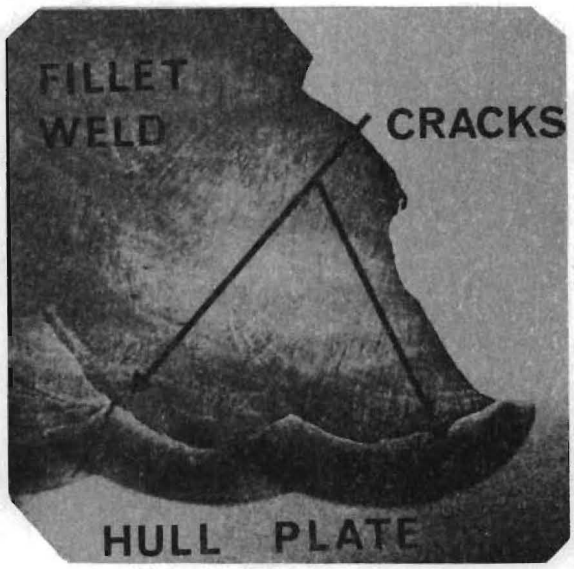

Figure 7 Transverse Section of a Frame-to-Hull Tee Joint Revealing Cracks in a Heavy-Gage-Composition HY-80 Steel Hull Plate. Ammonium Persulfate Etchant, 4X (modification of Figure 14 in Reference 21).

hydrogen dissolved in the weld pool diffuses to the adjacent base-metal region which has temporarily transformed to austenite. He further proposed that if the particular heat of HY-80 steel had a sufficiently high alloy content, or if for some reason the austenite grain boundaries became alloy enriched, the alloy-rich austenite would have a lower M_s temperature than the lower-alloy austenite in the weld metal and thus would not transform until after transformation of the weld metal was complete. In such a case, the late transforming, alloy-rich austenite regions would become sinks producing localized regions of abnormally high hydrogen content even with low-hydrogen welding procedures. According to this model, when the last vestiges of supersaturated austenite finally transformed to martensite and lost their relatively high solubility for hydrogen, every available inclusion or microfault would serve as a site for the precipitation of hydrogen gas. Then, under the influence of stresses resulting from both low temperature transformation and restraint, such sites could initiate fracture.

Doty and Grotke[21] also reasoned that the grain-boundary cracking in HY-80 steel weldments was identical to underbead cracking. They hypothesized that the cracking was due to alloy- and carbon-enriched prior-austenite grain boundaries which transformed to martensite near room temperature.

Such martensite would be embrittled due to a concentration of hydrogen which was unable to diffuse away rapidly enough. In their investigation, electron microscopy revealed a second phase at the prior-austenite grain boundaries in the maximum-grain-coarsened heat-affected zone. Tempering of the specimen resulted in the formation of agglomerates at the prior-austenite grain boundaries. It was claimed that the agglomerates were carbides.

At about the same time, an investigation by Emmanuel et al.[25] under sponsorship of the Bureau of Ships, concluded that hydrogen was primarily responsible for crack propagation but not crack initiation. It was postulated that hydrogen could initiate cracking at low temperatures only when present in amounts far greater than could be introduced when welding with a low-hydrogen electrode. Furthermore, upon comparing the composition of heats of HY-80 steel with the results of Controlled-Thermal-Severity (CTS) tests and hot-ductility tests, these investigators found a relationship between cracking and the sulfur content of the heat. Also, they noted a significant change in sulfide distribution between the as-received material and hot-ductility test specimens. Because of these observations, it was hypothesized that intergranular heat-affected-zone cracks were initiated, at temperatures near the melting point, by some mechanism involving sulfur.

Masubuchi and Martin[23] similarly argued that the cracking in HY-80 steel is a two-stage process. The first stage, which occurs during the passing of the weld pool, supposedly involves the formation of intergranular microcracks at prior-austenite grain boundaries in the heat-affected zone adjacent to the fusion boundary. The second stage, which occurs at much lower temperatures, involves the propagation of these microcracks into macrocracks. During this second stage, any embrittlement phenomenon, such as hydrogen embrittlement, would contribute to crack propagation.

Masubuchi and Martin concentrated their investigation on the first stage, the microcracking phenomenon. They hypothesized that the microcracking was the result of hot tearing of liquated grain boundaries. Although a clear mechanism for hot tearing was not presented, the material liquating was proposed to be low-melting sulfides which segregated to the grain boundaries at temperatures above 2500 F. As part of their investigation, electron beam microanalyses were made across typical intergranular cracks and segregated grain boundaries of the heat-affected zone. However, the results were inconclusive in that some traverses indicated an increased silicon and sulfur concentration with a slightly lower iron concentration while in other traverses, no significant variations from the matrix composition were found.

Sibley[26] noted nonmetallic segregates along prior-austenite grain boundaries in the heat-affected zone adjacent to the fusion boundary and occasionally along interdendritic boundaries in the weld metal. Surprisingly, he reported that the results of tests for sulfides were negative. Therefore, Sibley suggested that the segregates were a complex oxide, possibly mixed with a silicate.

Rathbone and Gross[22] showed a correlation between cracking in the cruciform test and the sulfur content and, to a lesser degree, the nickel content of 12 heats of HY-80 steel. They reasoned that the effect of sulfur was to cause the formation of hot microcracks which subsequently propagated due to the stresses accompanying the low temperature transformation occurring at or below the M_s. Thus, the nickel was believed to increase the crack susceptibility because an increase in nickel would lower the M_s temperature. However, direct measurements of the M_s temperatures of the heats were not made in this investigation. According to this model, a lower transformation temperature would allow higher microstresses to be built up, thus, facilitating the initiation and propagation of new cracks and also the propagation of the existing microcracks caused by the sulfur segregation. The elimination of cracking in the cruciform test by preheating was cited as evidence that a transformation-stress mechanism was the one primarily responsible for the cracking.

In an investigation by Interrante and Stout,[27] the cracking of HY-80 steel was assumed to be strictly a delayed cold-cracking phenomenon. Therefore, this investigation was particularly concerned with the role of hydrogen and neither any effect of sulfur nor any observation of microcracking was mentioned. In their work, the Lehigh Restraint Test was used to evaluate the susceptibility of HY-80 steel to delayed cracking. This susceptibility was found to be directly proportional both to the hardenability of the base metal as calculated from a modified Winterton carbon equivalent formula, and to the hydrogen content of the welding atmosphere. In addition, one heat of HY-80 steel was subjected to a range of heat treatments prior to welding. Surprisingly, annealed samples and spheroidized samples showed a greater susceptibility to cracking than either spray-quenched samples or spray-quenched-and-tempered samples. From these results, the investigators concluded that crack susceptibility of HY-80 steel increases as the size of the carbides increases. Unfortunately, metallographic evidence of the base-metal microstructures was not presented and, therefore, the role of carbides is not clear.

Analysis of the Problem

From the brief review above, it is apparent that the understanding of the mechanism of cracking in HY-80 steel

weldments is far from complete. In addition, considerable disagreement exists concerning the mechanism of crack initiation. Unfortunately, it is precisely this understanding that is necessary to avoid similar problems with the higher strength quenched-and-tempered low-alloy steels presently under development.

Apparently, there is considerable disagreement among investigators who maintain that high temperature microcracking is a prerequisite for further cracking at low temperatures and others who hold that hydrogen and/or transformation stresses are responsible for both the initiation and propagation of the cracking in HY-80 steel. However, those who maintain that cracks both initiate and propagate at low temperatures have not clearly explained the apparent significance of sulfur.

In general, most investigators[21,22,23,24,25] agree that the cracking in HY-80 steel is predominantly intergranular, at least in the early stages of propagation. Thus, it is highly probable that grain boundary segregation is involved in some fashion. However, the popularly held opinions that grain boundaries in the heat-affected zone accumulate solute by some sort of "sweeping" process or by equilibrium segregation have been strongly refuted by Duvall and Owczarski.[28] They reasoned that moving grain boundaries

would be unable to accumulate solute and that diffusion induced segregation at grain boundaries would be reduced, rather than enhanced, at the high temperatures that occur in the region of the heat-affected zone immediately adjacent to the weld where cracking usually occurs. Thus, although the available evidence suggests that grain boundary segregation is involved in the cracking, the mechanism by which the segregation arises is completely unresolved.

Several generalizations of the cracking problem in HY-80 steel suggest directions for further research. These generalizations are:

1. In normally prepared metallographic sections of both commercial and laboratory heterogeneous welds, the cracks, when they occur, usually appear as microcracks and macrocracks at, or immediately adjacent to, the fusion boundary. This seems to indicate that there is something unique about the fusion boundary as a site for crack initiation.
2. Not all heats of HY-80 steel exhibit cracking to the same extent. For example, two given heats can have nominal compositions that meet the pertinent specifications for the steel but one may be susceptible to cracking while the other is not. Why materials made to a particular specification can exhibit wide

differences in weldability has yet to be explained.

3. The cracking can occur under low-hydrogen welding conditions. Therefore, if hydrogen does play a role, either a relatively small amount is sufficient to cause cracking or other factors are extremely effective in concentrating the available hydrogen.

Based on the above analysis, the objectives of this investigation have been set forth in the following section.

OBJECTIVES

The objectives of this investigation were:

1. to study the metallographic structures and compositional gradients in the vicinity of the fusion boundary with the object of gaining a better understanding of the basic metallurgy of this region.
2. to establish a sound mechanism for explaining grain boundary segregation at the fusion boundary in weldments of quenched-and-tempered low-alloy steels.
3. to correlate the cracking in HY-80 steel with identifiable metallurgical features and the amount of hydrogen present during welding.

MATERIALS AND EXPERIMENTAL PROCEDURES

Material

The material used in this study was obtained from two heats of HY-80 steel plate supplied by the U. S. Steel Applied Research Laboratory, Monroeville, Pennsylvania. All plates were nominally 2-inches thick. The check analyses for the two heats are listed in Table III. The tensile and impact properties are given in Table IV.

These two particular heats were selected because of a well documented difference in their weldability in spite of a similarity in composition. For example, note that the Mn/S ratio is almost identical for both heats.* Both heats conform to specification MIL 16216E and to the "heavy gage" composition of the earlier MIL 16216D specification. However, it should be noted that Heat No. 72P305 (from here on referred to as Heat P) has a carbon content near the maximum permissable under MIL 16216D and Heat No. N51755 (from here on referred to as Heat N) has a nickel content at the minimum of the allowable range as well as a significantly lower carbon content.

The weldability of the two heats had been previously determined at the U. S. Steel Applied Research Laboratory by

---

* The Mn/S ratio is still incorrectly assumed by many investigators to be an accurate indicator of weldability.

Table III

Chemical Composition of HY-80 Steels Used in This Investigation

Heat No.	Furnace Practice	Check Analysis, percent											Total O_2*, ppm
		C	Mn	P	S	Si	Ni	Cr	Mo	Al Sol	Al Insol	N	
72P305	Open Hearth	0.18	0.30	0.018	0.013	0.20	2.99	1.68	0.41	0.022 0.024**	0.003	0.007	100
N51755	Electric	0.13	0.28	0.011	0.011	0.31	2.50	1.49	0.40	0.056 0.037**	0.009	0.014	95

Inclusion Analysis, + ppm

Heat No.	Oxides			Nitrogen in Nitrides	Sulfides or Oxides +++			
	Al_2O_3++	MnO	SiO_2		Cr	Ti	V	Zr
72P305	55	23	18	49	410	13	5	3
N51755	185	42	15	110	435	20	8	5

* Neutron-Activation Method.
** Second check analysis.
\+ Ester-Halogen Method.
++ Includes all AlN.
+++ In most cases, alloying elements such as Cr, Ti, V, or Zr are present in the inclusion form as carbides, nitrides, or sulfides, although, depending on the steelmaking practice, they may occur as oxides if they are added before the steel is killed.

Table IV

Mechanical Properties of the HY-80 Steels Used in This Investigation[22)]

Longitudinal Tensile Properties

Heat No.	Plate Thickness, inches	Type of Specimen	Yield Strength (0.2% Offset), psi	Tensile Strength, psi	Elongation, percent		Reduction of Area, percent
					1 in.	2 in.	
72P305	1/2*	0.252	95,000	115,000	24	+	74
72P305	2	0.505	88,000	108,000	+	25	74
N51755	2	0.252	83,000	103,000	27	+	78

* 1/2-Inch plate was not used in this investigation. The values are presented because 1/2-inch thick plate was used for cruciform tests, see Table V.

+ Not determined.

Longitudinal Charpy V-Notch Properties

Heat No.	Plate Thickness, inches	Energy Absorbed, ft-lbs	
		80 F	-120 F
72P305	2	143	121
N51755	2	153	140

means of the cruciform test.[22] The cruciform test will be briefly described in a subsection below. The results of these tests, as summarized in Table V, indicated that Heat P was considerably more crack sensitive than Heat N. The reason for the poorer performance of Heat P was not conclusively determined by investigators at U. S. Steel. However, the heats were part of a series of 12 heats used in a statistical investigation which showed a fair correlation between the amount of cruciform cracking and the sulfur and nickel contents of the individual heats.

Standard ASTM end-quench hardenability tests were also conducted at U. S. Steel. The ideal critical diameter, D_I, for the plates supplied was based upon the location along the end-quench specimen that corresponded to the hardness of 80 percent martensite. The results of the tests indicated that Heat P had a D_I of 7.0 inches and Heat N had a D_I of 4.5 inches. The hardenability of Heat P would be considered somewhat high for HY-80 steel, whereas, the hardenability of Heat N would be considered low. The difference in hardenability is a result of the higher nickel, carbon, and chromium in Heat P.

Metallographic Examination of the Base Metal

Samples for metallographic examination were cut from an as-received plate from each heat of HY-80 steel.

Table V

Single-Pass-Cruciform-Test Performance of the Heats of HY-80 Steel Used in This Investigation[22)]

Heat No.	Original Plate Thickness, inches	As-Welded Root-Cracking in Fillet C, Percent of Weld Length
72P305	1/2	73
N51755	2*	0

* The 1/2-inch-thick material required for the cruciform tests was machined from the quarter-thickness position of the 2-inch-thick plate.

Sections both longitudinal and transverse to the final rolling direction were polished, etched, and examined in the as-received condition under standard bright-field illumination.

Metallographic Examination of the Weld Fusion Boundary

Specimens for metallographic examination were obtained by sectioning bead welds transverse to the welding direction. The bead welds, about four inches long, were made on 2- by 2- by 5-inch-samples from both heats of HY-80 steel. Bead welds were made using an Airco Stickfeeder using 5/16-inch diameter E11018G electrodes. The electrodes were not baked because the possible formation of cracks due to hydrogen was not undesired. The bead welds were made transverse to the final rolling direction of the plate. Welds were placed both on the plate-edge and the rolled-surface of the sample. The welding conditions were 165 amperes, 22 volts, and 8.5 inches per minute.

Each bead weld was sectioned at six locations and the sections polished. Several etchants were tried and rated on their ability to reveal information about the fusion boundary. Examination was made using both standard bright-field illumination and Nomarski Interference Contrast as provided by a Natach-France Model TM. 74 microscope.[29)]

Electron Beam Microanalysis Across the Fusion Boundary

In order to determine the concentration profiles at the fusion boundary, electron beam microanalysis was performed for this investigation at the U. S. Steel Applied Research Laboratory.

Bead welds made on one specimen from Heat N and one from Heat P were sectioned transversely and the sections were subjected to thorough metallographic examination. Both welds were made with E11018G electrodes using 200 amperes, 22 volts, and a travel speed of 6.5 inches per minute. On the basis of the metallographic examination, suitable locations along the fusion boundary in each of the two sections were selected for traverses by the electron beam microanalyzer. The desired starting and stopping points for the microanalytical traverses were marked by hardness indentations. The two samples were then repolished with 3-micron diamond paste to remove the etched-surface and then re-etched, just sufficiently for the operator to orient the traverse.

The electron beam of the microanalyzer was operated at 30 kilovolts and 10 microamperes. The beam was traversed across the specimen at a constant velocity of 96 microns per minute. The speed of the chart paper was adjusted so that one-inch runout on the chart corresponded to 8 microns traversed on the sample. The spectrometer was adjusted to

record simultaneously CrK_{α} (λ = 2.292A) and MnK_{α} (λ = 2.108A). Analyses were made for manganese and chromium because the nominal compositions of these elements differ significantly between the weld metal and the base metal. Typical E11018G electrodes have a nominal content of 1.50 percent manganese and negligible amounts of chromium in contrast to the base metal which contained approximately 0.30 percent manganese and 1.5 percent chromium.

Varestraint Tests of the Weld Metal

The Varestraint Test was used to compare the weld-metal hot-cracking sensitivity of E11018G bead welds made on specimens from Heat P and Heat N. The purpose of the tests was to determine whether or not dilution from the crack-sensitive heat of HY-80 steel would affect the hot-cracking behavior of the weld metal.

The Varestraint Test, developed by Savage and Lundin, has been described in detail in the literature.[30,31] Briefly, the test involves the deposition of a bead weld on a specimen which is supported as a cantilever beam, as shown in Figure 8. At a predetermined instant during the welding operation, the specimen is forced to conform to the upper surface of a radiused-die-block. Die-blocks with different radii can be substituted to provide a series of specimens which have been subjected to different predetermined magnitudes of augmented

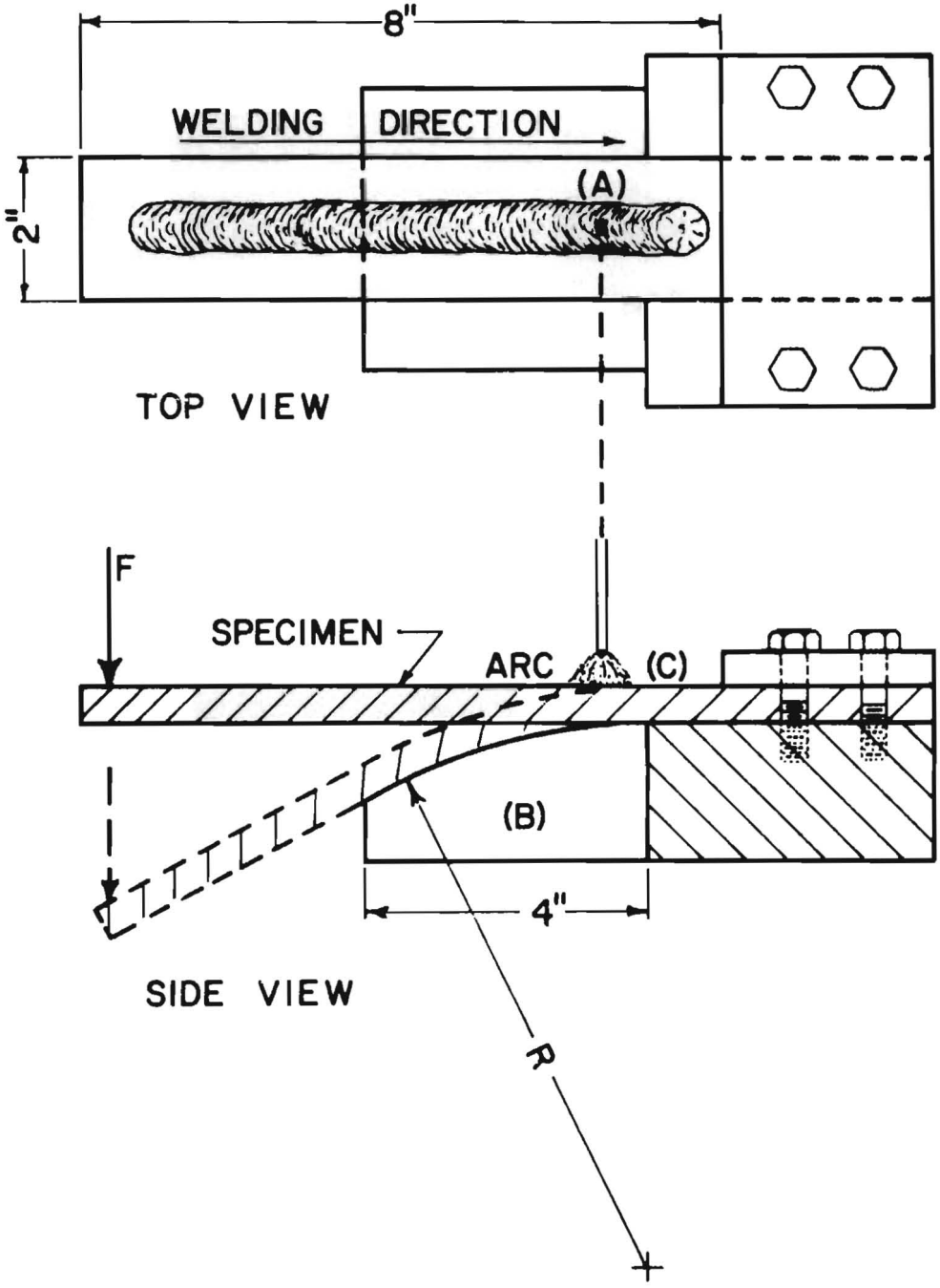

Figure 8. Schematic Illustration of the Varestraint Testing Device. When the Welding Arc Reaches Point A the Specimen is Forced to Conform to the Radius-Block B and the Arc Continues to Point C Where it is Extinguished.

strain in their outer fibers. When hot-cracking occurs, the cracks are usually located around the trailing edge and along the side of what was the instantaneous location of the weld pool at the time of load application.

For these tests, specimens 12- by 2-inches by 1/2-inch-thick were cut from plates from both heats of HY-80 steel in a manner shown in Figure 9. The specimens were taken in this manner so that in testing the bead weld would be made at the plate center where the segregation is the highest. All specimens were ground to a thickness of 0.500 $\pm$ 0.002 inch with a 30 RMS surface finish.

The bead welds were made with 5/16-inch-diameter E11018G electrodes by means of an Airco Stickfeeder attached to the Varestraint Test apparatus. The welding conditions were 200 amperes, 22 volts, and a travel speed of 6.5 inches per minute, providing a heat input of approximately 41,000 joules per inch. The electrodes were not baked before use.

The radii of the die-blocks used were 12.5, 25, 50, and 100 inches which provided nominal augmented strains of 2.00, 1.00, 0.50, and 0.25 percent, respectively. One specimen from each heat was used for each radius and, in addition, one specimen from each heat was welded but not strained. After welding and straining in the Varestraint apparatus, a sample containing the location of the weld puddle at the time

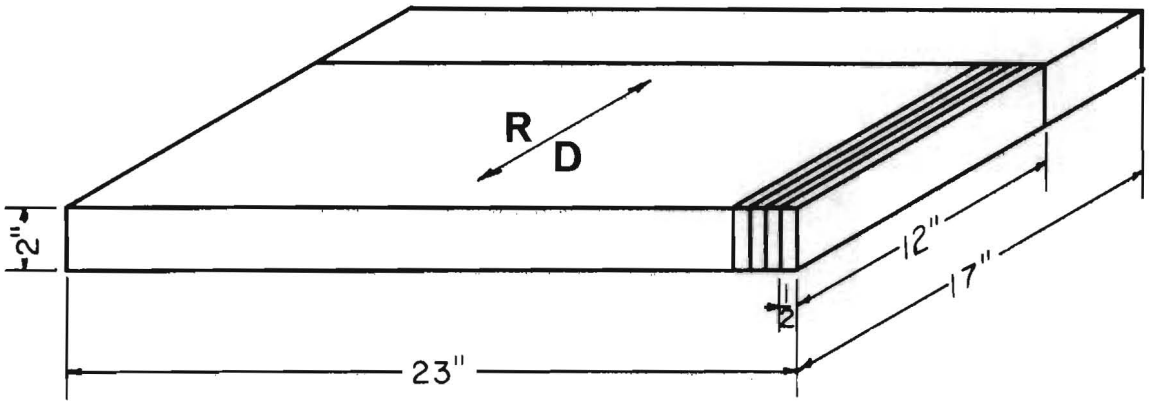

Figure 9 Orientation of the Varestraint-Test Specimens to the As-Received HY-80 Steel Plate.

of loading was removed from each specimen, as shown in Figure 10. The sample was then mounted in epoxy, ground to remove the weld reinforcement, and polished for metallographic examination. In addition, the metallographic samples from the specimens strained at 2 percent were sectioned transversely and prepared for examination of the fusion boundary.

Cold-Cracking Tests

Granjon[32] reported a technique used to study cold cracking which permitted direct microscopic observation of hydrogen bubble-evolution and crack formation in welded specimens of steels of relatively high hardenability and high carbon contents. For this investigation, the Granjon technique was modified in order to apply a bending load to small welded specimens during direct microscopic observation. The purpose of this modified technique was to obtain information about the nucleation of cold cracks. In contrast, most metallographic specimens taken from the common cold cracking tests provide little information about the nucleation of the cracks.

Specimens for the cold-cracking test were obtained by depositing a bead weld on specimens 0.30 by 0.50 by 2 inches long machined from both Heat N and Heat P. Two different specimen-to-plate orientations were selected in order to provide some specimens in which the banding was transverse and others in which the banding was parallel to the welding surface,

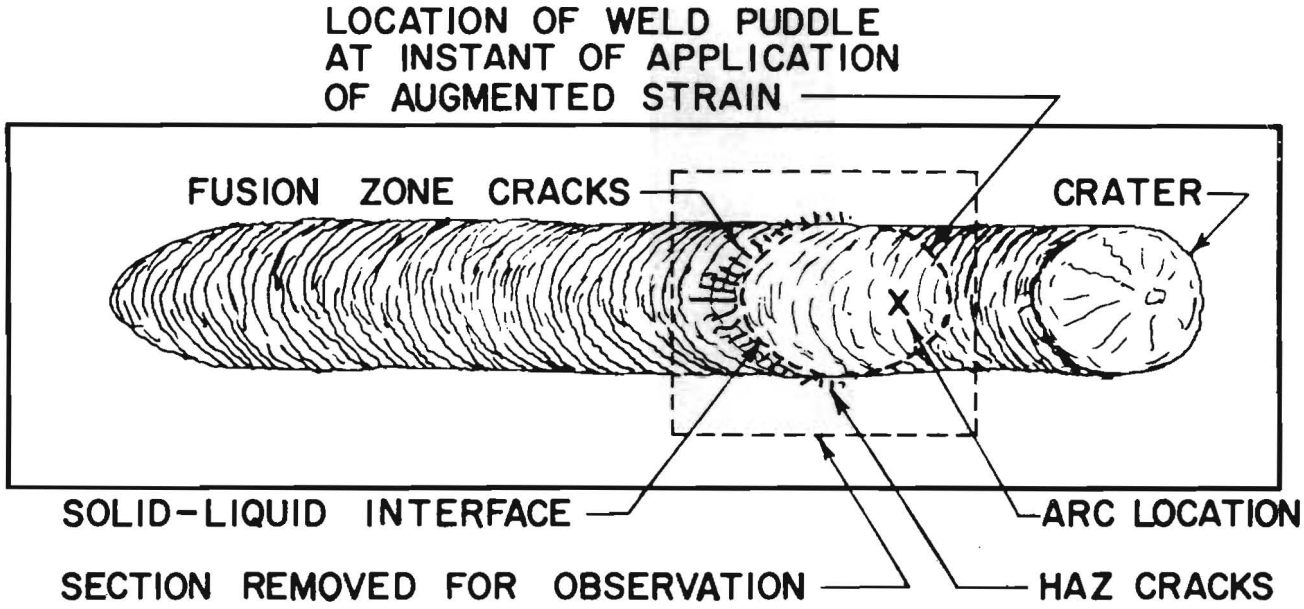

Figure 10 Schematic Illustration of the Top Surface of a Welded- and Tested Varestraint-Test Specimen Showing the Location of the Metallographic Sample.

refer to Figure 11. With the selected orientations, the location of the bead welds on the specimens correspond to the center of the as-received plate. All 0.5 by 2.0 inch surfaces were ground parallel, lapped, and rough polished with No. 600 grit polishing paper prior to welding.

Pairs of specimens with the same banding orientation, one from each heat, were clamped together between run-off tabs in a vise with the 0.5 x 2.0 inch rough-polished surfaces in contact while a bead-weld was deposited down the center of the composite weldment, as shown in Figure 12. E11018G welding electrodes were used with 165 amperes, 22 volts, and 7.5 inches per minute travel speed. High-hydrogen welds were made by wiping damp electrodes with a thin film of lubricating oil and also applying a few drops of oil to the surface of the specimens to be welded. The oil was necessary because preliminary tests indicated that simply wetting the electrodes did not introduce a sufficient amount of hydrogen into the welds to cause cracking or hydrogen bubble-evolution. Low-hydrogen welds were made with electrodes that were baked at 800 F for 1-1/2 hours and used soon after removal from the baking furnace. All welds were deposited with the Airco Stickfeeder.

Immediately after welding, the composite weldment was quenched to room temperature in water and then transferred

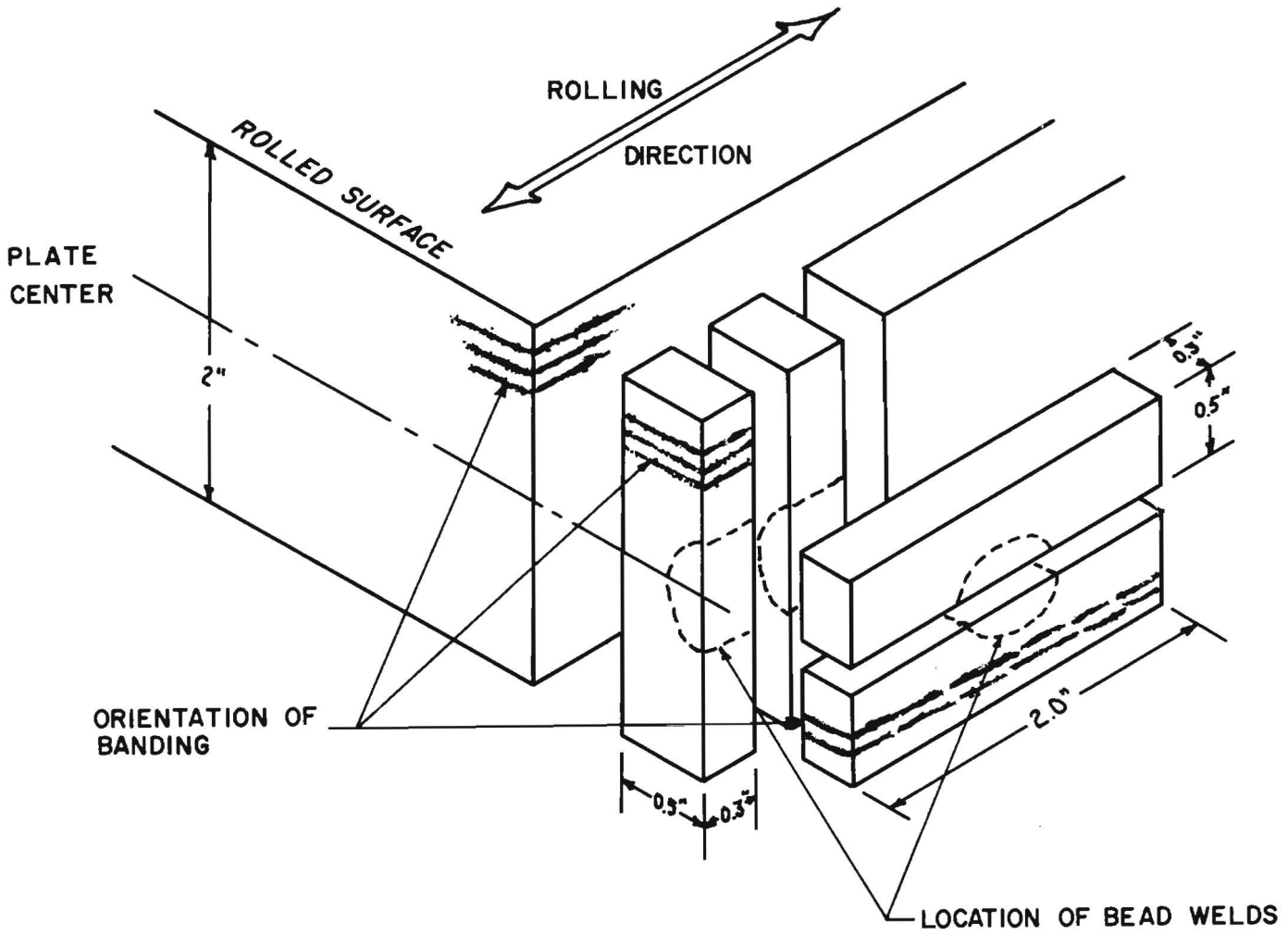

Figure 11 Orientation of the Cold-Cracking Test Specimens Machined From the As-Received HY-80 Steel Plates.

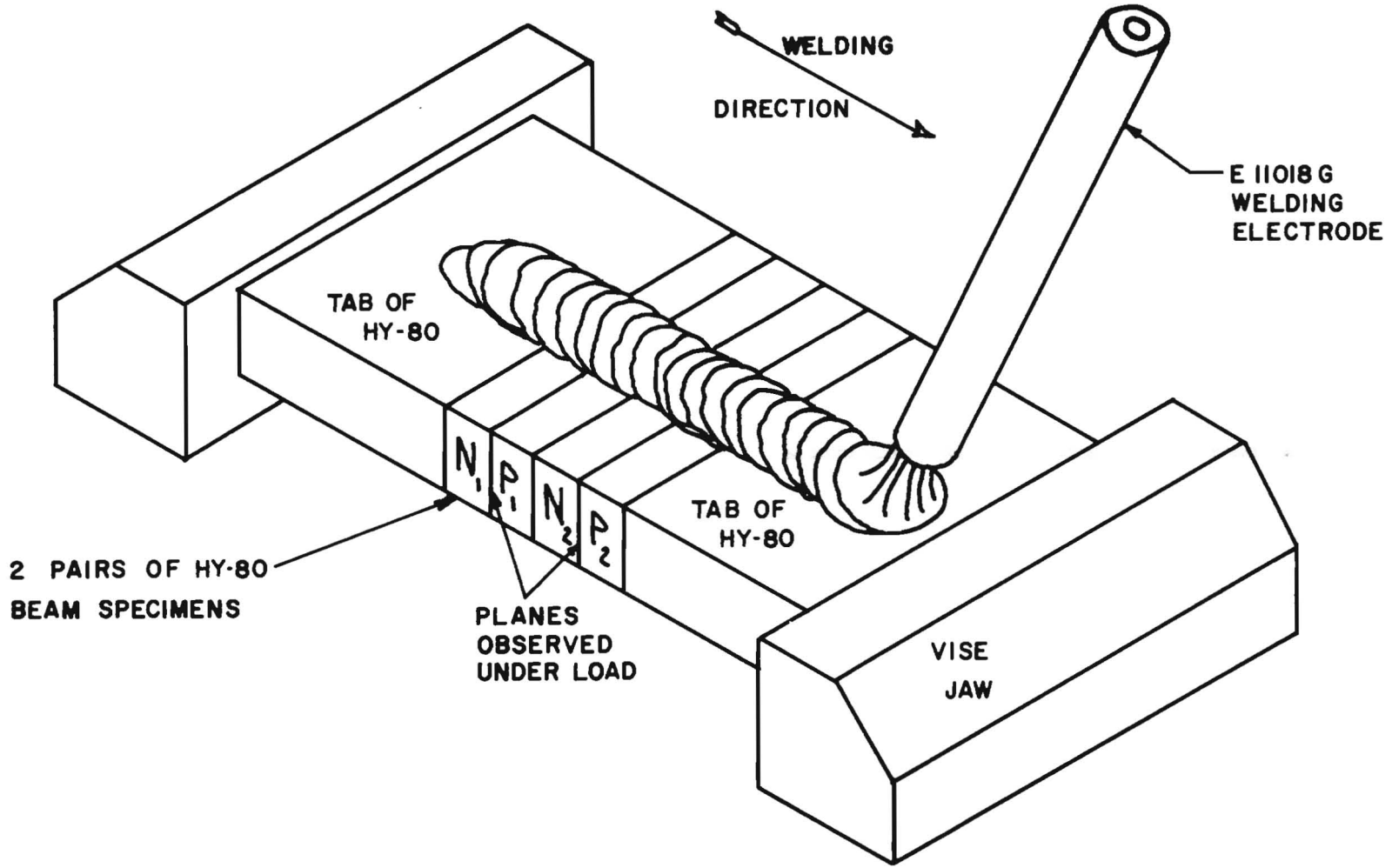

Figure 12 Schematic Illustration Showing the Welding of Cold-Cracking Test Specimens.

rapidly into a bath of dry ice and acetone (about -105 F). The specimens were stored in the dry-ice-acetone bath until they were to be tested. This quenching and holding procedure was used in order to minimize the loss of hydrogen from the specimens. A lower storage temperature, such as available with liquid nitrogen, was purposely avoided in order to minimize transformation of any retained austenite that possibly would be present in the heat-affected zone of the specimens. After quenching, the composite weldment was briefly removed from the bath in order to allow separation of the specimens and then all of the individual specimens were quickly returned to the bath.

The preparation of a specimen for testing consisted of removing it from the bath, allowing it to warm to room temperature, then quickly polishing and etching. In all cases, the surfaces prepared for examination were transverse to the weld and for a matched pair of specimens, the surfaces chosen were surfaces that had been adjacent to each other during welding (see Figure 12). This procedure for selecting the surfaces was used in order to insure that the instantaneous welding conditions would be identical when comparing specimens from a matched pair.

After polishing and etching, the specimen was then placed in a loading apparatus, detailed in Figure 13. This

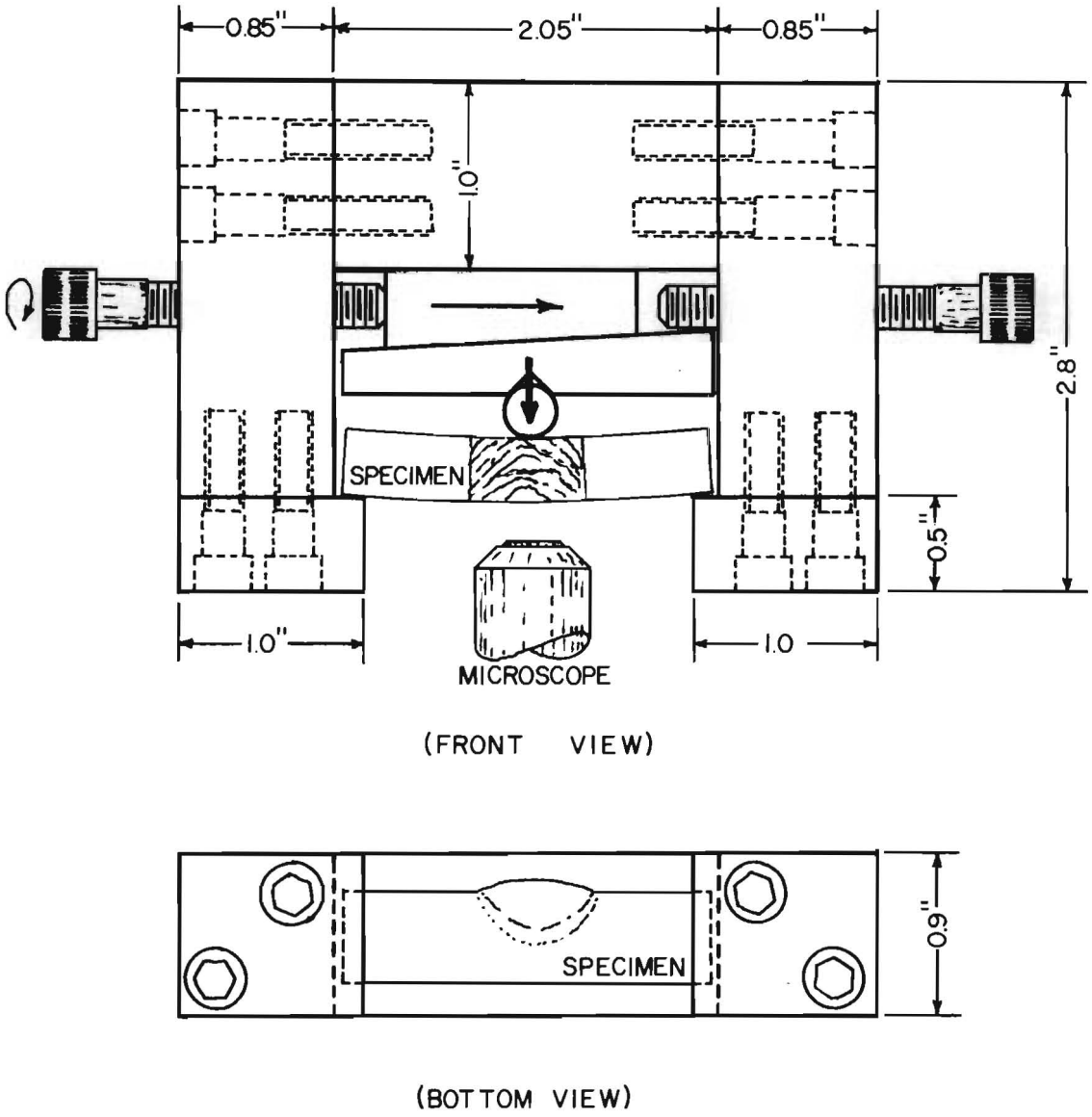

Figure 13 Detailed Drawing of the Loading Apparatus Used to Stress Specimens in the Cold-Cracking Test.

loading apparatus stressed the specimen as a simple beam with a concentrated load at the center. In order to be able to observe the evolution of hydrogen from the polished surface, a few drops of immersion oil was spread over the surface to be examined. The apparatus, with the specimen inserted, was then placed on the stage of a microscope, as shown in Figure 14. The specimen was observed under bright-field illumination, before and after stressing, to note any crack formation and/or bubble evolution. However, because of the design of the loading apparatus and the limitations on the movement of the stage of the microscope, observation of the specimen during testing could not be made above 250 magnification.

Examination of a Transverse Section From a Cruciform Test Specimen

The cruciform test is a frequently used method of evaluating base-plate weldability of HY-80 steel. The cruciform test has been described in the literature and will not be dealt with in depth here.[33,34] Figure 15 shows the details of a cruciform test specimen. Samples for metallographic examination of transverse sections are usually taken at the mid-length and at a one-quarter-length of the test specimen. In the cruciform test, general experience has shown that crack is found most frequently, and is developed to the greatest extent, under fillet weld C.[34] This has also been true with HY-80 steel.[22]

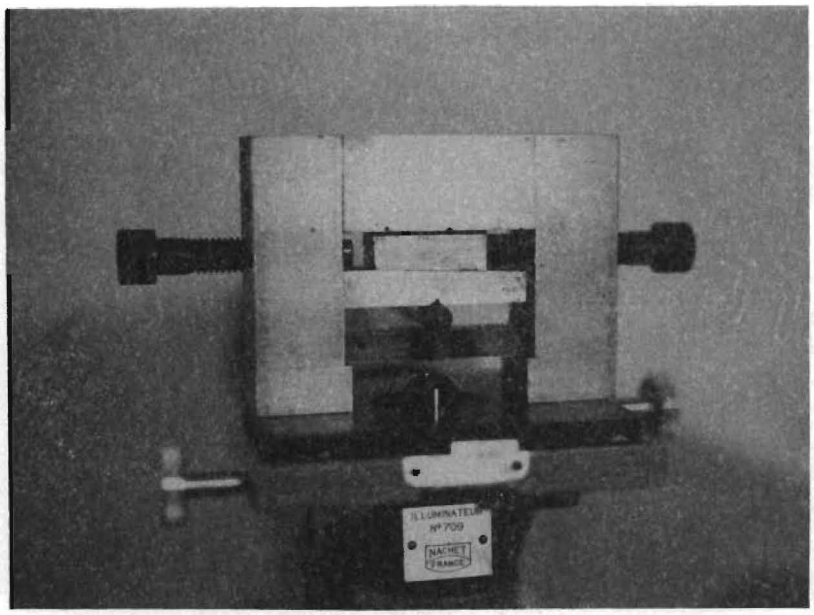

Figure 14 View of the Loading Apparatus, With a Cold-Cracking Test Specimen Inserted, Mounted on the Stage of the Microscope.

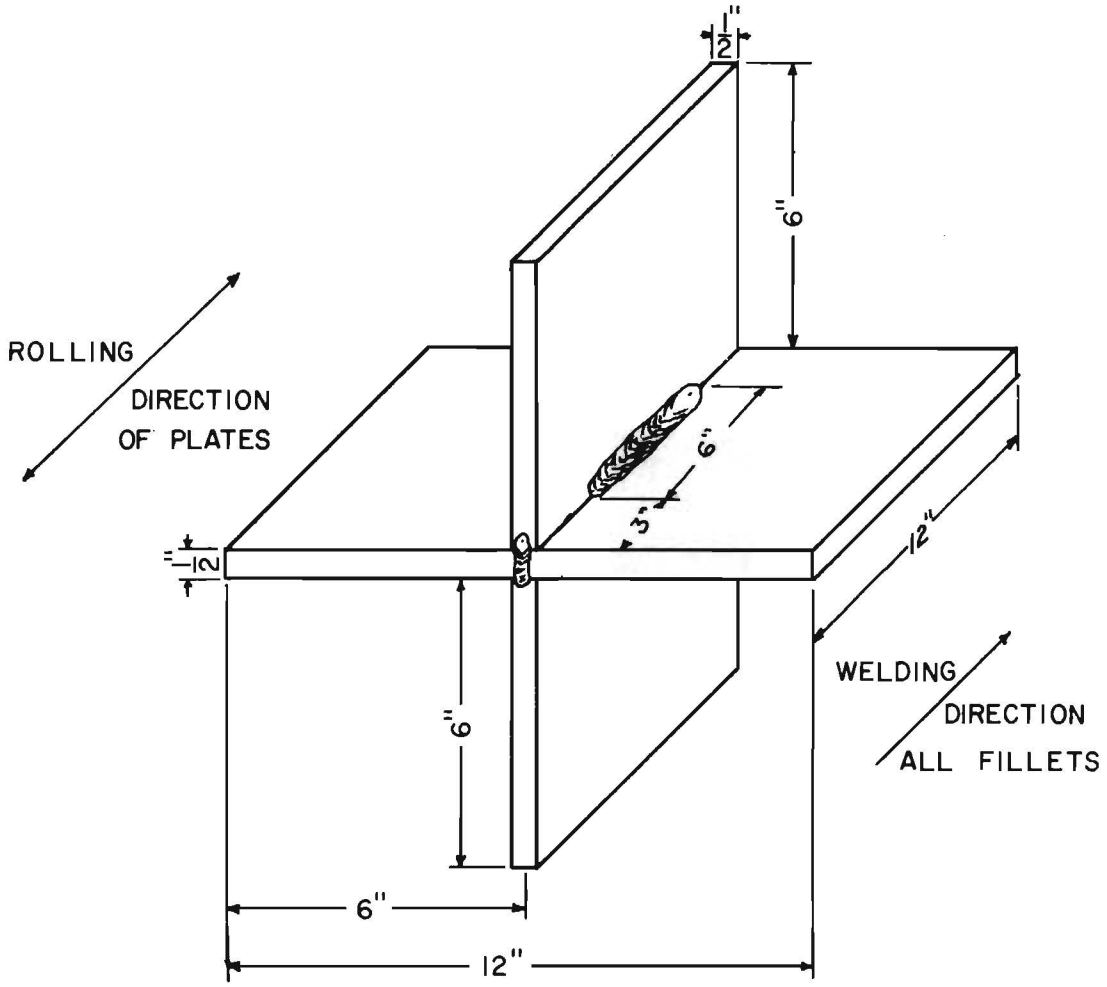

NOTE:

1. CONTACTING EDGES OF STEM PLATES ARE MACHINED STRAIGHT AND SQUARE
2. CONTACTING SURFACES OF THROUGH PLATE ARE MACHINED TO REMOVE MILL SCALE
3. ORDER OF WELDING: A, B, C, D.

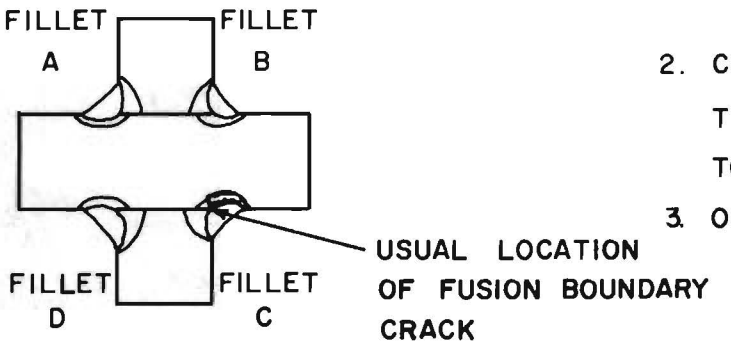

Figure 15 Details of the Cruciform Test Specimen Used to Evaluate the Weldability of Quenched-and-Tempered Low-Alloy Steel Plate.

In order to examine the nature of a typical crack in the cruciform test, a metallographic sample from a cruciform test specimen was requested from the U. S. Steel Applied Research Laboratory. Although no sample from a test specimen of either Heat N or Heat P was available, a sample from another heat of HY-80 steel was supplied. The composition of the heat was not available but the crack morphology was typical of that encountered in cruciform testing of HY-80 steels.

The sample, containing a crack under fillet weld C, was polished, etched using various etching procedures, and examined under standard bright-field illumination and oblique illumination.

RESULTS AND DISCUSSION

Metallographic Examination of the Base Metal

The metallographic examination of samples from the as-received plates of HY-80 steel yielded information concerning low-temperature transformation products, nonmetallic inclusions, and banding.

Transformation Products. The microstructures at the one-quarter-thickness of the as-received HY-80 steel plate, as revealed by a picral etchant at 100X, are shown in Figure 16. In both heats, the microstructure consisted entirely of low-temperature transformation products. No difference in the transformation products could be discerned between the two heats at this magnification.

Nonmetallic Inclusions. The nature of the nonmetallic inclusions, however, differed greatly between the two heats. Figure 17 shows a comparison of the inclusion content at 100X in the as-polished condition. Although both heats had elongated sulfide inclusions, Heat P, Figure 17A, had a greater amount of relatively large but thin elongated-type sulfide inclusions than Heat N. The sulfides in Heat N were generally smaller and more randomly distributed than those in Heat P. Figure 18 shows a comparison of the size of typical sulfides at 1000X. In turn, Heat N, Figure 17B, had a greater number of stringers (clouds)

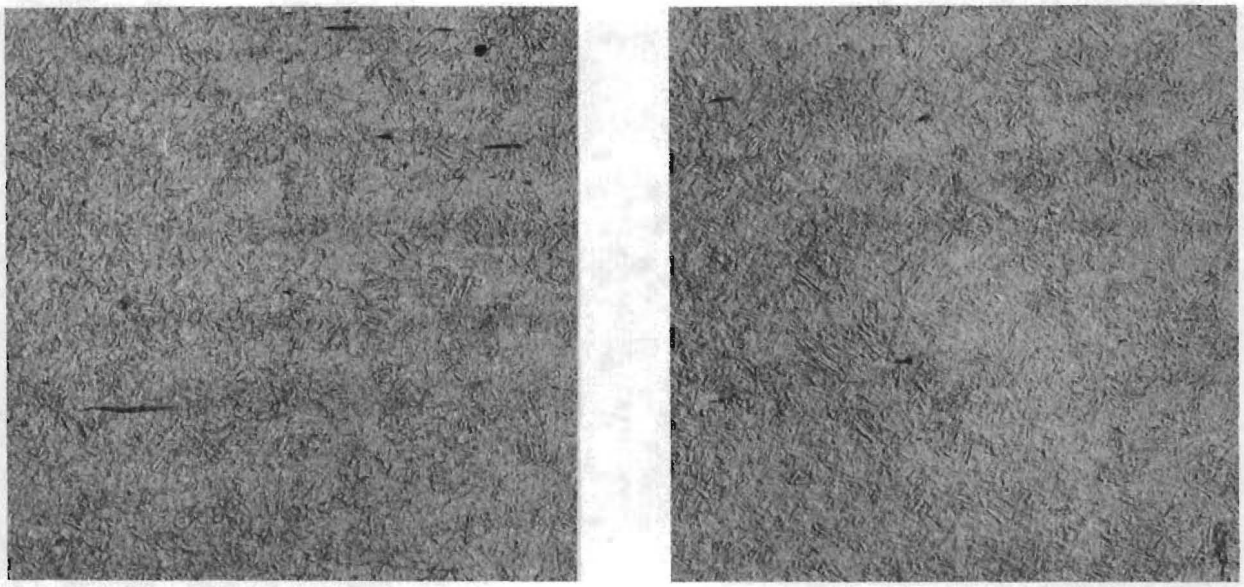

Longitudinal Transverse

A.

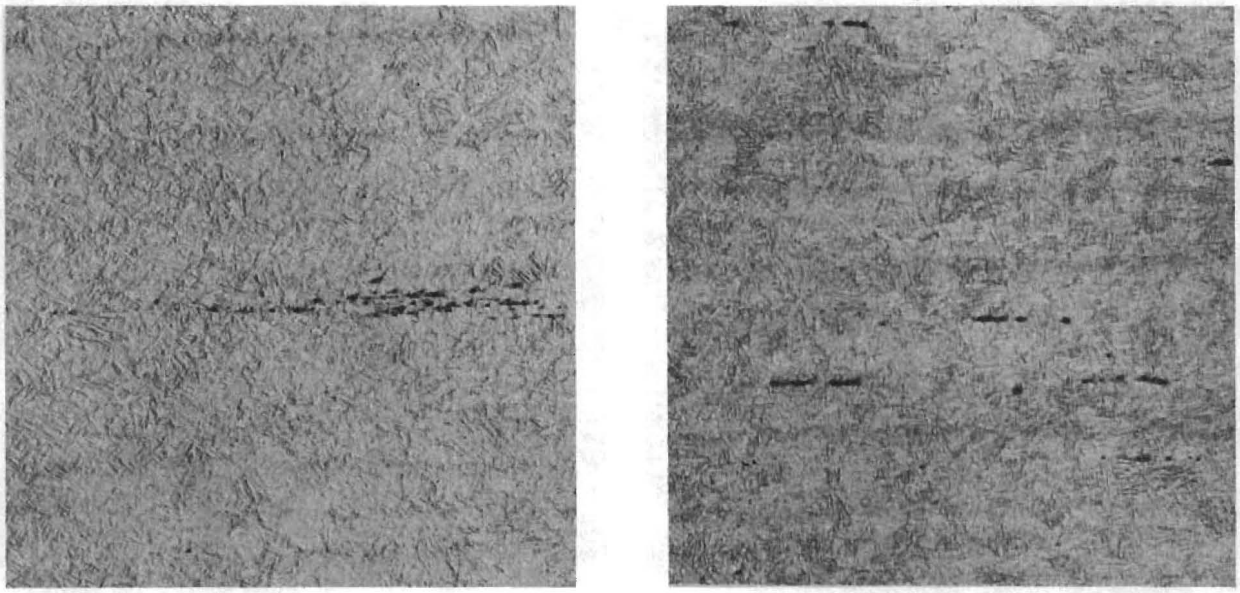

Longitudinal Transverse

B.

Figure 16 Microstructure of the As-Received HY-80 Steel Plates in Sections Longitudinal and Transverse to the Final Rolling Direction. Super-Picral Etchant, 100X. A. Heat No. 72P305. B. Heat No. N51755.

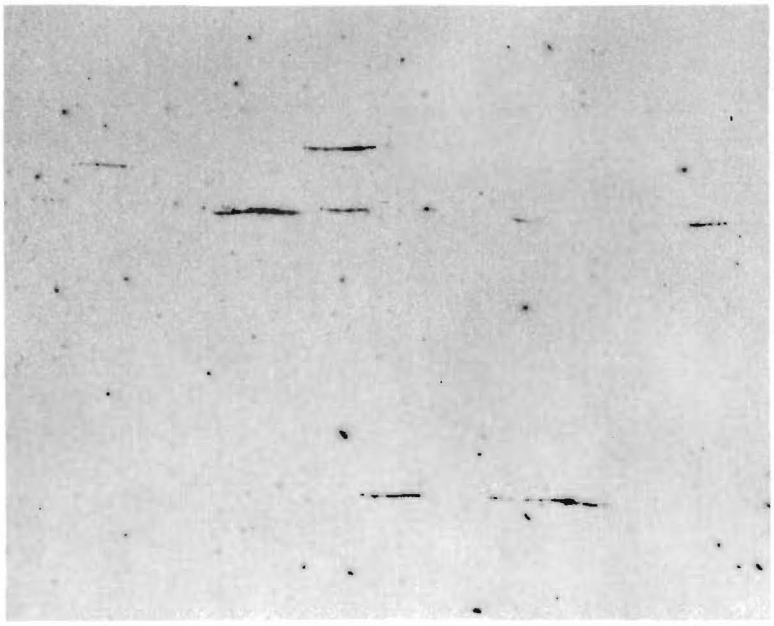

A.

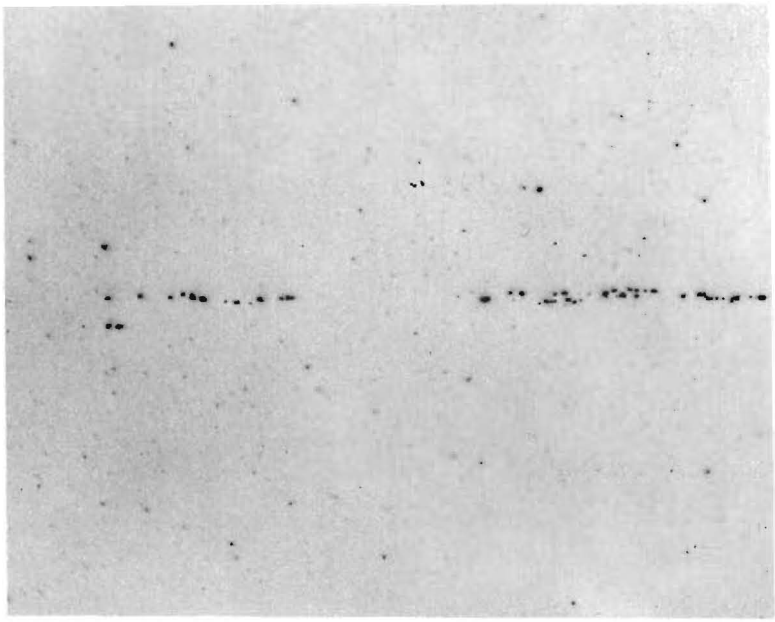

B.

Figure 17 The General Appearance of Nonmetallics in Sections of the HY-80 Steel Plates Longitudinal to the Final Rolling Direction. Polished and Unetched, 100X. A. Heat No. 72P305. B. Heat No. N51755.

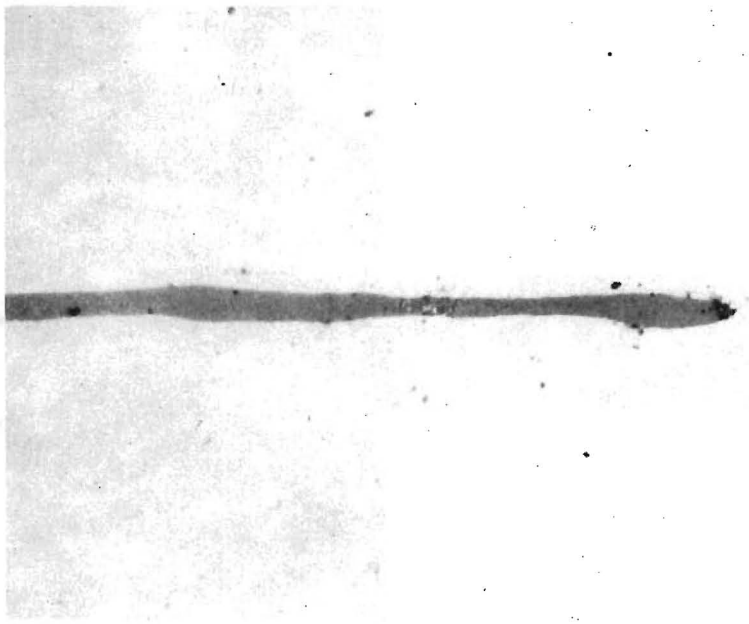

A.

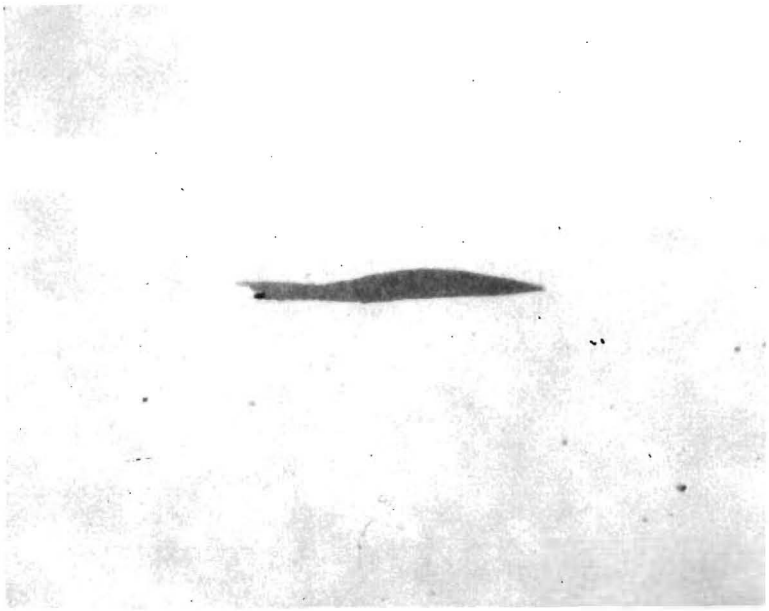

B.

Figure 18. Typical Sulfide Inclusions in Sections of the HY-80 Steel Plates Longitudinal to the Final Rolling Direction. Polished and Unetched, 1000X. A. The Edge of a Long Sulfide in Heat No. 72P305. B. A Relatively Long Sulfide in Heat No. N51755.

of oxide-like spherical inclusions. This observation is consistent with the inclusion analysis, see Table III, which indicates that Heat N had about double the oxide content of Heat P. Randomly dispersed between the large inclusions in both heats was a background of very fine spherical inclusions that were not identified.

In both heats, the largest sulfides occurred in the center-half of the plate thickness. This observation agrees with the observations of Salmon Cox and Charles[35] who reported that the size of the sulfides in an ingot of fully-killed tube steel increased on moving through the columnar and branched-columnar regions toward the center of the ingot. Even at the plate centers, however, the longest sulfide inclusions in Heat N were only as long as the medium-length sulfides in Heat P.

At 100 magnification, the volume fraction of sulfides in Heat N appeared to be less than that in Heat P since the oxide-like inclusions were, of course, not considered as sulfides. However, examination of the oxide-like spherical inclusions in Heat N at a high magnification revealed a great number of duplex oxide-sulfide inclusions, as shown in Figure 19. When the percentage of sulfides in the spherical inclusions was considered, it then appeared that the volume fraction of metal sulfides was approximately the same in both heats. Such a

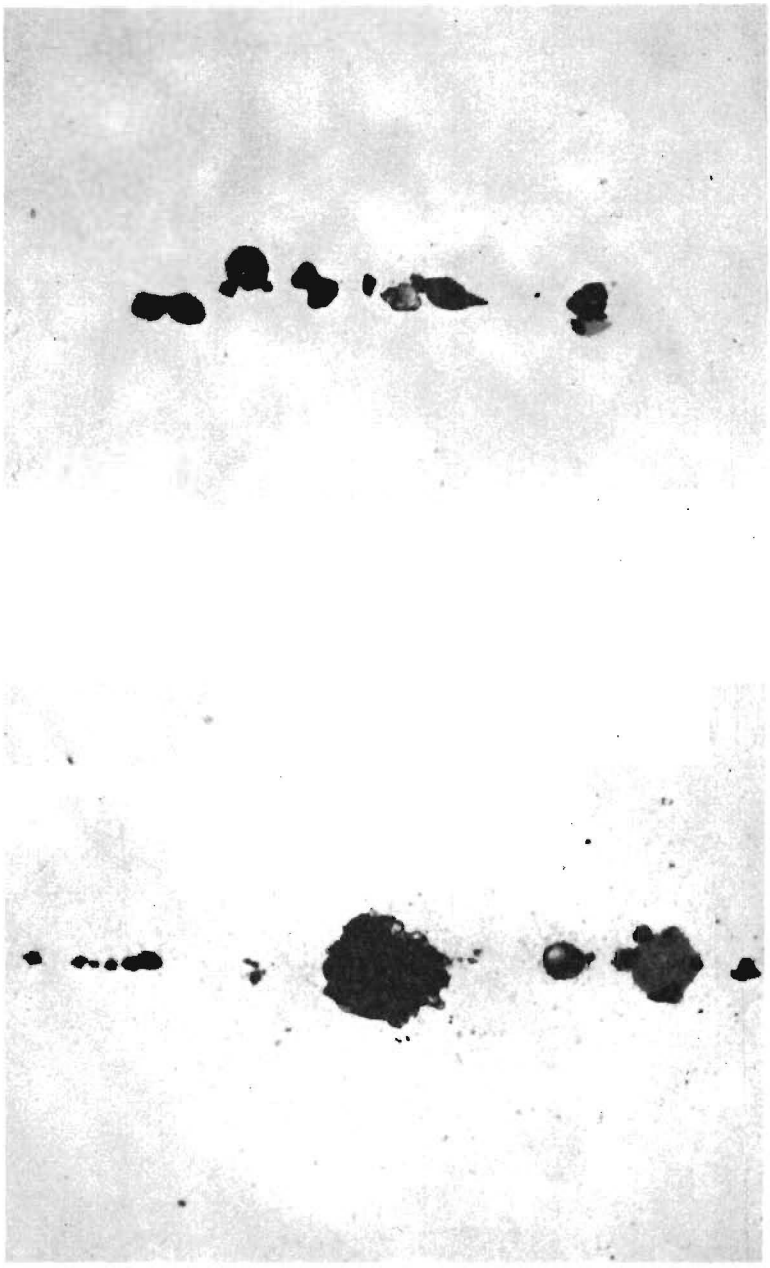

Figure 19 Typical Globular Inclusions in a Section of Heat No. N51755 Longitudinal to the Final Rolling Direction. Note the Many Duplex Oxide-Sulfide Inclusions. Polished and Unetched, 1000X.

similarity in the volume fraction of sulfides is not unexpected since the two heats of HY-80 steel did have similar sulfur contents, see Table III.

Aside from their greater size and length, the stringered sulfides in Heat P appeared to be somewhat thinner than the sulfides in Heat N. This may be a result of the plate from Heat P being rolled at a lower temperature than the plate from Heat N and/or a difference in the inclusion composition between the two heats. The rolling temperature affects the relative deformability of the matrix in comparison to the inclusion.[36] In other words, at a lower rolling temperature the matrix around the inclusion is less deformable and consequently the inclusion is forced to become thinner and more elongated. In addition, Van Vlack[37] *et al*. have proposed that the presence of a siliceous liquid at steel-rolling temperatures could provide a fluxing action that aids in the elongation of sulfide inclusions.

However, the most significant difference in the nature of the sulfide inclusions between Heat N and Heat P was related to the size and distribution of the sulfides. There are at least two factors which influence the size and distribution of sulfide inclusions:

1. the degree of deoxidation of the ingot
2. the solidification conditions of the original ingot, particularly the freezing rate.

The degree of deoxidation may well determine the location at which sulfides precipitate during solidification of the ingot. In HY-80 steel ingots there may be two distinct locations where sulfides can precipitate during the solidification, they are:

1. between dendrite arms and between parallel dendrite stalks or subgrains (intra-dendritic)
2. between colonies of parallel dendrite stalks (intergranular).

Intra-dendritic precipitation would result in smaller and more-uniformly distributed sulfides, whereas the sulfides formed by intergranular precipitation would be larger and their distribution more non-uniform.

During the solidification of the ingot, the sulfides precipitate as liquid globules. However, both oxygen and carbon greatly increase the activity coefficient of sulfur in iron.[38] Therefore, a high oxygen and/or carbon content in a heat could cause the solubility of the sulfides to be low. A low solubility, in turn, would cause the sulfides to precipitate relatively early in the ingot-freezing process, thereby allowing them to achieve large sizes.[39,40,41] On the other hand, a low oxygen and/or carbon content could cause the sulfides to precipitate late in the freezing process, thereby preventing them from achieving large sizes. Yeo[36] has

discussed in more detail how a high oxygen content during solidification of resulfurized steels results in relatively large sulfides. However, comparisons between low-alloy steels and resulfurized steels must be made carefully.

Nevertheless, it could be argued that the difference in the carbon content and deoxidation of the two heats of HY-80 steel used in this investigation accounts for the difference in size and distribution of sulfide inclusions. When the fact that the total oxygen content was approximately the same for both heats is compared with the fact that Heat N has more than twice the aluminum oxide content of Heat P, it can be concluded that during solidification the oxygen dissolved in the molten Heat N ingot was probably low compared to that of Heat P. With respect to carbon, note that Heat P had 5 points more carbon than Heat N (See Table III). Therefore, the lower carbon content and the lower dissolved oxygen content in Heat N would have probably caused the sulfides in Heat N to remain in solution until a relatively late stage in solidification, resulting in primarily inter-arm sulfides. Under such conditions, when the sulfides finally came out of solution in Heat N, they probably nucleated preferentially on available oxides that were also trapped between the dendrite arms thereby producing duplex inclusion and preventing agglomeration of the sulfides.

On the other hand, in an ingot of Heat P, the solubility of the sulfides during solidification may have been lower because of the higher carbon content and higher oxygen content (due to less deoxidizer). Therefore, the sulfides in Heat P could have precipitated earlier during solidification, probably within the still-open channels between the dendrite tips, consequently becoming primarily intergranular sulfides. Also, if they had precipitated early, the globules in Heat P would have had a greater opportunity to coalesce and thus achieve relatively large diameters.

The difference in the size and distribution of the sulfides between Heat N and Heat P could have also been due to a difference in the rate of freezing of the ingots because of a difference in ingot-size. In the production of steels like HY-80 steel, usually ingots from electric furnace heats (e.g. Heat N) are smaller than ingots from open hearth heats (e.g. Heat P). Therefore, it is highly probable that the freezing rate of the ingot from Heat N was faster than the freezing rate in the ingot from Heat P. In general, a faster freezing rate causes the spacing between dendrite arms to be smaller which, in turn, would mean that any sulfides precipitating between the dendrite arms would be smaller and more randomly distributed.

Banding. Metallographic examination revealed that the two heats of HY-80 steel were about equally banded, as may be seen by comparing Figures 20A and 20B. The banding shown in Figure 20 appears very marked because the base metal samples were etched with a two-stage nital and sodium bisulfite procedure (to be discussed in the following subsection). The light-etching bands, in Figure 20, are higher in alloy content than the dark-etching bands and thus correspond to the regions last to freeze between the dendritic arms in the original ingot. During subsequent hot-rolling, these segregated regions are converted to bands which, contrary to frequent postulations, are not readily eliminated by normal homogenizing treatments. With regard to the bands, it should be emphasized that the sulfide inclusions were usually observed to be located in light-etching alloy-rich bands.

Metallographic Studies of the Fusion Boundary

Present American Welding Society (AWS) terminology[5] defines two distinct regions in a fusion weld as follows:

1. weld metal - that portion of a weld which has been melted during welding
2. heat-affected zone - that portion of the base metal which has not been melted, but whose mechanical properties or microstructures have been altered by the heat of welding or cutting.

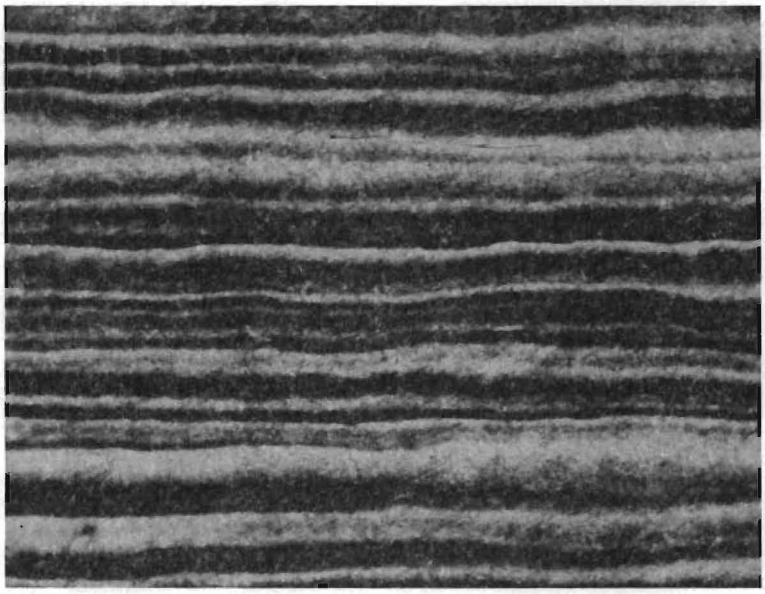

A.

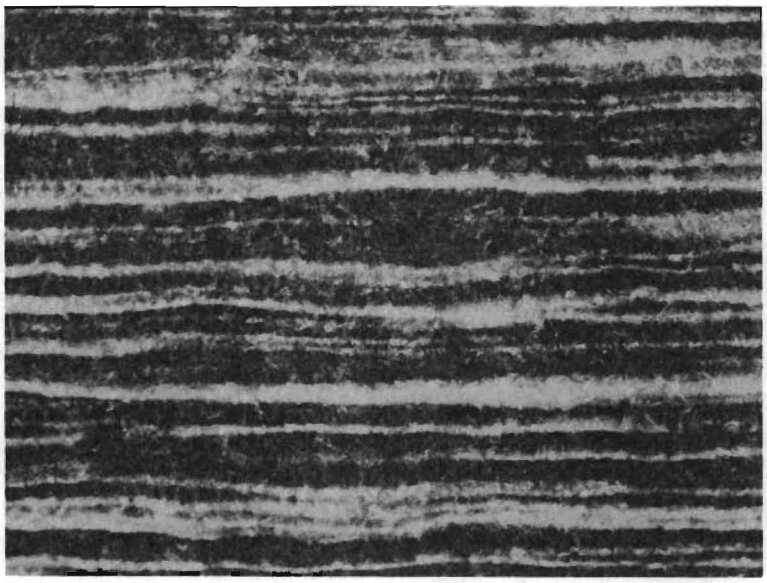

B.

Figure 20 The Appearance of Banding in Sections of the HY-80 Steel Plates Longitudinal to the Final Rolling Direction. Nital and Sodium Bisulfite Etchant, 100X. A. Heat No. 72P305. B. Heat No. N51755.

However, when subjected to very careful metallographic examination, the structure in the vicinity of the fusion boundary* appears to be more complex than these simple definitions suggest. Consequently, the first major phase of this investigation was a thorough metallographic examination of the fusion boundary of welds in HY-80 steel.

Evaluation of Etching Procedures. The results of the evaluation of the etching procedures indicated that a two-stage nital and sodium bisulfite etching procedure, Procedure A in Table VI, is remarkably effective in revealing information about the fusion boundary of bead welds on HY-80 steel. This procedure is a modification of a three-stage picral, nital and sodium bisulfite procedure first suggested by the David Taylor Model Basin[42] for use on HY-80 steel and later modified by the Air Reduction Company.[43] The success of the two-stage procedure is primarily due to the sodium bisulfite which selectively stains the regions of high iron content (the nital only improves the contrast obtained with the sodium bisulfite). In other words, alloy-rich regions such as cell boundaries in the weld metal and bands in the base metal are not readily stained by the sodium bisulfite. This selective staining feature is important in understanding photomicrographs of structures

* The term fusion boundary will be used to describe the general vicinity of the junction between the weld metal and the base metal, pending the introduction of more exact terminology.

Table VI

Etching Procedures Used to Reveal the Weld-Metal Base-Metal Junction in Bead Welds in HY-80 Steel

Procedure	Etchant	Etching Technique	Remarks
A	1% Nital	Dip-etch for 2 - 8 sec. and rinse with ethanol only.	For best results, the nital etch should be very light.
	3% Aqueous Sodium Bisulfite with Aerosol OT wetting agent.	Swab with sodium bisulfite @ 100 F until weld metal turns dark, then quickly rinse with water. Final rinse with ethanol.	See Note 1, below.
B	2% Nital	Swab-etch for 2 - 10 sec. and rinse with water. Final rinse with ethanol.	This etchant is commonly used to reveal transformation products but a very light etch and oblique lighting can reveal solidification substructure.
C	5% Ammonium Persulfate	Swab-etch for 1 - 4 sec. and rinse with water. Final rinse with ethanol.	Same as for Procedure B.

Note 1: The results produced by the sodium bisulfite step were greatly dependent upon (1) the care used in the final polishing of the specimen, (2) the degree of etching by the nital in the first step, (3) the age of the sodium bisulfite etchant, and (4) the amount of Aerosol OT in the solution. Further work will be required to standardize this procedure.

revealed by the two-stage procedure and will be referred to several times below.

The significance of the nital and sodium bisulfite procedure is apparent in Figure 21. This figure shows the striking difference between the appearance of a location along the fusion boundary, as revealed by the two-stage procedure, see Figure 21A, and the identical location, as revealed by a conventional nital procedure, see Figure 21B (a microhardness indentation was used as a marker to locate the same area after repolishing and etching). It should be noted that the conventional nital procedure, Procedure B in Table IV, primarily reveals transformation products, whereas the nital and sodium bisulfite procedure reveals a distinct light-etching zone which exhibits a solidification substructure. The substructure in the light-etching zone is cellular and appears as a pattern of white and gray stripes. The white stripes represent the unstained cell boundaries which are solute-rich. The gray stripes represent the lightly-stained cores of the cells which are solute-lean, i.e., iron-rich.

Furthermore, it should be noted that the light-etching zone is below the apparent location of the "fusion line" revealed by the nital etchant, as shown in Figure 21B. In fact, the nearly-horizontal demarcation between the dark-etching weld metal at the top in Figure 21A and the light-etching zone at

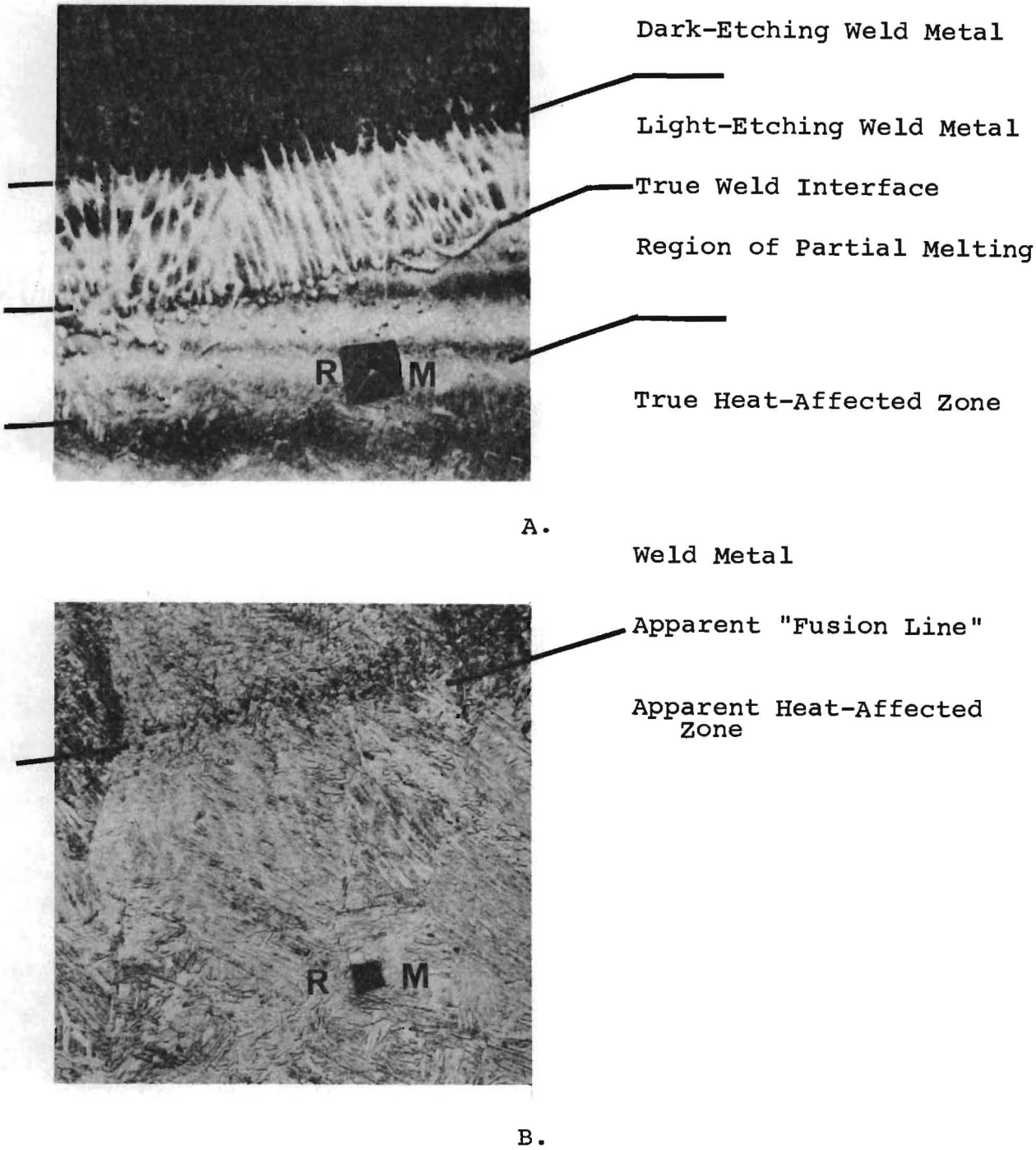

Figure 21 Comparison of Two Etching Procedures Used to Reveal the Fusion Boundary on a Transverse Section of a Shielded Metal-Arc Bead-Weld in HY-80 Steel, 250X. A. Location at a Reference Mark Etched With the Two-Stage Nital and Sodium Bisulfite Procedure. B. The Identical Location Repolished and Etched With Nital Only.

the center corresponds roughly to the "apparent fusion line" as revealed by the nital etchant. For the bead welds, the thickness of the light-etching zone exhibiting a solidification substructure when etched by the two-stage procedure usually varied from zero at the toe of the weld to several mils at the root of the weld. Note that for the location shown in Figure 21, the true fusion boundary, revealed by the two-stage procedure, is nearly three mils beyond the apparent boundary identified with the conventional nital etchant.

Another important feature which is revealed by the two-stage procedure and not by the nital procedure should be noted in Figure 21A. Localized melting in the heat-affected zone adjacent to the true fusion line can be seen in the form of a network of broad, light-etching grain boundaries and numerous isolated light-etching dots. This type of partial melting has been reported in other alloys[3,4] and the two-stage etching procedure reveals that a similar region of partial melting occurs in welds in HY-80 steel. The mechanisms responsible for, and the significance of, such localized melting will be discussed in more detail in subsections below.

Some degree of success in revealing substructure beyond the normally-apparent fusion line was also achieved with an ammonium persulfate etching procedure, Procedure C in Table IV, as may be seen by inspection of Figure 22 which shows

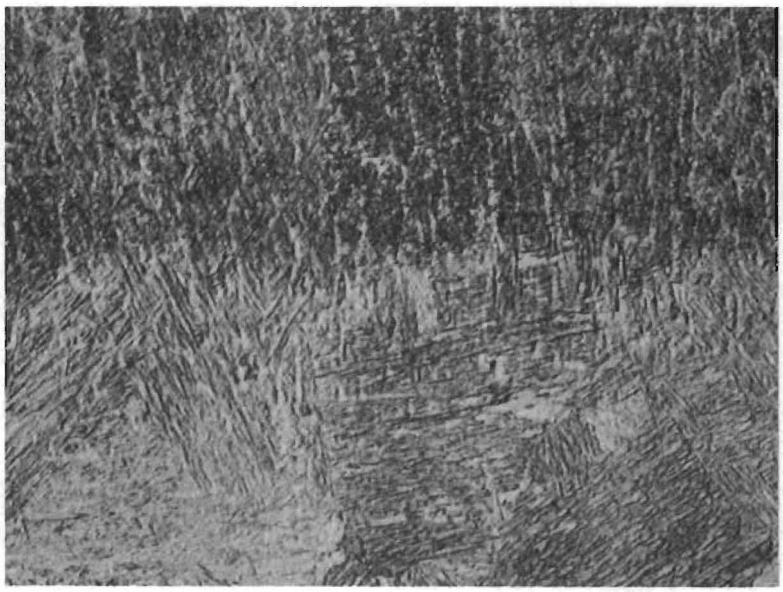

A.

B.

Figure 22 Comparison of Two Etching Procedures Used to Reveal the Fusion Boundary on a Transverse Section of a Shielded Metal-Arc Bead-Weld in HY-80 Steel, 250X. A. A Location Etched With Nital. B. The Identical Location Repolished and Etched With Ammonium Persulfate.

a comparison of the results obtained with ammonium persulfate and those obtained with nital. The section shown in Figure 22A was etched with 2 percent nital and the demarcation between the darker-etching region at the top and the lighter-etching region below is obvious. By comparison, the same section is shown in Figure 22B after repolishing and lightly etching with ammonium persulfate. Note that in Figure 22B, evidence of the solidification substructure extends below the apparent fusion boundary revealed by the nital procedure. The ammonium persulfate etchant, however, requires the use of oblique lighting to accent subgrain boundaries which are less rapidly attacked by the etchant than is the intervening cell matrix. The use of Nomarski Interference Contrast, as provided by the Nachet TM 74 microscope,[29] was extremely helpful in high-lighting the weld metal substructure revealed by ammonium persulfate, as shown in Figure 23.

Recognition of an Unmixed Zone. The cellular solidification substructure in the zone beyond the normally-apparent fusion line, as shown in Figures 21, 22, and 23, is evidence that this zone was completely molten during the passage of the weld pool. Thus, this zone should be considered as actually part of the weld metal.

An explanation of the origin of this zone of weld metal is afforded by Figure 24. In this figure, it can be seen

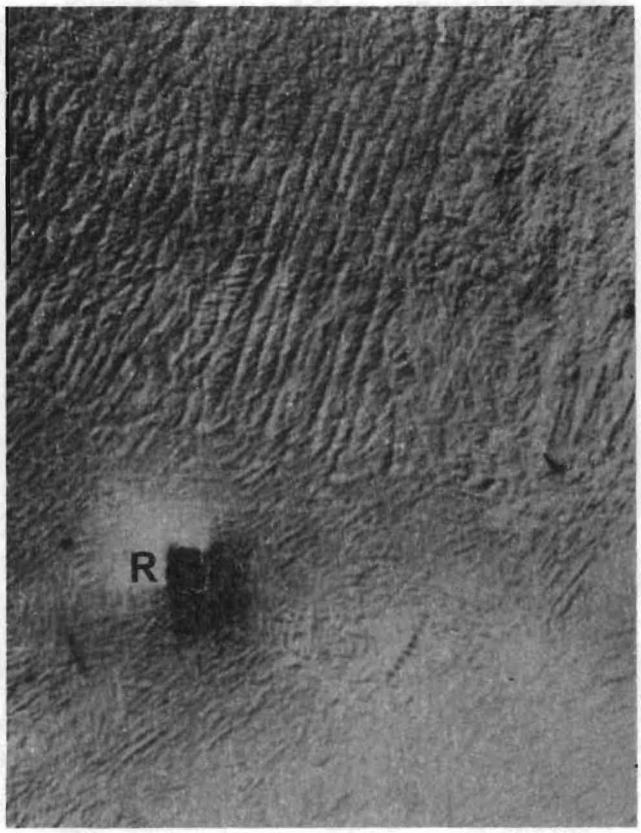

Figure 23 Substructure at the Weld Interface as Highlighted by Nomarski Interference Contrast.[29] The Location is Identical to that Shown in Figure 21 Except the Image is Inverted. Ammonium Persulfate Etchant, 250X.

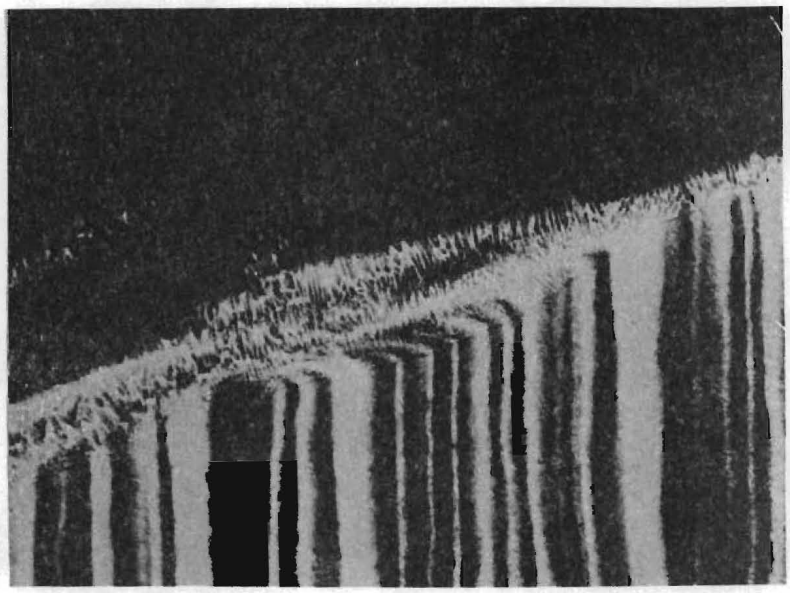

Figure 24 A Transverse Section of a Shielded Metal-Arc Bead Weld Showing Evidence of Laminar Flow Within an Unmixed Zone of Molten Weld Metal. Note the Sharp Angle Between the Bands in the Base Metal and Those in the Unmixed Zone. Nital and Sodium Bisulfite Procedure, 100X.

that the bands in the base metal, as revealed by the two-stage procedure, provided excellent "markers" by which the liquid motion at the fusion boundary could be ascertained. The motion at this location was obviously laminar while at other locations, outside the field shown in Figure 24, the bands in the light-etching weld metal were not as severely distorted, indicating the presence of a more nearly stagnant liquid zone. The very fact that the bands of the base metal remain clearly apparent in the weld metal that was completely melted shows that a zone of fused but essentially unmixed base metal can exist at the fusion boundary in heterogeneous welds. Such an "unmixed zone" would be the result of a lack of turbulent fluid motion at the boundary of the weld puddle. Even with considerably hydrodynamic motion in a weld pool, the velocity of liquid motion must approach zero at the solid-liquid interface.[8,44] Therefore, irrespective of the degree of turbulence in the bulk of the weld pool, there exists either a stagnant layer or a laminar-flow layer immediately adjacent to the solid base metal.

Summarizing the above results, it can be stated that in metallographic sections of heterogeneous welds prepared by conventional means, the unmixed zone can remain undistinguishable and would be mistakenly identified as part of the heat-affected zone. This results from the fact that there is usually a marked difference in the etching characteristics between the

mixed weld metal and its surroundings. On the other hand, the melted and solidified base metal in the unmixed zone is nominally the same in composition as the adjacent heat-affected zone and the only difference in the as-etched appearance between the two is due to the solidification substructure of the unmixed zone. If the etching procedure is simply intended either to contrast the weld metal or to reveal only transformation products, the substructure in the unmixed zone can easily be masked. This is the case with the conventional etchants on HY-80 steel; so it is not surprising that the existence of the unmixed zone has not been reported previously. Further evidence of the presence of an unmixed zone at the fusion boundary was obtained from electron beam microanalysis.

Electron Beam Microanalysis of the Fusion Boundary. The paths of the electron beam traverses on the specimen from Heat P and the specimen from Heat N are illustrated in Figures 25 and 26, respectively. Note that all of the scans traversed dark-etching weld metal, light-etching weld metal, and unmelted base metal.

The concentration profiles for manganese and chromium across the fusion boundary obtained by scan AA' and BB' on the specimen from Heat P are shown in Figures 27 and 28, respectively. The profiles obtained during scans CC', DD', and EE' in the specimen from Heat N are shown in Figures 29, 30, and 31,

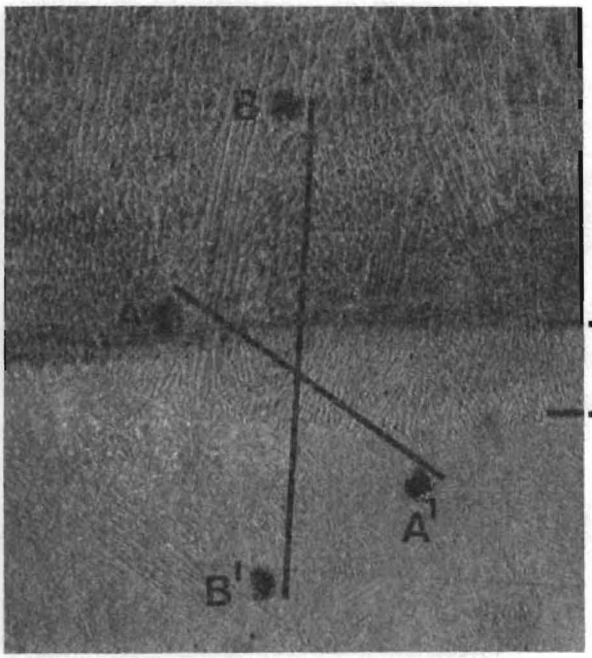

Figure 25 Traverses AA' and BB' of the Electron Beam Microanalyser Across the Fusion Boundary of a Bead Weld in a Specimen From Heat No. 72P305. Ammonium Persulfate Etchant, 100X.

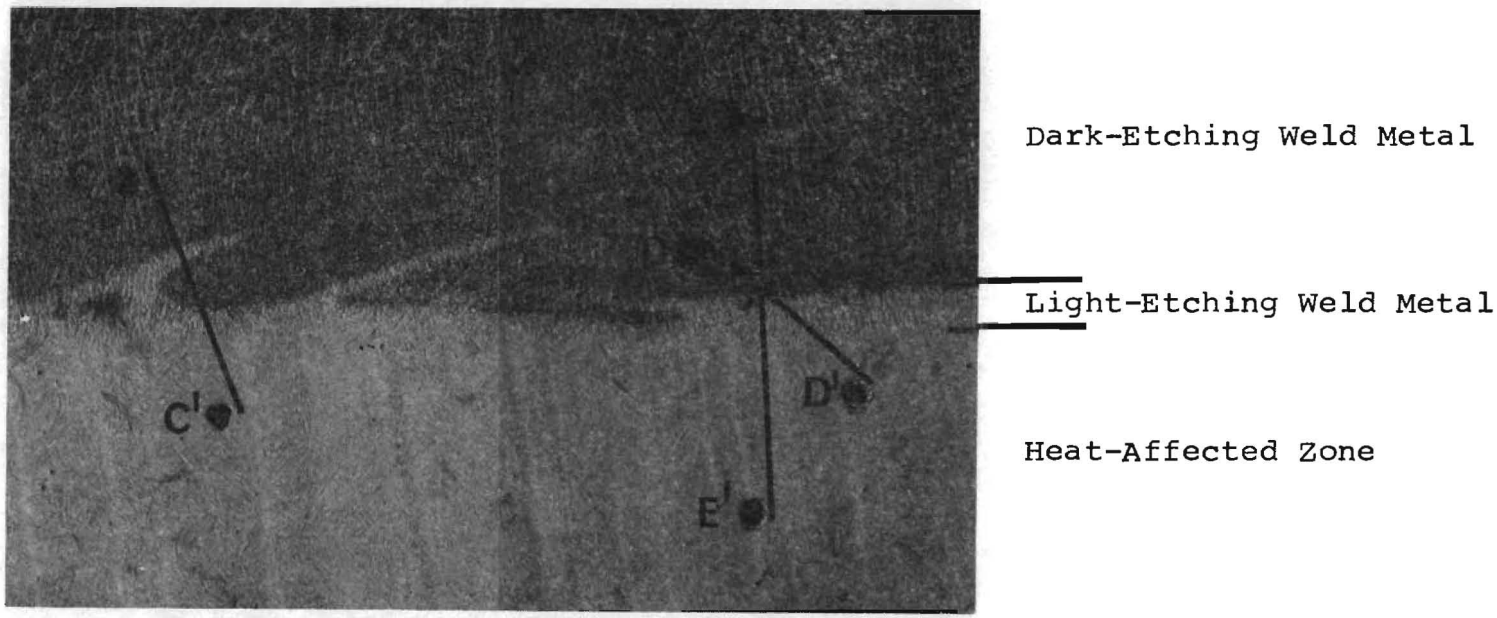

Figure 26 Traverses CC', DD', and EE' of the Electron Beam Microanalyser Across the Fusion Boundary of a Bead Weld in Heat No. N51755. Ammonium Persulfate Etchant, 100X.

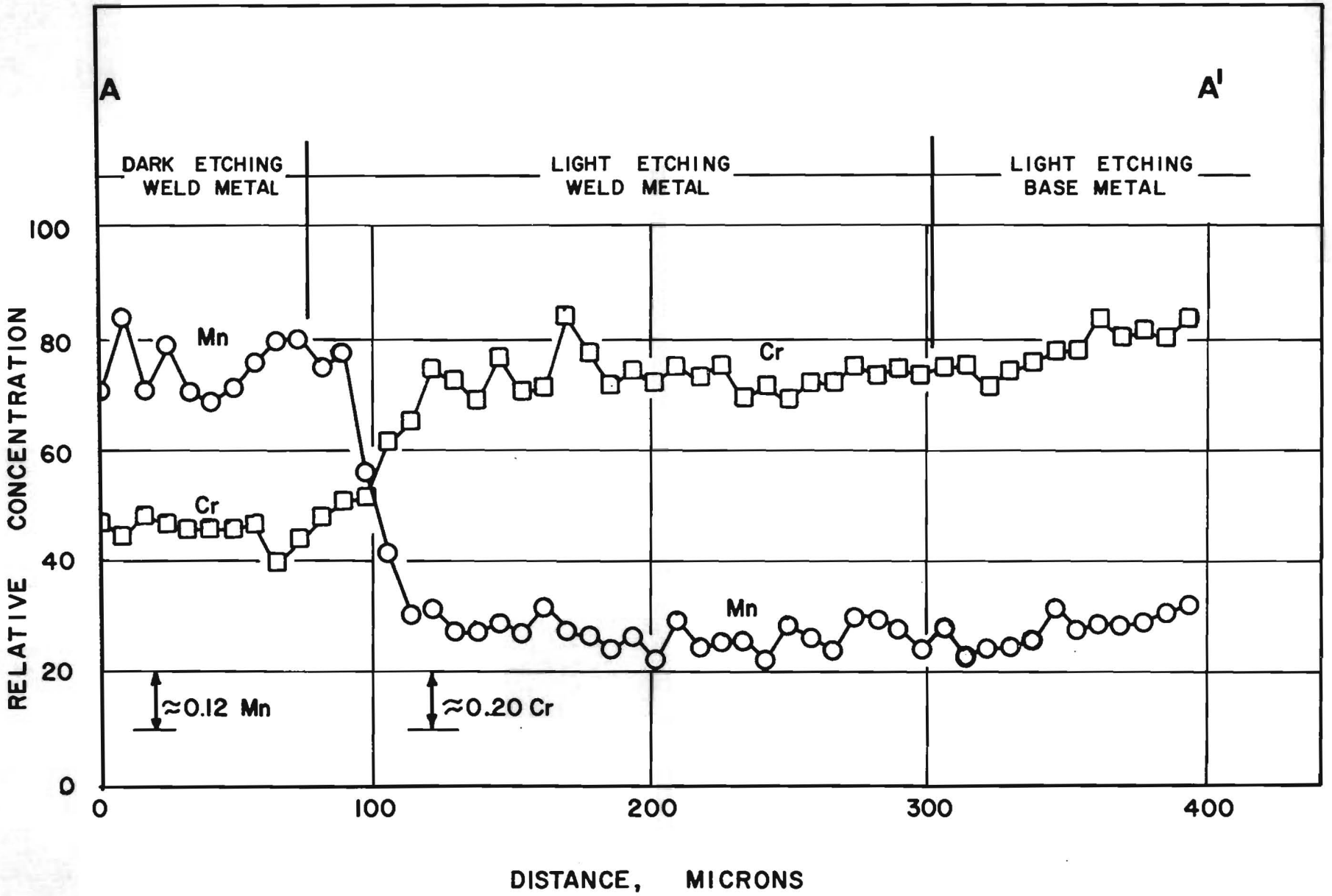

Figure 27 The Concentration Profiles for Manganese and Chromium Obtained by Traverse AA' Across the Fusion Boundary of a Bead Weld in Heat No. 72P305.

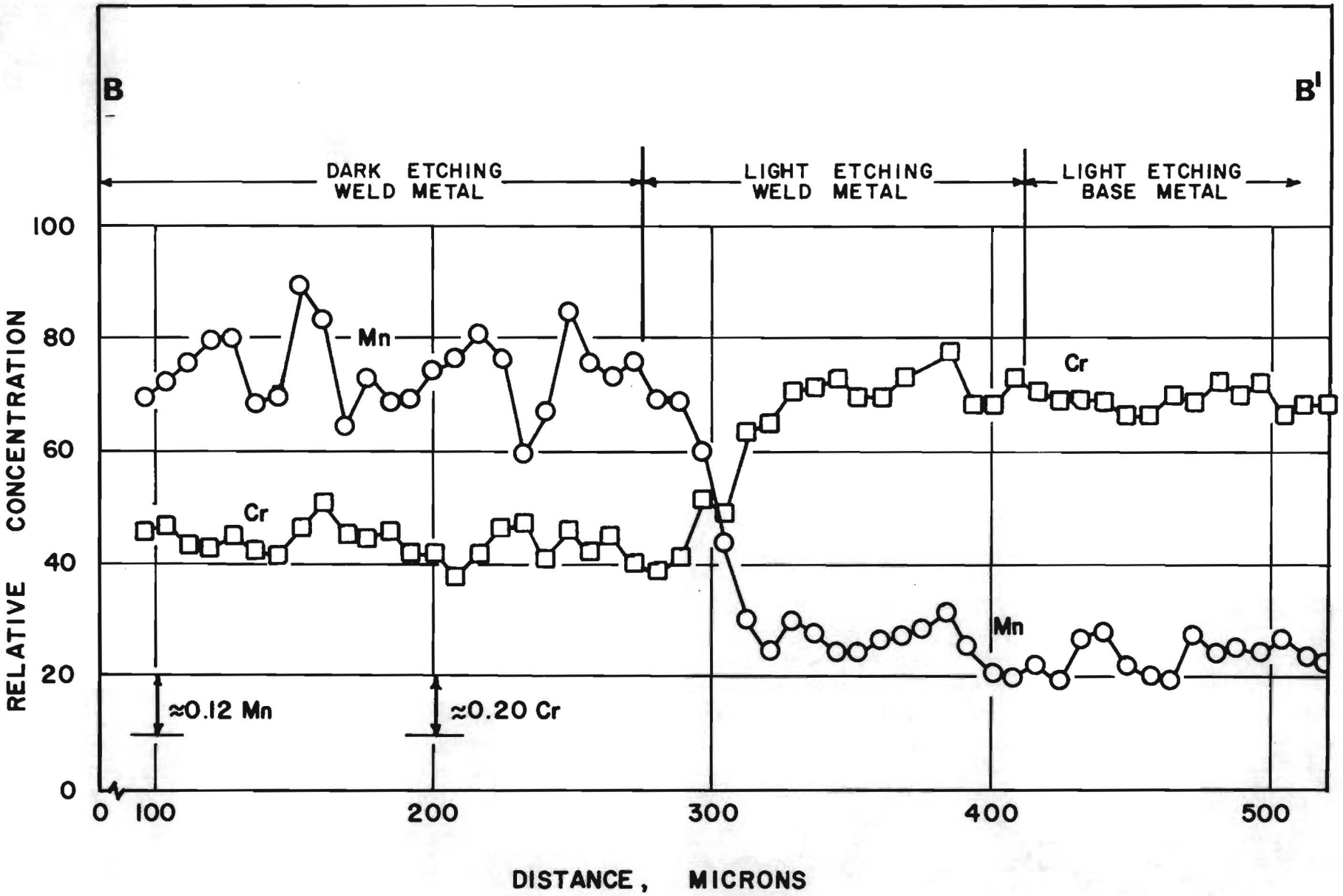

Figure 28 The Concentration Profiles for Manganese and Chromium Obtained by Traverse BB' Across the Fusion Boundary of a Bead Weld in Heat No. 72P305.

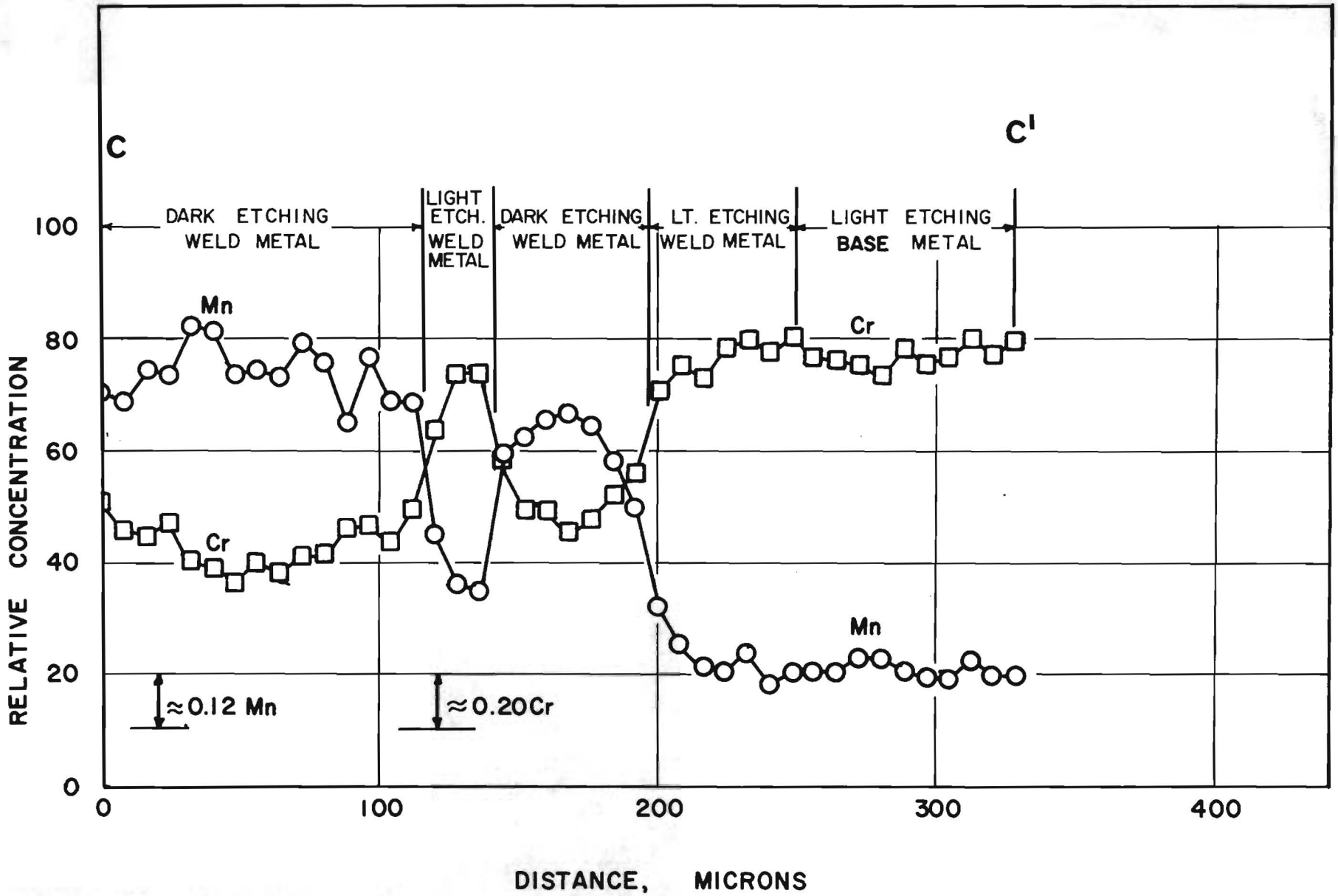

Figure 29 The Concentration Profiles for Manganese and Chromium Obtained by Traverse CC' Across a Fold in the Weld Metal and Across the Fusion Boundary of a Bead Weld in Heat No. N51755.

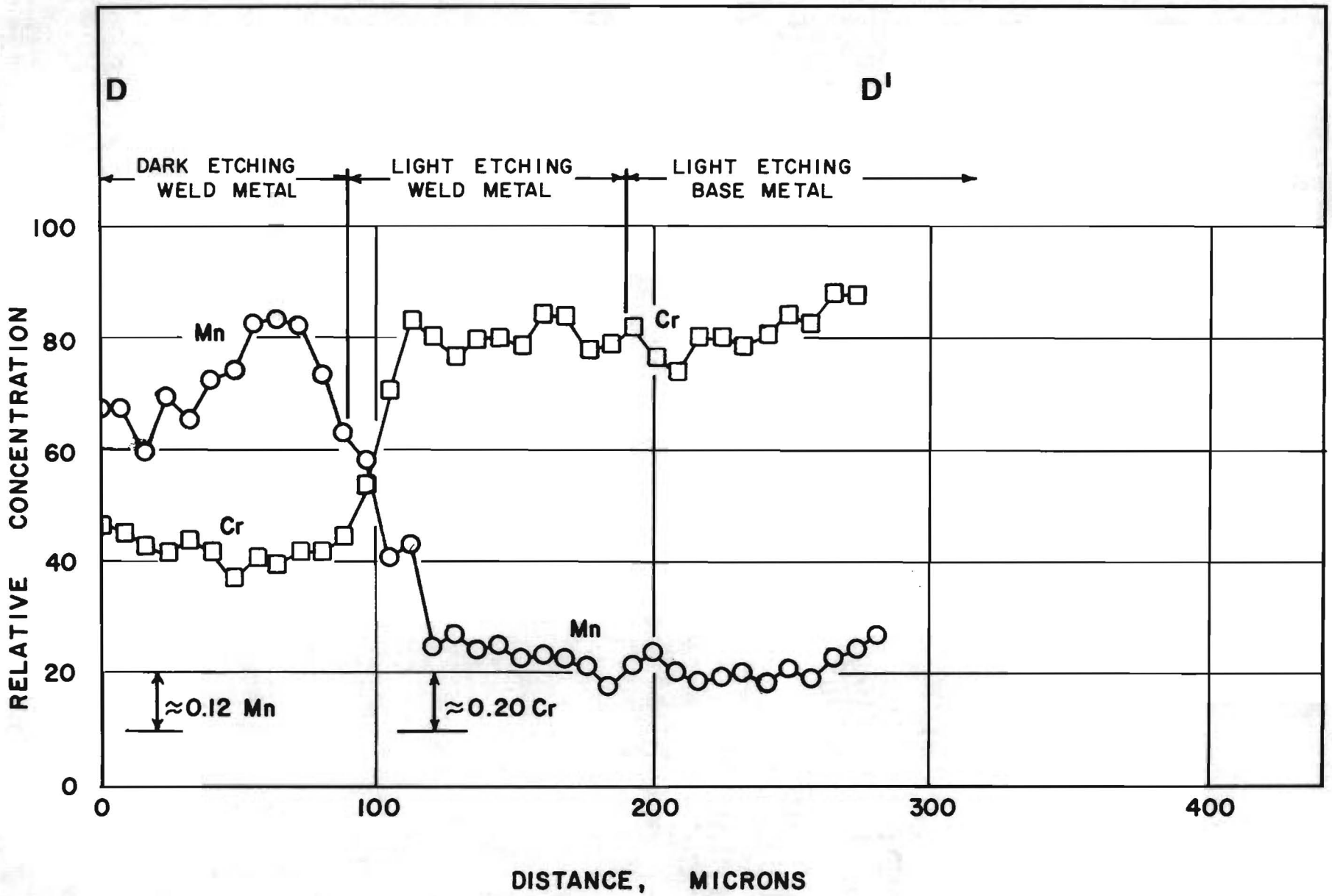

Figure 30 The Concentration Profiles for Manganese and Chromium Obtained by Traverse DD' Across the Fusion Boundary of a Bead Weld in Heat No. N51755.

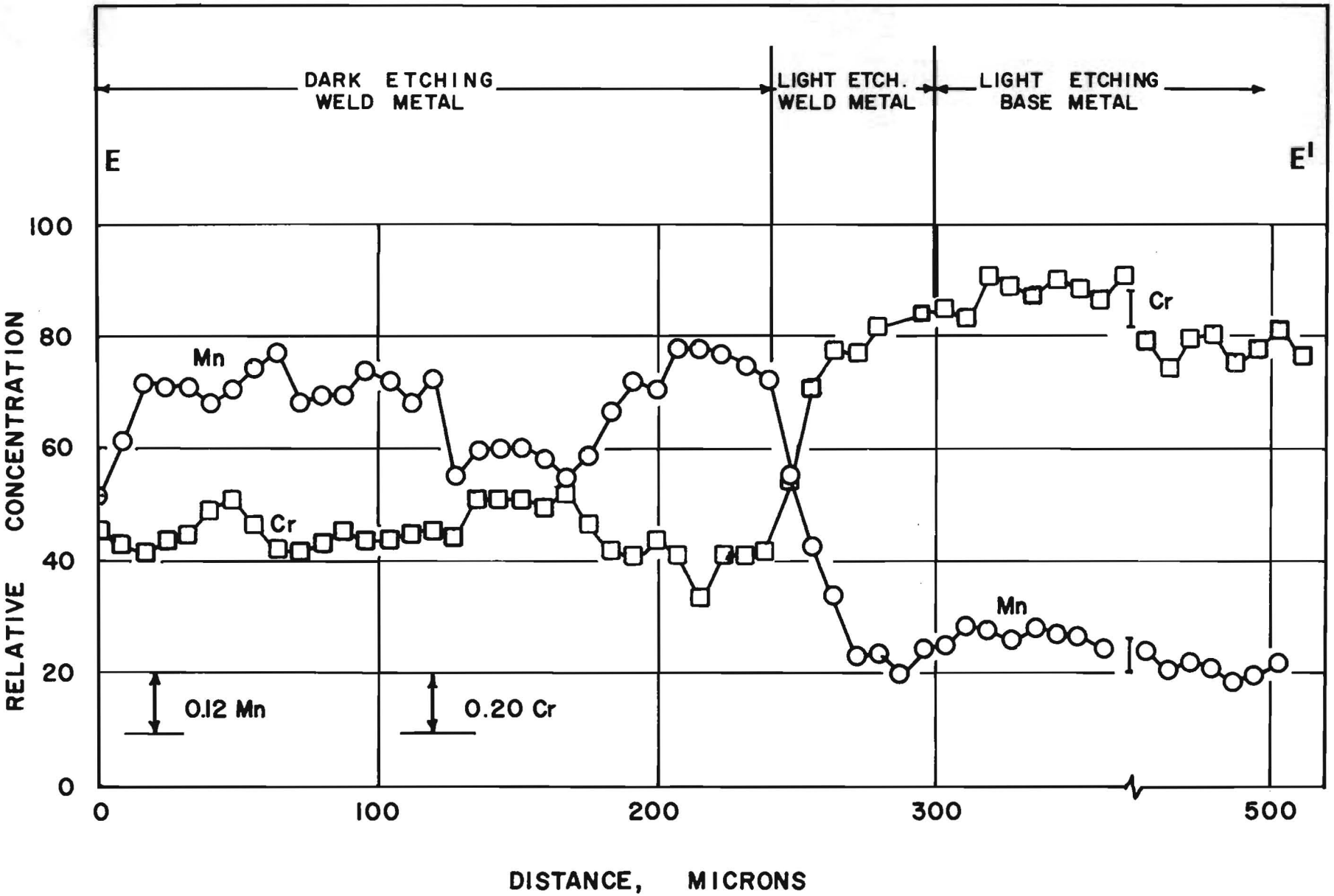

Figure 31 The Concentration Profiles for Manganese and Chromium Obtained by Traverse EE' Across the Fusion Boundary of a Bead Weld in Heat No. N51755.

respectively. The concentration scale (microanalyser intensity) of all of the graphs is relative because manganese and chromium standards in the composition range of HY-80 steel were not available for the microanalyser. However, shown in each figure is an approximate correlation between both the manganese and chromium composition and the relative concentration scale. This correlation was obtained by equating the manganese and chromium composition given in Table III to the average output intensity of the microanalyser during the period the beam was impinging on base metal. Also, the graphs shown in Figure 27 through 31 have been corrected for background intensity.

Across the top of the graphs in Figures 27 through 31, the extents of the various etched regions are indicated as they correspond to the paths shown on the photomicrographs in Figures 25 and 26. Because the electron beam left no visible trace on the specimen, correlation between the chart-paper plot from the microanalyser and measurements on the photomicrographs was obtained by means of a reference mark placed on the chart paper by the operator at the instant the beam was seen to cross the junction between the dark-etching and light-etching regions of the weld metal.

It is apparent from the concentration profiles shown in Figures 27 through 31 that a significant portion of the light-etching weld metal has a manganese and chromium composition

equal to that of the base metal. Scan CC', which traversed a fold of light-etching fused metal, is particularly enlightening. The concentration profiles, shown in Figure 29, show that as the fold was crossed, the manganese concentration decreased and the chromium concentration correspondingly increased. Note further that after the beam crossed the light-etching region of the weld metal and re-entered the dark-etching region, the manganese content increased and the chromium content decreased. Finally, as the beam again impinged upon light-etching weld metal, the manganese and chromium contents again corresponded to those of the base metal. Therefore, it is obvious that the fold was a portion of the melted but unmixed base metal that was washed away from the fusion boundary. Such folds appeared frequently in all of the sections of the bead welds examined and some of the folds extended a considerable distance into the weld metal. Similar folds have also been observed in gas metal-arc welds in maraging steel.[45] It is probable that the folds or washes of unmixed base metal are characteristic of all heterogeneous fusion welds and thus preclude any unqualified assumption of homogeneous mixing of the entire weld pool.

The results of the electron beam microanalysis show that the narrow zone of light-etching fused metal revealed both by the two-stage etching procedure and the ammonium persulfate

etchant is comprised, to a great extent, of metal with a manganese and chromium concentration identical to that of the base metal. However, it is not certain if it is the manganese or the chromium or a combination of the two which is responsible for the observed etching response. It is possible that some other element or combinations of elements besides manganese and chromium causes the as-etched color. Also, it should be noted that the chromium and manganese profiles generally break at the same point, however, further work is required to determine if other elements, including carbon, exhibit a similar concentration profile in the unmixed zone.

The results of electron beam microanalyses further confirms that the light-etching region metallographically observed at the fusion boundary consisted of HY-80 steel base metal that melted but did not become mixed with elements from the filler metal during the passage of the weld pool. Some consequences of the presence of an unmixed zone in heterogeneous welds will become apparent in later subsections.

Suggested Revisions in Terminology

The junction of the weld metal and the base metal is generally viewed as simply a two-dimensional surface of demarcation between completely-melted weld metal and completely-solid base metal.[5] Based upon the metallographic and analytical evidence presented above, it can be stated that this

"classical" view, while possibly adequate for macroscopic examination, is without a doubt inadequate when considering the microscopic fusion boundary of heterogeneous welds in low-alloy steels such as HY-80 steel.*

The results of this investigation have shown that the completely-melted weld metal is not a single homogeneous region but actually consists of two distinct regions with a diffusion gradient between them. One of these regions comprises the bulk of the weld metal which appears to be at least fairly well mixed with the elements of the filler metal. Therefore, this region will be called the composite region. The other region, at the extremities of the weld metal, is the easily masked narrow band consisting essentially of melted-and-solidified base metal which has already been referred to as the unmixed zone. In this investigation, the unmixed zone will also include the composition gradient between the composite region and the bulk of the unmixed zone since a concentration gradient should not be a characteristic of a well-mixed region.

In general, the terms "unmixed zone" and "composite region", while applicable to heterogeneous welds, are not applicable to truly autogenous and homogeneous welds. For example, Figure 32A shows the fusion boundary of a weld in HY-80 steel

* Also, it is evident that the classical view is likewise inadequate for welds in other types of alloys.[3,4]

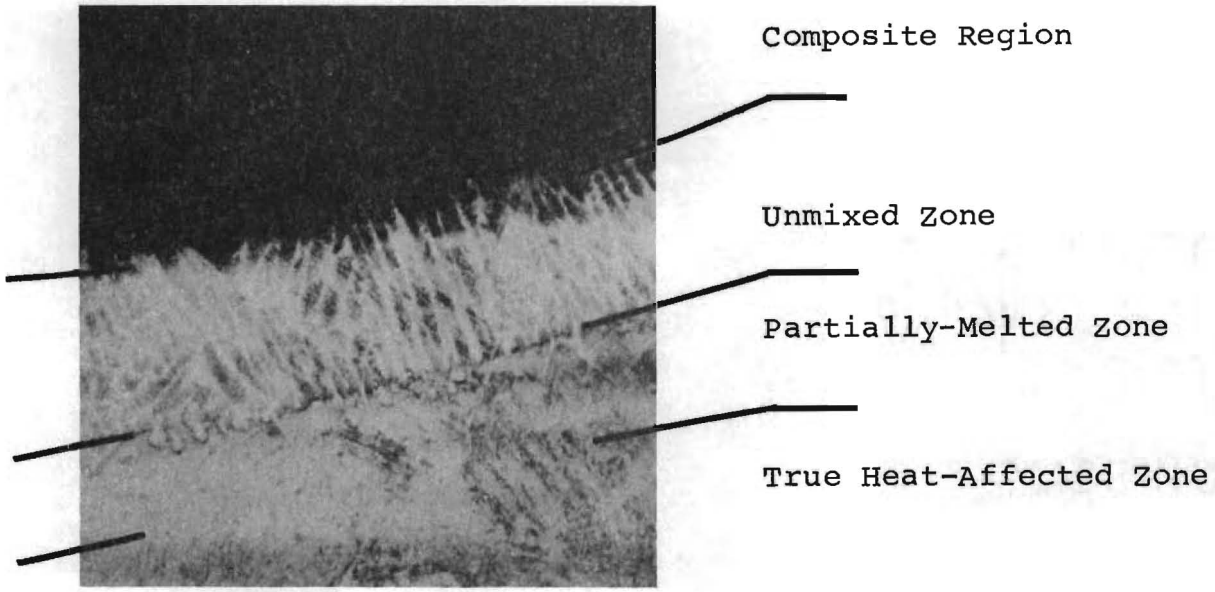

A.

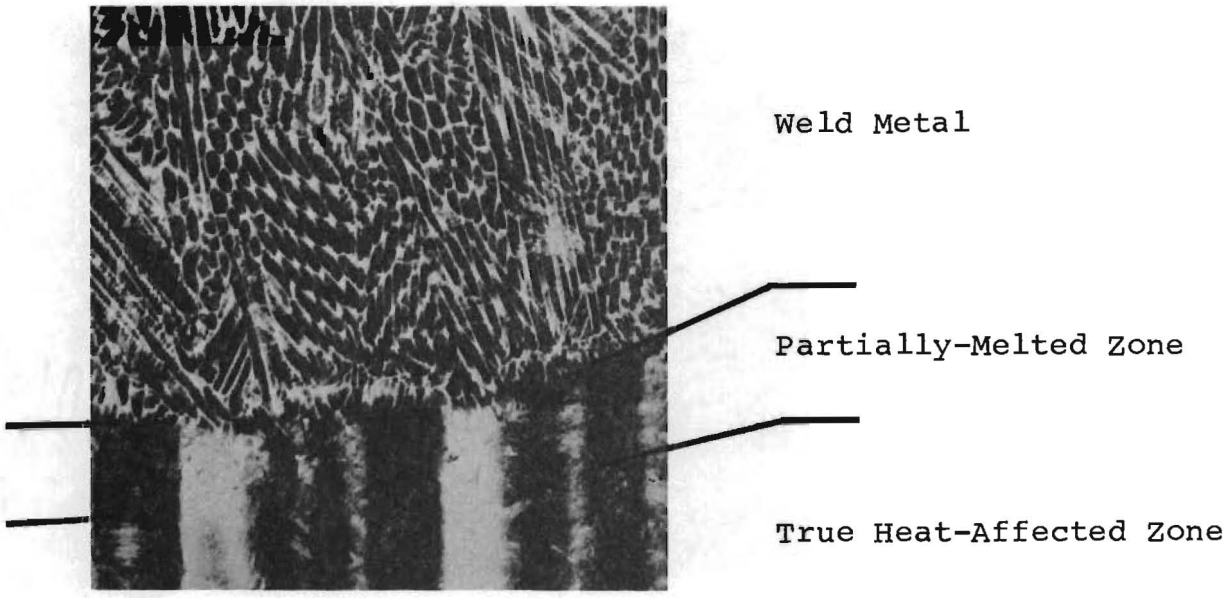

B.

Figure 32 A Comparison of the Regions at the Fusion Boundary Obtained With Different Welding Processes. Nital and Sodium Bisulfite Procedure, 250X. A. Weld Made by the Heterogeneous Shielded Metal-Arc Process. B. Weld Made by the Autogenous Gas Tungsten-Arc Process.

made by the shielded-metal-arc process and the various regions associated with the weld are labeled at the right on Figure 32A. In comparison, Figure 32B shows the fusion boundary of a weld in the same heat of HY-80 steel made by the autogenous gas tungsten-arc process. Note, in Figure 32B, that the entire volume of weld metal is uniform in response to the etchant. This uniform response results from the fact that all portions of the weld zone shown in Figure 32B are essentially identical in both composition and substructure.

The equivalence between the unmixed zone in a heterogeneous weld and the overall weld metal in a homogeneous or autogenous weld is particularly significant in cases where the primary purpose of adding a filler metal is to avoid some problem associated with an autogenous weld metal. In other words, no matter how well the composition in the composite zone is modified, the problem can still persist in the narrow unmixed zone where the composition remains essentially identical to that of the base metal. This should serve as a warning to those who would attempt to eliminate a problem in autogenous welds by simply changing to heterogeneous welding.

In addition, it should be cautioned that even in autogenous and homogeneous welds, the resulting composition of the bulk weld metal may be significantly different from the base metal due to absorption, outgassing, oxidation, or vaporization

of certain elements during welding. In such welds, therefore, an unmixed zone, or at least a zone unaltered in composition, may be present and should only be dismissed as a possibility after verification that one is not present.

Returning to the subject of terminology, the term weld interface is suggested when referring specifically to the surface beyond which the degree of melting is not complete. It is intended that this term replace such terms as bond, fusion line, and true fusion boundary. However, the term fusion boundary will be retained here when referring to the general vicinity that may include the partially-melted zone, the weld interface, and the unmixed zone.

This investigation also shows that there is a need for revision of the terms presently being used to indicate the heat-affected base metal. The evidence that has been presented above and which will be presented below, indicates that partial melting does occur adjacent to the weld interface. Therefore, the definition of the heat-affected zone as given in the Welding Handbook can only apply to what, in this text, will be referred to as the true heat-affected zone. The term partially-melted zone will be used to describe the portion of the heat-affected base metal that has undergone any amount of localized melting. This zone will be documented and described in detail in the following subsection.

The proposed terminology and definitions of the various regions resulting from a heterogeneous welding process are summarized in Table VII. In addition, the application of these terms is schematically illustrated in Figure 33.

Mechanisms of Partial Melting

Careful metallographic examination of the sections of the bead welds in HY-80 steel revealed evidence of localized melting immediately adjacent to the weld interface, as shown in Figure 34. This localized melting was manifested in four forms:

1. constitutional liquation of sulfide inclusions
2. constitutional liquation of small spherical inclusions
3. grain boundary wetting
4. super-solidus grain boundary melting.

Constitutional Liquation of Elongated Sulfide Inclusions. Constitutional liquation is the formation, under nonequilibrium conditions, of a liquid phase between the matrix and a solid second-phase particle. The liquation is the result of a diffusion-controlled reaction occurring at the particle-matrix interface at elevated temperatures. For liquation to occur, the reaction product must have a solidus temperature below the actual local temperature. Once formed, the liquid phase will persist until either diffusion changes the local composition to one that has a solidus temperature above the actual temperature,

Table VII

Proposed Terminology and Definitions of Discrete Regions in Heterogeneous Welds

Proposed Terminology	Proposed Definition	Present Applicable AWS Terminology[5]
Composite Region	The bulk portion of the weld metal within which hydrodynamic motion causes the chemical composition to be modified by dilution of the filler metal with material melted from the surrounding base metal.	Weld Metal
Unmixed Zone	A boundary layer at the outer extremities of the weld metal, consisting of base metal which is melted and solidified during welding without experiencing mechanical mixing with the filler metal.	
Weld Interface	The surface bounding the region within which complete melting was experienced during welding as evidenced by the presence of a definite solidification substructure.	Bond
Partially-Melted Zone	That portion of the base metal, located just outside the weld interface, within which the degree of melting due to such phenomena as constitutional liquation, grain boundary melting, etc., ranges from 0 to 100%.	Heat-Affected Zone
True Heat-Affected Zone	That portion of the base metal within which all microstructural changes produced by welding occur in the solid state.	

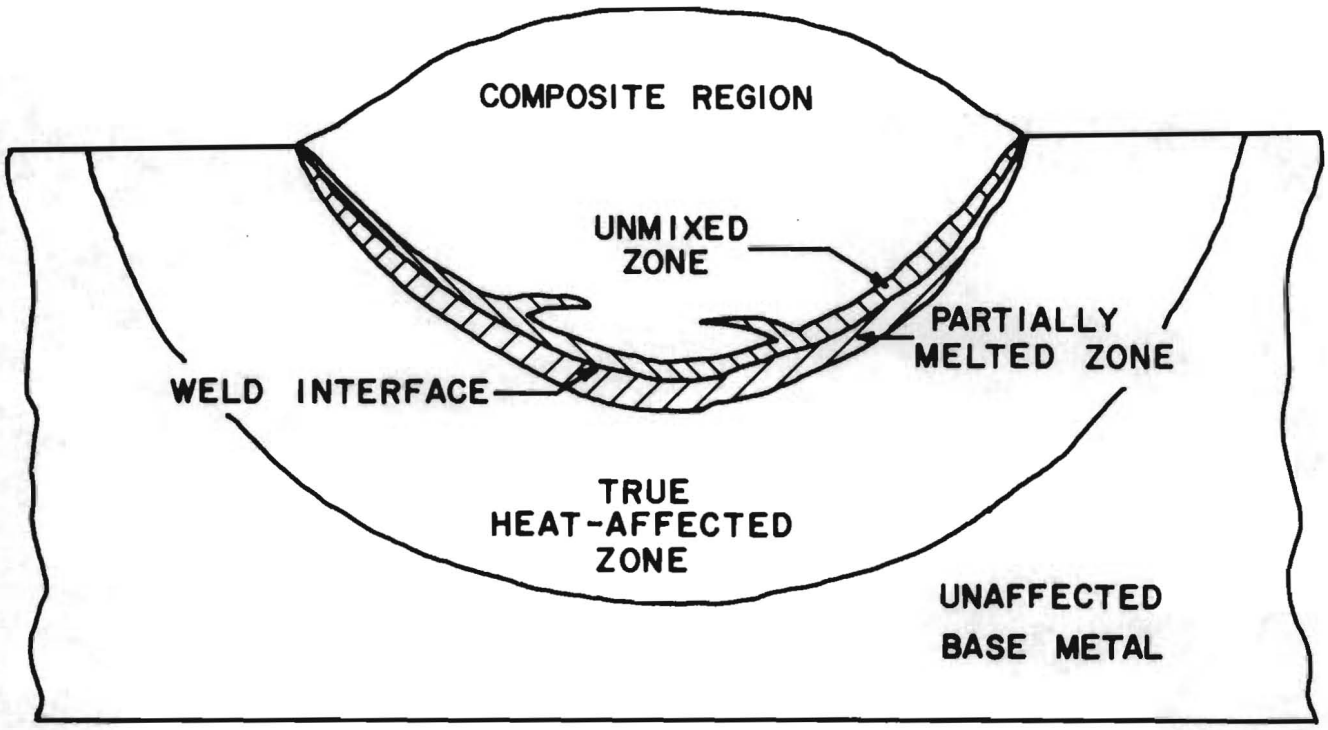

Figure 33 Schematic Illustration Showing the Regions of a Heterogeneous Weld Recognized in This Investigation and the Proposed Terminology to Identify These Regions.

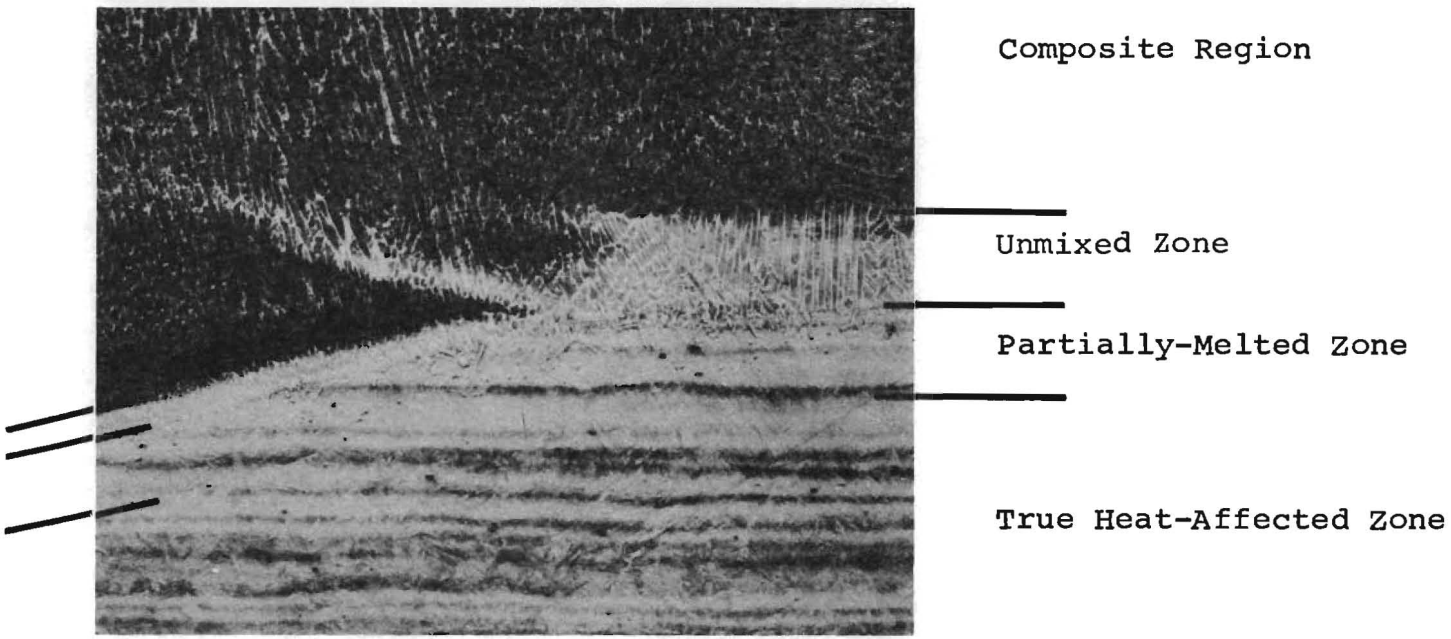

Figure 34 Transverse Section of a Bead Weld in a Specimen from Heat No. 72P305 Showing the Fusion Boundary. Note the Evidence of Various Types of Partial Melting in the Heat-Affected Zone Adjacent to the Fully-Molten Weld Metal. Nital and Sodium Bisulfite Procedure, 100X.

or until the local temperature is reduced by cooling to below the effective local solidus.

Although constitutional liquation in HY-80 steel has not been previously reported, details of the liquation phenomenon in other alloys have been discussed.[1,3,4,46] It should be noted, however, that not all of the investigators have used the specific term constitutional liquation.

In an investigation reported by Pepe and Savage,[4] constitutional liquation in 18Ni maraging steel weldments was found to involve titanium sulfide inclusions. In the present investigation, one form of constitutional liquation involved elongated sulfide inclusions in the HY-80 steel. Some specific examples of such liquation in HY-80 steel are shown in Figure 35. The light-etching area around the remnant of each of the inclusions is the region that was molten during the passage of the weld pool. The dark-etching area at the top of each photomicrograph in Figure 35 is the composite region. The incidence of constitutional liquation was much more severe in the specimens from Heat P than in the specimens from Heat N simply because Heat P had more large elongated sulfides.

Note that within the light-etching region around each of the primary inclusions in Figure 35 there is an array of smaller particles that also have the characteristic appearance of sulfides. A higher magnification photomicrograph of one of

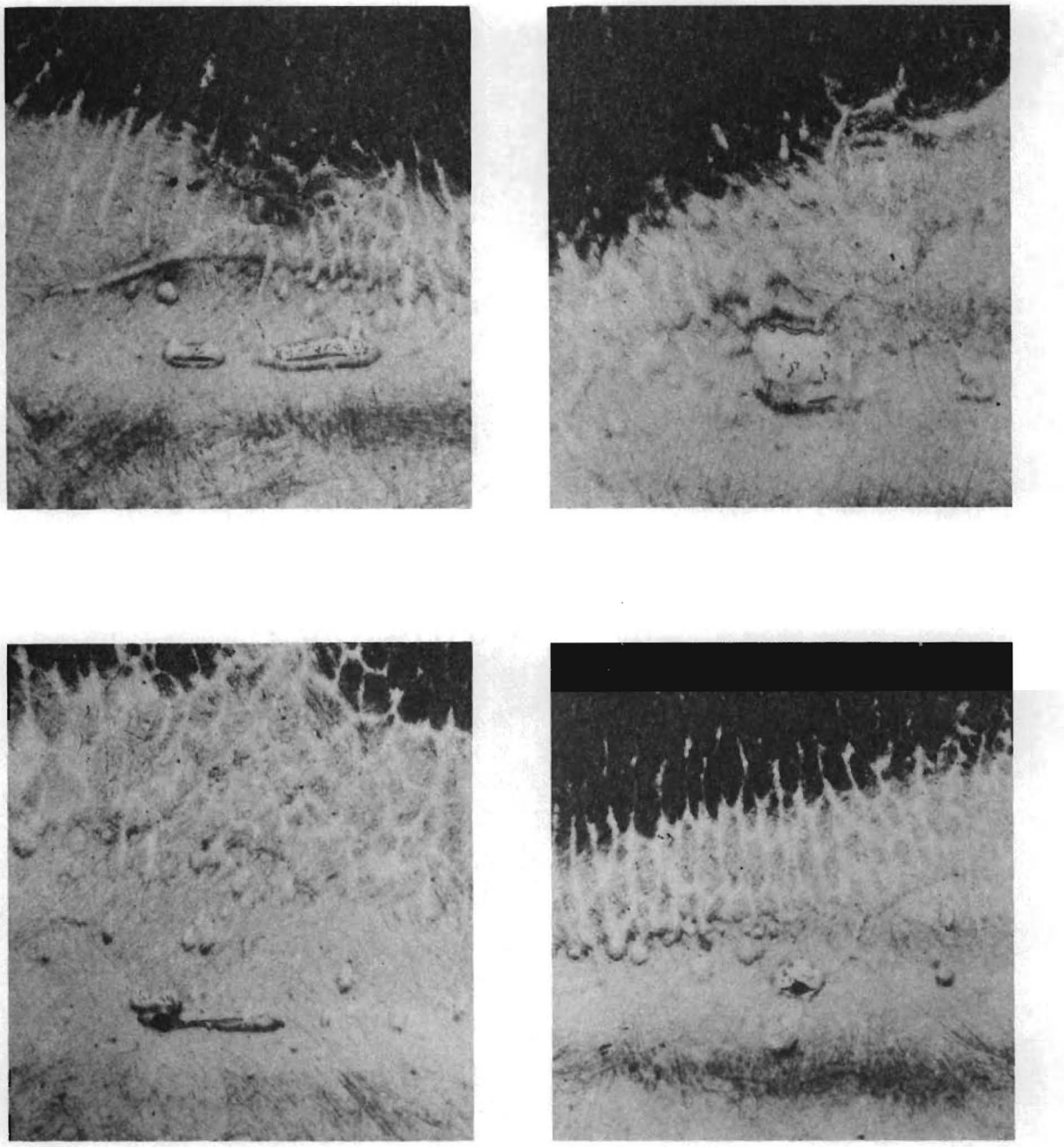

Figure 35 Some Examples of Constitutional Liquation of Sulfide Inclusions in the Partially-Melted Zone. Note the Small Globular Precipitates in the Vicinity of the Remnant of the Original Inclusion. Nital and Sodium Bisulfite Procedure, 500X.

the examples of liquation is shown in Figure 36 and the globular shape of the smaller particles within the liquated volume is more clearly apparent. The globular shape of the particles indicates that they precipitated from the liquid. Boneszewski and Baker[47] found evidence of similar small globular particles around alpha-manganese sulfides in the heat-affected zone of bead welds on a high-carbon, high-sulfur ferritic steel. In their investigation, the globular particles could not be identified definitely, but diffraction analysis indicated that they were complex sulfides and not simply alpha-manganese sulfides.

In addition, Boneszewski and Baker noted that in replicas of etched metallographic sections a white halo surrounded the decomposed sulfides. They suggested that the halos represented ferrite that resulted from carbon depletion in the region around the primary inclusion. However, in the present investigation a significant carbon depletion in the liquated region around the sulfides did not appear to have occurred. This conclusion is based on the fact that platelets of low-temperature transformation products were observed to be continuous across the interface between the liquated region and the matrix, see Figure 36. This observation indicates that the carbon concentration in the liquated region was not altered sufficiently to affect the martensite-transformation temperature.

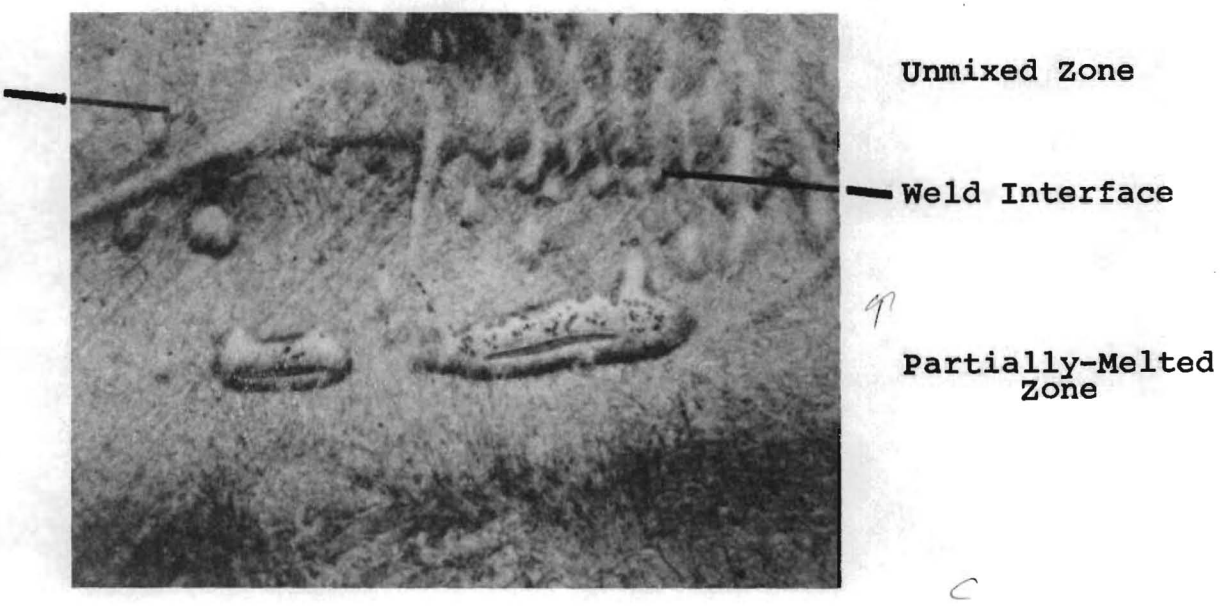

Figure 36 A Greater Magnification of One of the Examples of Constitutional Liquation in Heat No. 72P305. Nital and Sodium Bisulfite Procedure, 1000X.

It is possible that the halo Boneszewski and Baker observed was a result of the response of the liquated region to the nital etchant they used and not a consequence of the region around the inclusions being ferrite. The nital may have etched the liquated region more uniformly than the surrounding matrix, thereby producing a smooth area on the replica.

Without further work involving electron beam microanalysis, a model for the constitutional liquation of sulfide inclusions in HY-80 steel would be highly speculative. This is true because sulfides in HY-80 steel are undoubtedly complex manganese-iron-chromium sulfides. Furthermore, diffusion of elements between a sulfide and the matrix would probably be affected by oxygen, silicon, etc. Nevertheless, the mechanism for constitutional liquation probably involves diffusion of iron into the sulfide and manganese out of the sulfide. It should be noted that the iron sulfide/manganese sulfide binary diagram has a eutectic point at about 2156 F,[41] well below the solidus temperature of HY-80 steel.

Three additional features of the constitutionally liquated regions in the HY-80 steel which can be noted in the photomicrographs in Figures 35 and 36 are:

1. the precipitated particles tend to be located on the side of the liquated volume that is nearest the fusion boundary.

2. a dark-etching rim is predominant on the side of the liquated region that is furthest from the fusion boundary (this rim is definitely not due to oblique lighting or a relief effect).
3. although the constitutionally liquated regions have maximum dimensions that are several times larger than the average diameter of the cells in the fully-molten weld metal, none of the liquated regions solidified by a nonplanar mode.

The first two of these features are the result of redistribution of solute during unidirectional solidification of the liquated region. This unidirectional solidification is a very important, but previously overlooked, aspect of constitutional liquation adjacent to welds. A liquated region usually solidifies from the surface furthest from the fusion boundary toward the weld because of the dictates of the temperature gradient in the heat-affected zone. During this unidirectional solidification of the liquated region, solute is rejected into the remaining liquid as the solid-liquid interface advances. Therefore, the final concentration profile across a solidified liquated region contains an initial transient as well as a terminal transient. The initial transient is solute-lean and is etched dark by the nital and sodium bisulfite procedure,

hence, the dark-etching rim on the side away from the weld. On the other hand, the terminal transient is solute-rich, and therefore, is not stained by the sodium bisulfite. The solute-rich portion that develops in the liquated region on the side near the weld is, of course, the preferred location for the precipitation of the globular particles.

It should be emphasized, at this point, that although only a few elements in the alloy may be involved in the reaction responsible for the constitutional liquation, the subsequent solidification of the liquated volume results in the redistribution of all of the elements that are within the liquated volume. Since sulfides in HY-80 steel primarily occur within already alloy-rich bands, further redistribution of the solutes as a result of the solidification of constitutionally liquated volume can produce local regions in the heat-affected zone that have extremely high solute concentrations and are, therefore, very crack-susceptible.

The third feature, which is the absence of nonplanar solidification mode within the liquated region, is probably a result of the high temperature gradients in the liquated region. Because of its small size, the temperature gradient within the liquated volume could not have differed significantly from the steep gradients in the surrounding heat-affected zone during the passage of the weld pool. On the other hand, in the molten

weld metal near the freezing interface the usual temperature gradients are much lower and a non-planar solidification mode is obtained. When considering this significant difference between the temperature gradients in the liquated region and the temperature gradients in the weld metal, and then noting that the Chalmers number is inversely proportional to the temperature gradient in the liquid, see equation (2), it becomes apparent that the steep temperature gradients within the liquated region could have easily resulted in a Chalmers number below unity. Recalling that a Chalmers number below unity predicts a planar solidification mode, it appears that constitutional supercooling was not established in the liquated volume and, thus, a non-planar solidification mode was not possible. On the other hand, it is obvious from the cellular solidification mode that exists in the bulk weld metal that the gradients there were low enough to give a Chalmers number above unity.

Liquation of Small Spherical Regions. In addition to the constitutional liquation of sulfide inclusions, small spherical liquated regions also appeared as scattered white spots in a narrow zone adjacent to the weld interface. The largest spots were about 12 microns in diameter. A few of the spots contained a small second phase particle at the center but the majority did not. The zone in which this partially melting occurred was associated with the banding in that the

last vestiges of spherical melting usually extended back further along the alloy-rich light-etching bands than along the dark-etching bands.

Although no quantitative measurement was made, the spots appeared to be somewhat more prevalent in Heat P than in Heat N. However, the fact that numerous spherical liquated regions were present in both heats of HY-80 steel at locations where the matrix phase itself showed no evidence of melting indicates that constitutional liquation began well below the bulk solidus of either Heat N or Heat P.

The composition of the particles causing the liquation is not known. However, the distance between the white spots suggests that they are not the result of carbides, since carbides in the untempered or self-tempered maximum-grain-coarsened heat-affected zone are usually much too fine and closely spaced to give the type of distribution seen in Figure 34. It is possible that the liquating inclusions are the ones that were referred to as background inclusions in the examination of the as-received plate. Since the background inclusions did not elongate during rolling, they may be very fine complex-sulfides or oxides.

Randall _et al._[48] have reported the occurrence of similar spherical liquated regions in ultrahigh-strength steel. Most of the liquated regions that they observed contained small

inclusions. They reasoned that the white spots were interdendritic areas of the original ingot. This argument, however, ignores the fact that interdendritic regions of the ingot become considerably elongated in the reduction-to-plate and only non-plastic inclusions remain spherical. Therefore, a more plausible explanation is that the white spots observed in the material used by Randall et al. and in the HY-80 steel used in this investigation were actually regions of constitutional liquation of fine spherical inclusions. The reason that remnants of the inclusion could be seen in only a very few white spots is believed to be due to the small size of the spherical inclusions. Very fine inclusions would be decomposed more readily by the matrix-particle reaction during the constitutional liquation process.[46)]

Grain Boundary Wetting. Grain boundary liquation in the base metal at the fusion boundary has been proposed as a possible mechanism by which cracks can be nucleated in high-strength low-alloy steels under the thermal and stress conditions of welding.[49)] However, the mechanism by which solute accumulates at the grain boundary to provide the segregation necessary to produce significant liquation has only recently become clear. To explain the liquation of grain boundaries in copper-nickel alloys, Savage et al.[50)] proposed a mechanism of grain boundary wetting.

Applying similar reasoning to the observations in this investigation, it can be argued that small spherical second-phase particles in the base metal immediately adjacent to the weld interface experience constitutional liquation and the resulting liquid pools retard the migration of grain boundaries adjacent to the weld interface. This delay occurs because the liquid phase formed by the liquation is apparently of such composition that a migrating grain boundary encountering the liquid region is wetted by the liquid. Once wetting occurs, pinning of the boundary results and the normal grain-growth process is arrested in that vicinity. After passage of the weld pool the liquid film along wetted grain boundaries solidifies thereby unpinning the boundaries and allowing them to continue migrating. Therefore, by the time that the temperature becomes low enough to allow the austenite-to-martensite transformation, the remains of the grain boundary liquation do not necessarily coincide with a prior-austenite grain boundary. Of course, nonmetallics may possibly become aligned in such a way as to prevent some prior-austenite or delta-ferrite grain boundaries from resuming their migration.

Figure 37 shows evidence that this mechanism of grain boundary wetting can be applied to explain grain boundary liquation in HY-80 steel. In Figure 37 the spherical liquated regions, which are a prerequisite for grain boundary wetting,

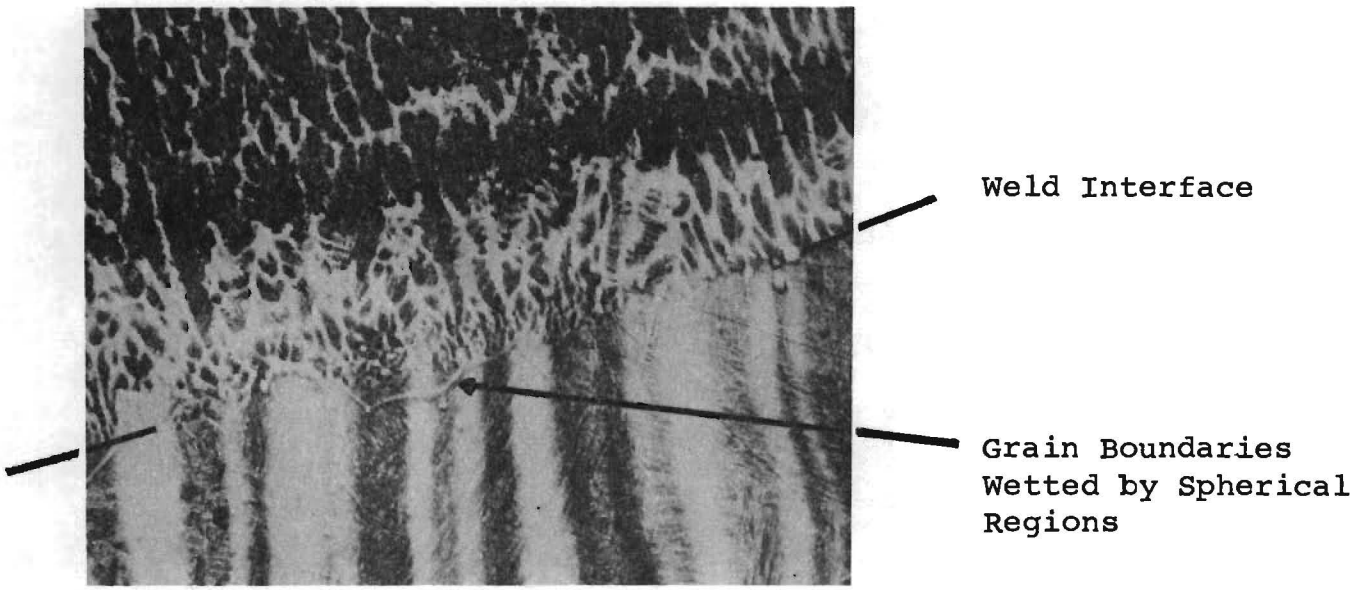

A.

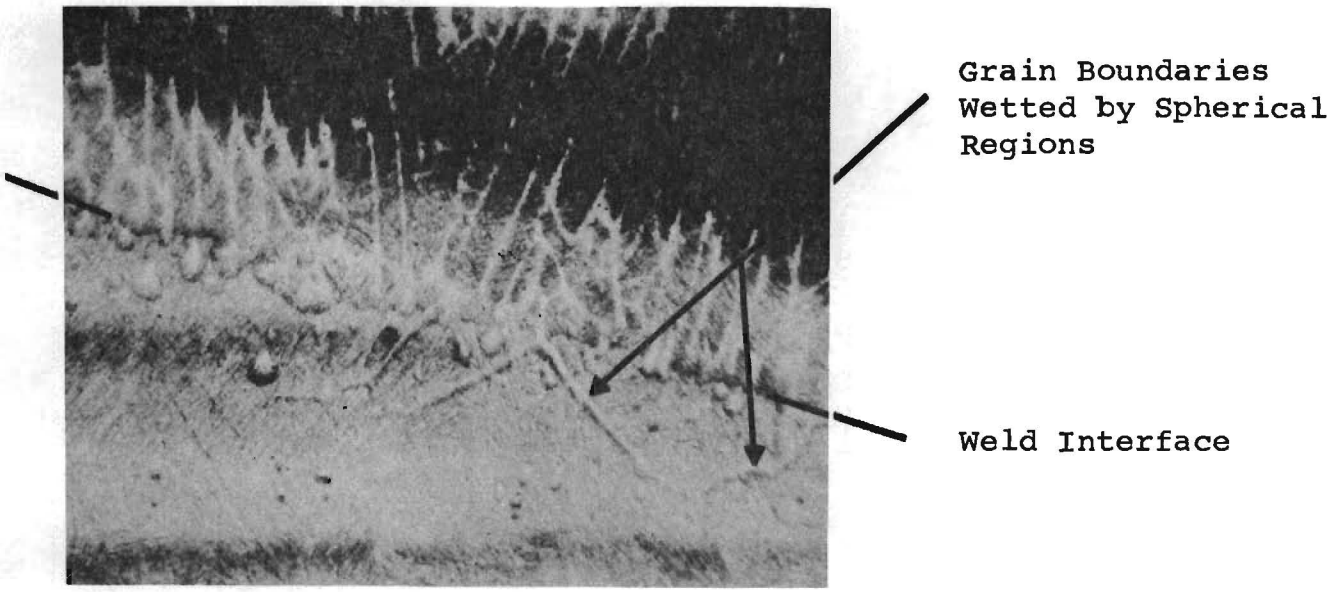

B.

Figure 37. Examples of Grain Boundary Wetting in the Partially-Melted Region of Bead Welds in HY-80 Steel. Nital and Sodium Bisulfite Procedure. A. Specimen from Heat No. N51755, 250X. B. Specimen from Heat No. 72P305, 500X.

can be clearly seen. The origin of these spherical regions was discussed in the previous subsection. In addition, the association of the wetted grain boundaries with the spherical regions is evident in Figure 37. Note in Figures 37A and 37B that the spherical liquated regions exhibit a cusp-shaped intersection with the broadened white-etching grain boundaries near the weld interface, thereby providing further support for the proposed mechanism. Specifically, the low dihedral angles indicate that the surface free-energy between the spherical liquated phase and the matrix favors grain boundary penetration. Furthermore, the broadness of the liquated grain boundaries indicate the extent to which wetting has occurred.

Broad grain boundary wetting is metallographically observable, under correct procedures, because the solidification of the liquid phase at the grain boundary is accompanied by a redistribution of solute. However, it should be realized that further away from the weld interface the liquid film along wetted grain boundaries is probably too thin to allow for an observable amount of solute redistribution. This would explain why liquated grain boundaries are not always seen to extend back as far as the last vestiges of constitutional liquation.

Similar to the occurrence of spherical liquated regions, the occurrence of wetted grain boundaries was more

infrequent and less extensive in Heat N than in Heat P. Also, in both heats the grain boundary wetting was more extensive at locations where alloy-rich light-etching bands intersected the fusion boundary.

It appears that the grain-boundary-wetting process in HY-80 steel can also produce a re-alignment of small sulfide globulars. This re-alignment can result from the intersection of migrating grain boundaries with liquated regions that were formed by constitutional liquation of large sulfide inclusions. For example, Figure 38 shows a location in a specimen from Heat P where prior-austenite grain boundaries intersected a liquated region resulting from a sulfide-matrix interaction. In Figure 38, small globular precipitated inclusions are identifiable within the liquated region. Furthermore, it can be seen that the primary inclusion had almost completely decomposed, leaving only a small remnant of the inclusion floating in the liquid. In Figure 38 it also appears that during solidification of the liquated region and the liquated grain boundary, one of the inclusions precipitated in film-like fashion along the prior-austenite grain boundary. It should be pointed out that the richer such inclusions are in iron, the more effective they are in forming grain boundary films. Therefore, the suggestion by Boneszewski and Baker[47] that sulfide films may be due, in some cases, to grain boundary

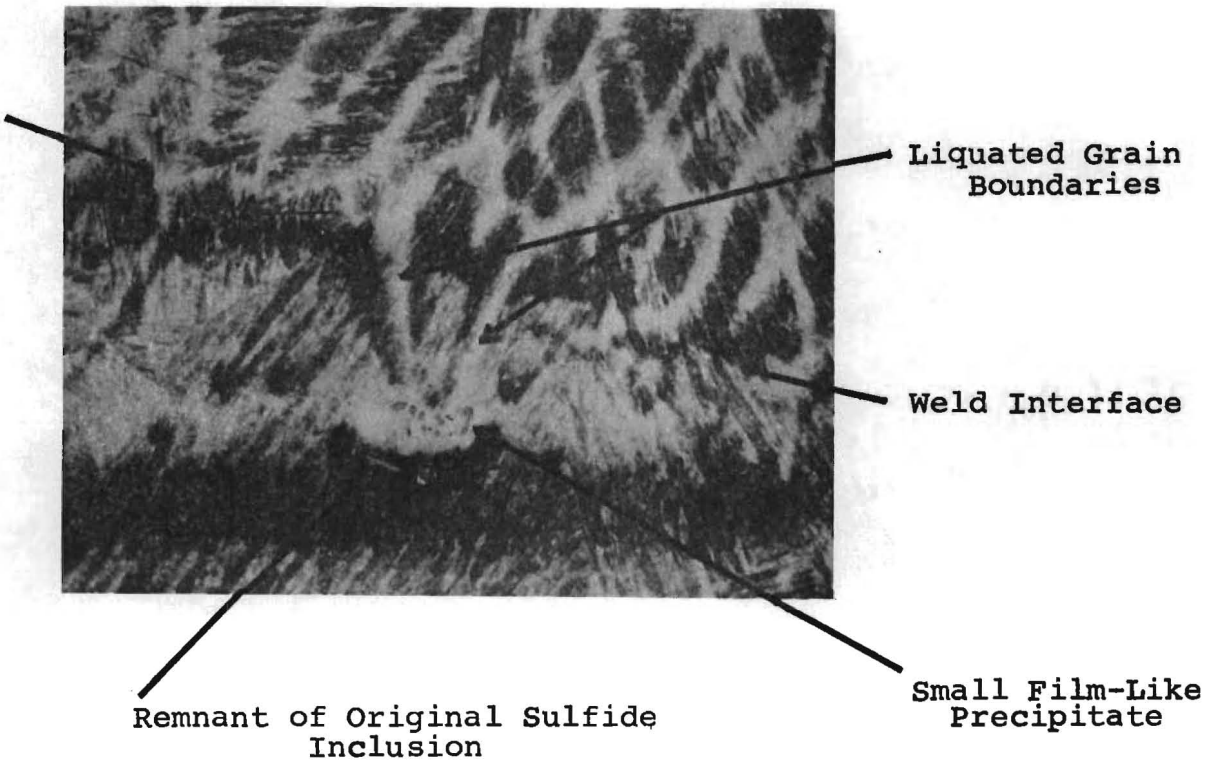

Figure 38 Grain Boundary Wetting Resulting From the Intersection of a Prior-Austenite Grain Boundary and a Constitutionally Liquated Region. Note the Alignment of an Inclusion Along the Liquated Boundary. Nital and Sodium Bisulfite Procedure, 1000X.

wetting rather than to the diffusion of sulfur from the grain interior to the boundaries, is probably a valid mechanism in welds in HY-80 steel.

In addition, chromium may significantly influence the morphology of sulfide inclusions. For example, Brammer and Honeycombe[51] have shown that while manganese sulfides were globular in as-cast iron-manganese-sulfur alloys, they tended to be lath- or sheet-like in non-manganese chromium-sulfur alloys and in alloy steels containing chromium.

Super-Solidus Grain Boundary Melting. All alloys except syntectic, eutectic and congruent-melting alloys exhibit a melting temperature range as defined by the separation between the liquidus and the solidus temperatures. For example, in low-carbon low-alloy steels such as HY-80 steel, the melting temperature range for the nominal composition is of the order of 50 to 75 F. However, in these materials the presence of the steep temperature gradient at the fusion boundary of normal fusion welds (about 10,000 F/in.) causes the 50 to 75 F temperature range to correspond to a distance of approximately 0.5 to 0.8 mils. Since these dimensions are of the same order of magnitude as the dimensions of the substructure in the adjacent unmixed zone, this type of partial melting is not easily distinguished metallographically in HY-80 steel. However, it should be emphasized that super-solidus grain boundary melting

has been observed in welds in copper-nickel alloys[50] and would probably be recognizable, with correct metallographic procedures, in higher-alloy steels or in the presence of less drastic temperature gradients.

The role of super-solidus grain boundary melting in the two heats of HY-80 steel used in this investigation may best be predicted after reference to Figure 39 which shows the peritectic portion of the iron-carbon binary diagram.[52] Note in Figure 39 that both the bulk solidus and the phases existing just below the solidus are markedly influenced by the carbon content. Assuming that the combination of alloying elements in HY-80 steel is not sufficient to invalidate the use of the iron-carbon peritectic as a first approximation, and also assuming homogeneous base metal, then Heat P, with 0.18 percent carbon, is slightly hyper-peritectic. However, it is very probable that the alloy-rich light-etching bands in Heat P have higher-than-nominal carbon contents, thereby making such bands even more hyper-peritectic. In comparison, Heat N, with 0.13 percent carbon, is hypo-peritectic to such a degree that even the alloy-rich bands would probably be also hypo-peritectic.

During the passage of a weld pool in base metal from Heat P, partial melting should begin well below the peritectic temperature. At the solidus temperature, melting would occur by direct transformation of austenite to liquid. Further, just

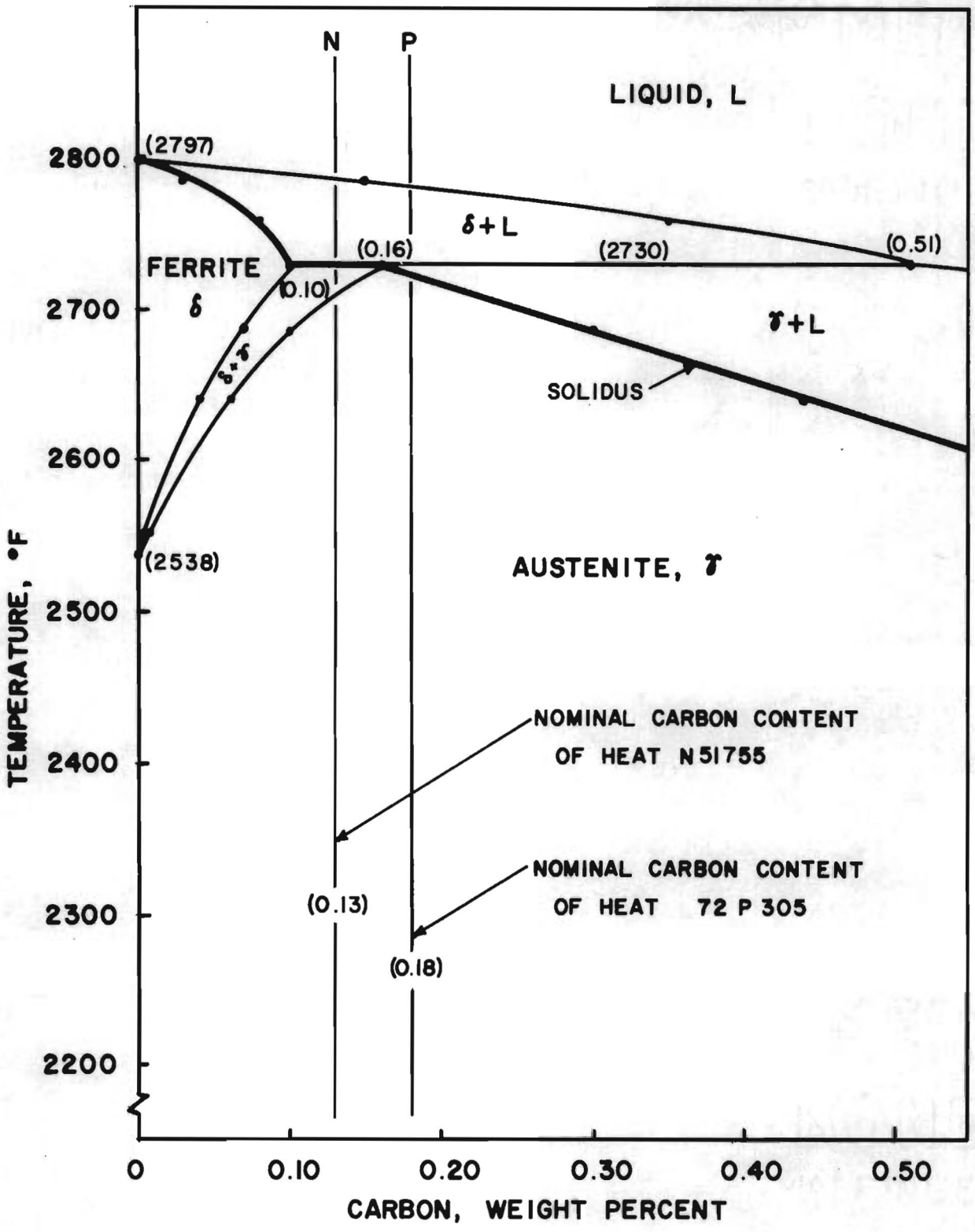

Figure 39 The Peritectic Portion of the Iron-Carbon Binary Diagram (Data From Reference 52).

above the peritectic temperature, the lever law applied to Figure 39 predicts that the amount of liquid present in a hyper-peritectic band would be at least 20 percent.* Thus, in Heat P a significant amount of melting takes place at or below the peritectic temperature and this melting probably contributes to the observed width and frequency of liquated grain boundaries near the weld interface (however, the relative amount of super-solidus grain boundary melting in comparison to grain boundary wetting cannot be differentiated metallographically).

On the other hand, Figure 39 indicates that because of the hypo-peritectic nature of Heat N, no melting of the matrix phase should occur below the peritectic temperature under equilibrium conditions. In fact, just below the peritectic temperature an alloy-rich band would be a mixture of about 50 to 65 percent austenite and the remainder delta-ferrite. Just above the peritectic less than 10 percent melting would be expected. This amount of melting is significantly less than that calculated for Heat P at the same temperature. Furthermore, because the austenite-to-delta-ferrite transformation in

* It should be emphasized that the conditions in a weld do not approach equilibrium. However, any departure from equilibrium would probably influence the metallurgical behavior of both hypo- and hyper-peritectic alloys in a similar fashion, and therefore, it seems reasonable to use equilibrium behavior in a first approximation. Also, limiting consideration to very minute regions at the weld interface makes equilibrium more tenable.

Heat N, the 10 percent melting would have to be distributed over a greater number of grain boundaries (delta-ferrite boundaries) than in Heat P (austenite boundaries). This fact suggests that with a given amount of liquid phase, either the proportion of the total grain boundary area melted would be less in Heat N or the thickness of the liquid grain boundary film would be less. Either case could account for the less extensive grain boundary liquation noted in bead welds in Heat N.

Furthermore, upon cooling Heat N from temperatures at or above the peritectic temperature, the delta-ferrite formed on heating should transform back to austenite. Thus, assuming that nucleation occurs at the ferrite grain boundaries, a new network of austenite grain boundaries would grow through the matrix and thus become divorced from the liquid films located at the prior delta-ferrite grain boundaries. On the other hand, Heat P, being hyper-peritectic in carbon content, would retain a fully austenitic matrix upon heating up to the peritectic temperature. Therefore, on heating to, or cooling from a peak temperature below the peritectic temperature it would not undergo any ferrite-to-austenite transformation. Thus, a significant number of liquated grain boundary films would be exclusively associated with austenite, and would tend to impede motion of austenite grain boundaries, making it more

diffucult for the grain boundaries to divorce themselves from the segregated regions.

This inherent difference in the nature of the matrix phase present at the time constitutional liquation is present could also have a profound influence on the tendency of the liquid phase to penetrate the grain and interphase boundaries. However, no quantitative data are available on the surface free energies of the interphase interfaces involved and so no definite conclusions can be drawn at this time.

Other Defects Due to Sulfide Inclusions

Evidence was presented in the preceding subsection indicating that sulfides can cause undesirable conditions at the fusion boundary of welds in HY-80 steel. In the present subsection, examples of other undesirable phenomena involving sulfides are presented.

Microvoid Formation at the Weld Interface. A phenomenon that was observed at the weld interface of bead welds on HY-80 steel was the association of microvoids with elongated sulfide inclusions. Typical examples of microvoids at the edge of sulfide inclusions are shown in Figure 40. Figure 40A shows a microvoid that occurred in a specimen from Heat P and Figure 40B shows a similar condition that occurred in a specimen from Heat N. Note in both Figures 40A and 40B that some degree of constitutional liquation appears to have occurred at

the edge of the inclusion nearest the weld interface. Furthermore, the liquated region partially surrounds the void, indicating that the void formed during the period that liquation occurred.

Although the exact mechanism of the microvoid formation is not clear, it may involve a reaction between some element, possibly oxygen or hydrogen, and either the liquated region or the sulfide inclusion itself. It has been reported that manganese sulfide inclusions in the base metal can react with explosive violence during welding and create gas pockets at the fusion boundary.[53] Also, Herres[54] has proposed that porosity in welds can be the result of a reaction of hydrogen and sulfur to form H_2S during welding.

The fact that the microvoids shown in Figure 40 are not back-filled with weld metal is evidence that their formation may indeed be due to a reaction which forms a gas bubble. It can be assumed that at the instant that liquation is present at the tip of the inclusion, the adjacent weld metal is molten. Thus, if the microvoid had been a hot crack formed by strain, the void would be at least a partial vacuum which would have, to some degree, back-filled with weld metal. In addition, the microvoids shown in Figure 40 do not extend into the composite region where hydro-dynamic motion may have diluted any high-sulfur region resulting from the dissolution of the sulfide inclusion.

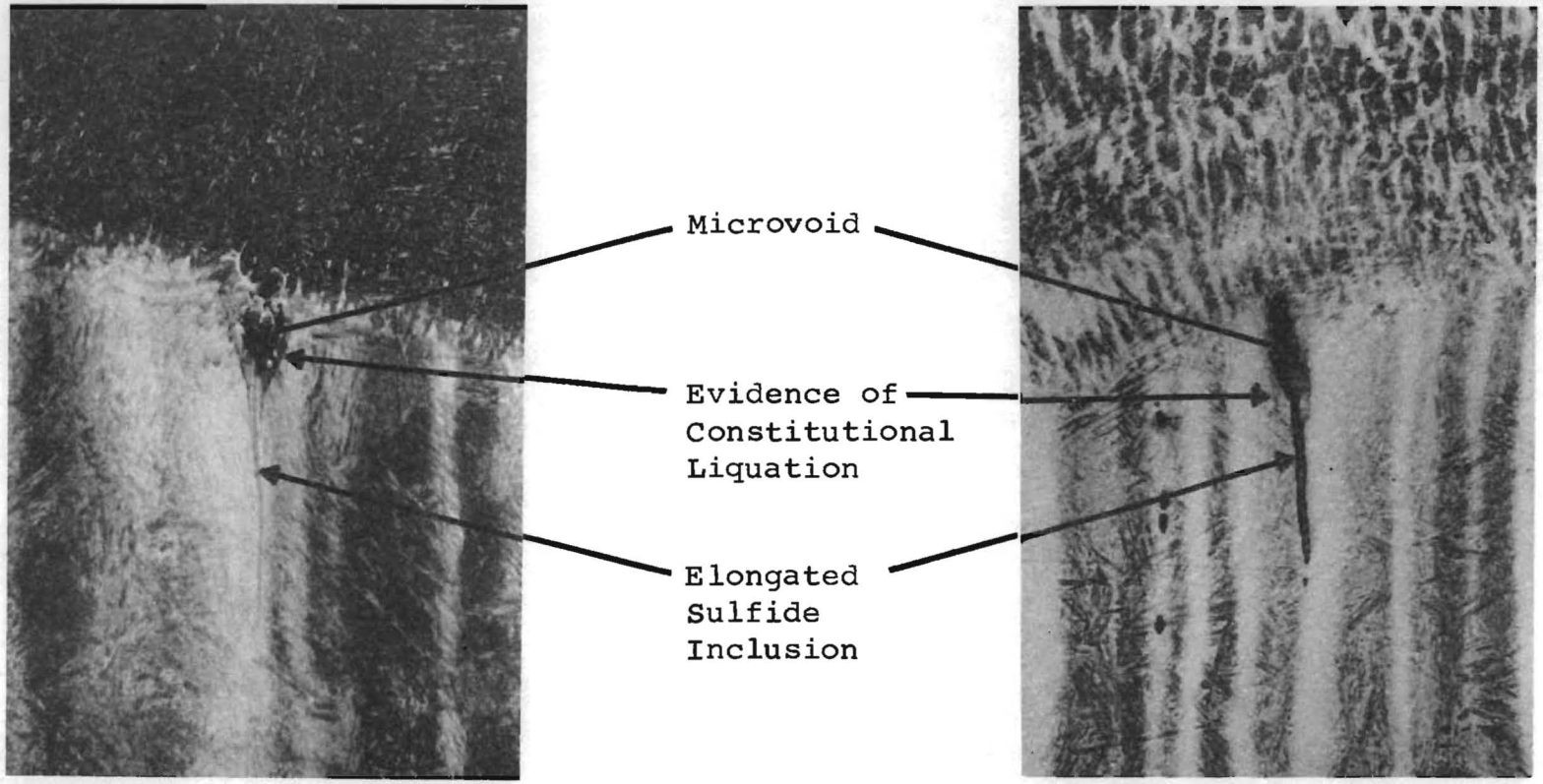

Figure 40 Microvoids Caused by Sulfide Inclusions at the Fusion Boundary of Bead Welds in HY-80 Steel. Nital and Sodium Bisulfite Procedure, 250X. A. Specimen from Heat No. 72P305. B. Specimen from Heat No. N51755.

Irrespective of the mechanism of their formation, the fact that such microvoids can occur at the fusion boundary of welds in HY-80 steel is indeed ominous. Such microvoids would be traps for any hydrogen present and the locations could become the initiation sites for cracking at lower temperatures. Since this microvoid formation phenomenon was only observed with elongated-type sulfides and since Heat P had more and larger elongated-type sulfides, it is not unreasonable to assume that Heat P would have more microvoids at the fusion boundary of welds and that this mechanism could have contributed to the report that Heat P had poorer weldability than Heat N. However, because the occurrence of sulfide-caused microvoids was relatively infrequent in the bead welds used in this investigation, a more quantitative evaluation of this phenomenon was not made.

Sulfide Alignment in the Unmixed Zone. In an above subsection describing mechanisms of partial melting, it was shown that sulfides can become aligned along liquated grain boundaries in the partially-melted zone (see Figure 38). Similarly, the alignment of sulfides along grain boundaries in the unmixed zone was observed. For example, Figure 41 shows small globular sulfide inclusions aligned along prior-austenite grain boundaries in the unmixed zone of bead welds in specimens from Heat P. Such alignments are believed to be a result of large

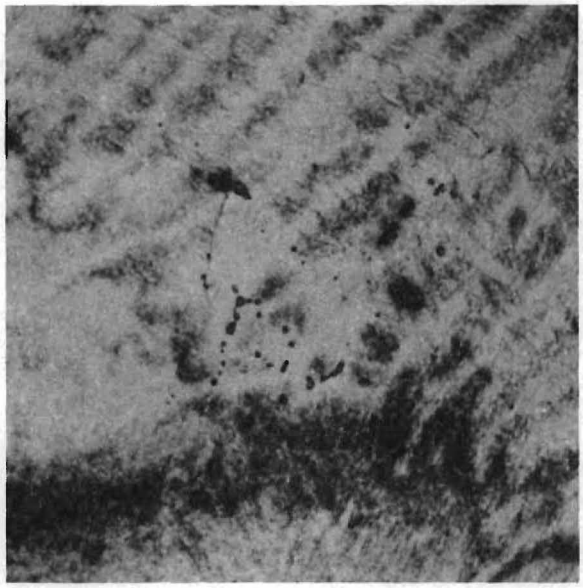

A.

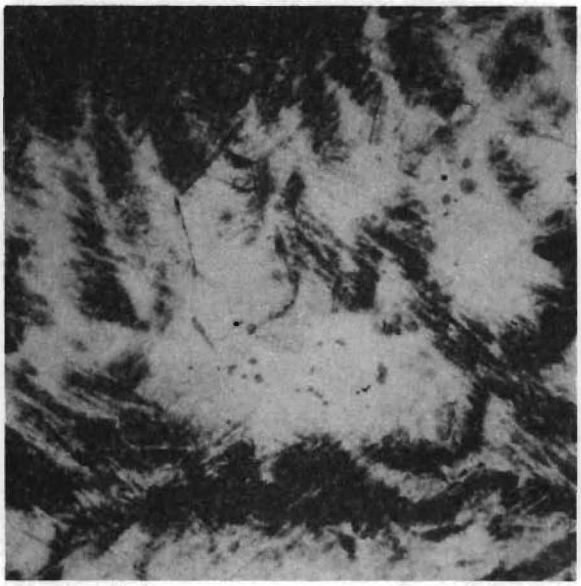

B.

Figure 41 Examples of the Alignment of Small Sulfide Globules and Films Along Prior Austenite Grain Boundaries in the Unmixed Zone of Bead Welds in Specimens from Heat No. 72P305. Nital and Sodium Bisulfite Procedure, 1000X.

sulfides from the base metal which completely dissolved in the unmixed zone, thereby creating local sulfur-rich regions. These regions would remain localized because of the short periods available for diffusion and because the liquid in the unmixed zone is either stagnant or experiencing only laminar fluid motion. Subsequently, during the epitaxial solidification of the unmixed zone, sulfur segregates to a great degree at solidification grain boundaries which, being solute-rich, probably remain liquid for some distance back from the general solid-liquid interface. Small globular or even film-like sulfides can then precipitate and become aligned at the solidification grain boundaries. After the last vestiges of liquid solidify, most grain boundaries with aligned sulfides would probably be unable to migrate away.

Boniszewski and Baker[47] have noted arrays of small globular sulfides on fractographs from specimens of ferritic steel. Therefore, alignments of sulfides at prior-austenite or prior-delta-ferrite grain boundaries may be an important source of nucleation sites for the cracking that frequently extends from the fusion boundary of welds in low-alloy steels.

Varestraint Tests of Heterogeneous Weld Metal

The composite-region cracking that was observed on the polished and etched surfaces of the Varestraint test specimens was evaluated qualitatively but not quantitatively

because the cracking had an extremely irregular nature. An example of this type of cracking, with its many interconnecting branches, is shown in Figure 42. This irregular cracking appears to be typical of that produced by the Varestraint test in welds made with a filler metal.

The results of the Varestraint tests of specimens from both heats of HY-80 steel are summarized in Table VIII. Despite the irregular nature of the cracking, the qualitative results clearly indicate that since the heterogeneous welds in both heats performed similarly, the heat from which the test specimens were taken did not influence the degree of hot-cracking produced in the composite region of the weld metal. Note also that the maximum augmented strain that did not produce cracking, termed the threshold strain, was 0.33 percent for both heats.

In a previous investigation by Bell,[55] Varestraint tests of specimens from Heat N and Heat P were welded by the autogenous gas tungsten-arc process. The results of that investigation, summarized in Figure 43, showed a considerable difference in the degree of weld-metal cracking between the two heats. It is also apparent in Figure 43 that the threshold strain for autogenous welds was greater for Heat N than for Heat P. In addition, Bell found that Heat P had the greater number of cracks as well as the longer maximum-crack-length.

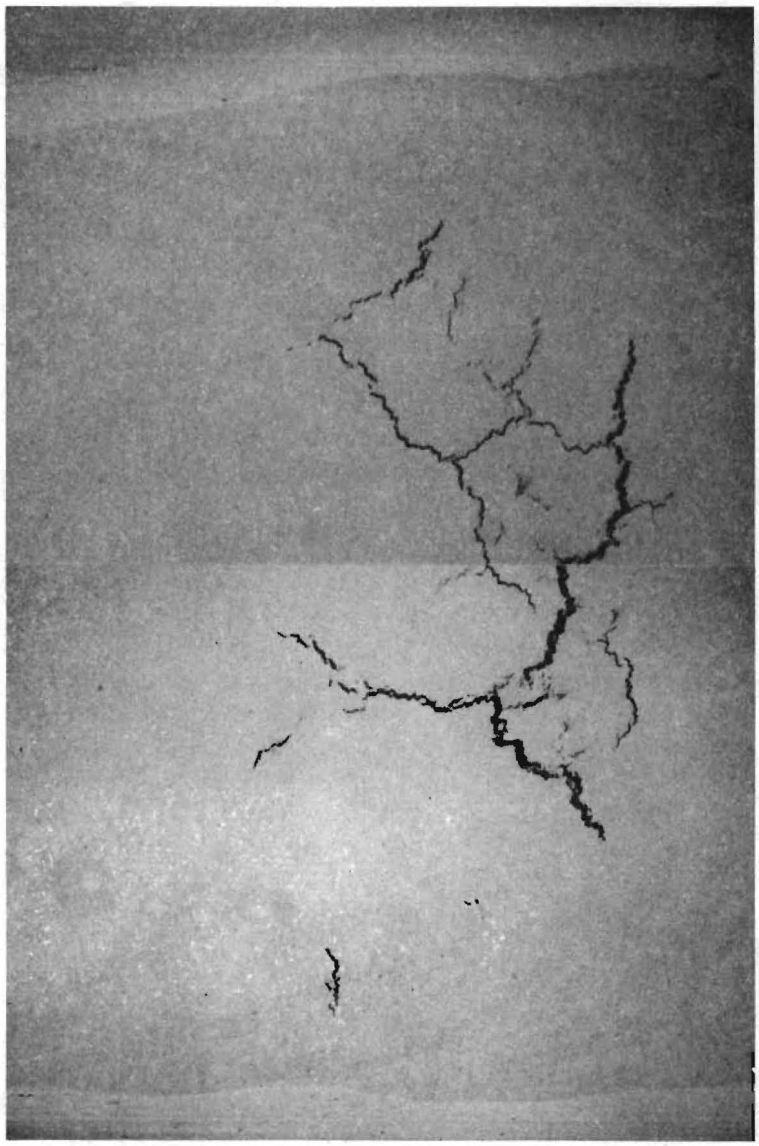

Figure 42 Irregular Weld-Metal Cracking in the Varestraint-Test Specimen From Heat No. 72P305 Strained 2.00 Percent. Ammonium Persulfate Etchant, 10X.

Table VIII

Qualitative Results of the Varestraint Test for Weld Metal Crack-Susceptibility

Heat No.	Augmented Strain, percent					
	0	0.25	0.33	0.50	1.00	2.00
72P305	None	None	None	Slight	Severe	Severe
N51755	None	None	None	Slight	Severe	Severe

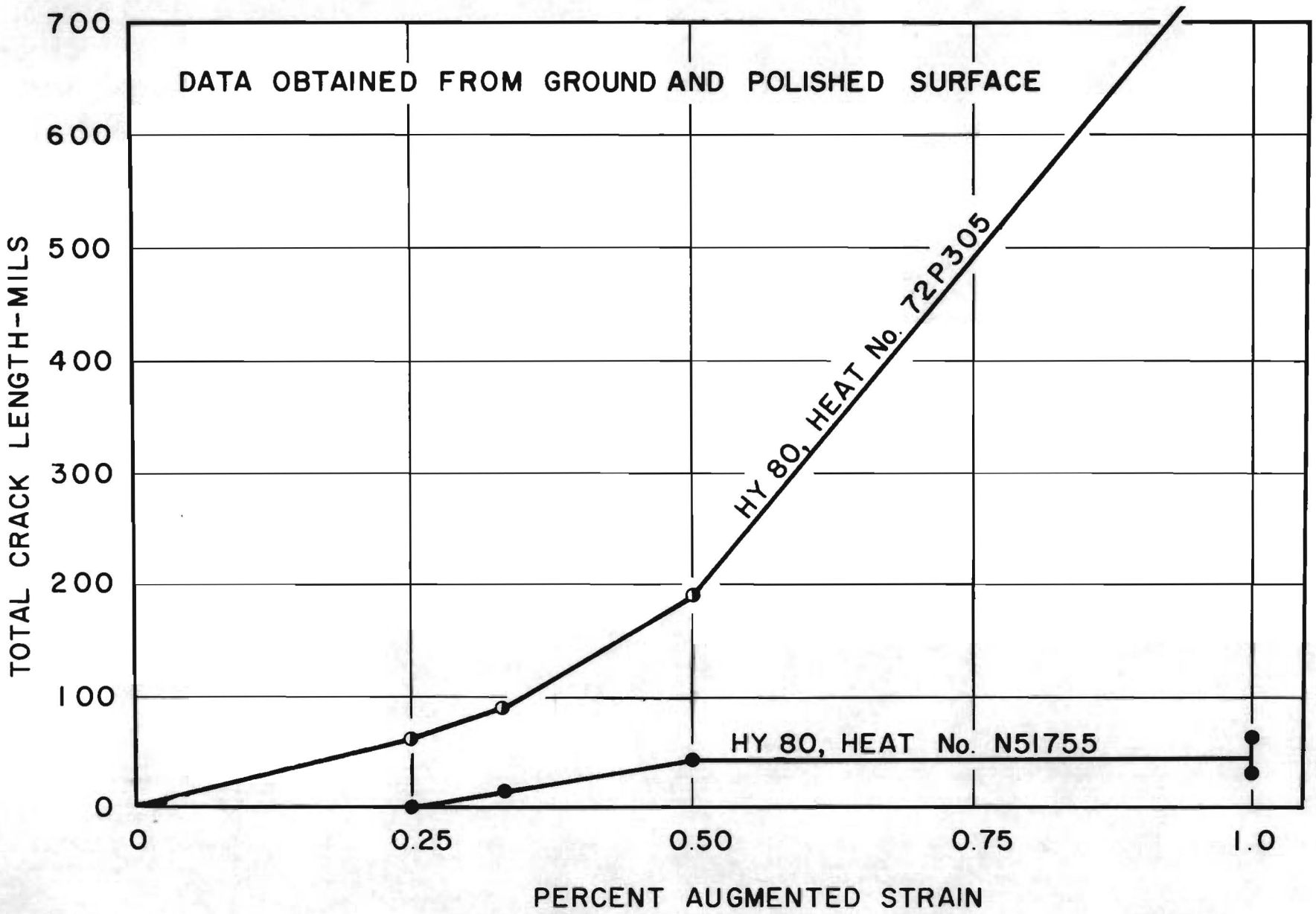

Figure 43 Results of Previous Varestraint Tests on Specimens From Heat Nos. 72P305 and N51755 Welded by the Gas Tungsten-Arc Process (from Reference 55).

Therefore, in comparing the results obtained by Bell with the results found in this investigation, it is apparent that the difference in the crack susceptibility of autogenous welds in Heat N and Heat P was not manifested in the composite region of the heterogeneous bead welds made with E11018G electrode. However, this result should not be construed to mean that the composite region of all types of heterogeneous welds made with E11018G electrodes on the two heats would fail to show a difference in crack-susceptibility. For example, in the first pass at the root of a grooved joint, typical of those used in the fabrication of heavy sections, the composite region would probably be much more diluted with base metal than the composite region of the bead welds produced in the Varestraint specimens in this investigation. Thus, the composite region of such root-pass welds in base metal from Heat N and Heat P should tend to show a difference in crack susceptibility similar to that shown by Bell.

In an examination of the transverse cross section of the welds strained at 2.00 percent, only one fusion-boundary crack was found. This crack, shown in Figure 44, occurred in a specimen from Heat P. Although it is not possible, on a single section, to ascertain the nucleation point of a crack, the location of the crack shown in Figure 44, with its center at the weld interface, strongly suggests that it was

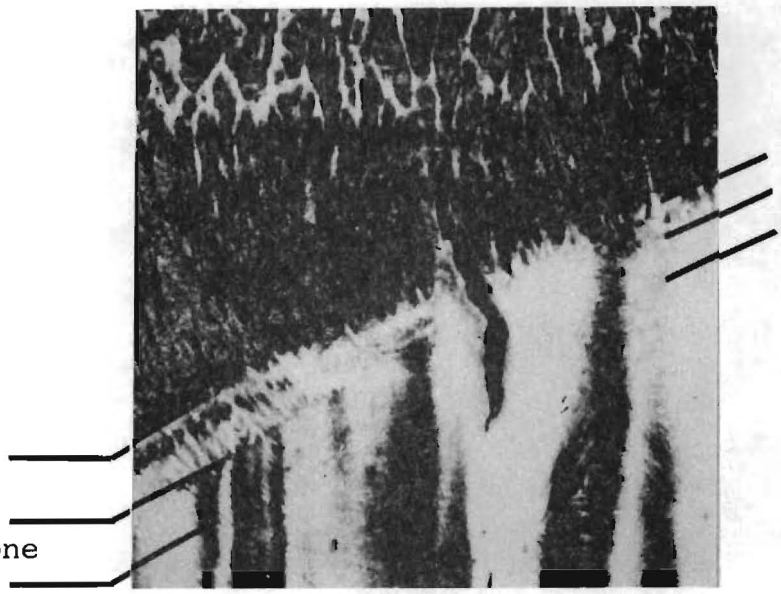

Figure 44 A Transverse Section Showing the Fusion-Boundary Crack in the Varestraint Test Specimen from Heat No. 72P305 Strained 2.00 Percent. Nital and Sodium Bisulfite Procedure, 300X.

nucleated either in the unmixed zone or in the partially-melted zone. In light of the aforementioned analogy between the unmixed zone of a heterogeneous weld and the weld metal of an autogenous weld, the possibility that the fusion boundary crack shown in Figure 44 did nucleate in the unmixed zone is completely consistent with the results of Bell which showed that autogenous welds in Heat P were more crack susceptible than those in Heat N.

In light of the fact that the unmixed zone is not revealed by usual metallographic procedures, it is very probable that many of the "fusion line" failures in weldments of low-alloy quenched-and-tempered steels reported in the literature were actually failures associated with the unmixed zone. Because it is simply melted and solidified base metal, the unmixed zone, in welds in low-alloy quenched-and-tempered steel, may have mechanical properties poorer than either the composite region, the partially-melted region, or the poorest part of the true heat-affected zone.

Also, it should be noted that the fusion boundary crack shown in Figure 44 occurred at a location where a light-etching alloy-rich band intersected the fusion boundary. The fact that such intersections of alloy-rich bands with the fusion boundary appear to be preferential sites for crack initiation will be elaborated upon in later subsections.

Cold-Cracking Tests

The modified Granjon technique described in the above Materials and Experimental Procedure section proved to be an excellent method of studying the mechanism and morphology of cold cracking in the two heats of HY-80 steel. However, it should be emphasized that in its present form the technique is primarily qualitative and not quantitative. Such modifications as provisions for strain and temperature monitoring and more exacting determinations of the hydrogen distribution in the test specimens (the hydrogen content of the specimens is not as important as the hydrogen distribution) would be necessary in order to make the test quantitative.

The light film of immersion oil that was spread uniformly over the vicinity examined on each specimen permitted observation of any hydrogen evolution without seriously impairing optical resolution. However, preliminary tests had indicated that the immersion oil caused discoloration of the etched surface obtained with the two-stage nital and sodium bisulfite procedure. In addition, with the ammonium persulfate etching procedure, the oil film impaired the optical resolution when the lighting was obliqued in order to reveal substructure. Consequently, the specimens were etched with nital for observation during testing. Although this procedure clearly delineated the composite region, it unfortunately

precluded positive identification of either the unmixed zone or the partially-melted zone during the cold-cracking test. However, cracking associated with these zones as well as the true heat-affected zone was studied further after the test specimens were removed from the loading apparatus, repolished and etched with the two-stage procedure.

General Observations. The observations of the welded specimens from Heat N and Heat P tested at room temperature in the loading apparatus are summarized in Table IX. These observations revealed the following general features:

1. None of the specimens from either Heat N or Heat P welded under low-hydrogen conditions exhibited hydrogen bubble evolution or cold cracking.
2. All specimens welded under high-hydrogen conditions exhibited bubble evolution and some degree of cold cracking in one or more of three regions;
   a. in the true heat-affected zone,
   b. at the fusion boundary, subsequently determined to be associated with the unmixed zone and/or the partially-melted zone,

Table IX

Summary of General Observations of Cold-Cracking-Test Specimens of HY-80 Steel

Heat No.	Relative Hydrogen Content	Banding-to-Stress Orientation	Amount of Bubble Evolution	Relative Cracking Observed* Fusion Boundary**	Relative Cracking Observed* True Heat-Affected Zone
72P305	High	Transverse	Profuse	very many	very many (long)
		Parallel	Profuse	few	few (short)
	Low	Transverse	None	few	none
		Parallel	None	none	none
N51755	High	Transverse	Profuse	several	many (medium length)
		Parallel	Profuse	none	none
	Low	Transverse	None	none	none
		Parallel	None	none	none

* Approximate rating of the incidence of cracking: few - 1 to 3, several - 4 to 6, many - 7 to 12, very many - over 12.

** Includes cracks associated with the unmixed zone and/or the partially-melted zone.

c. in the composite region. (However, cracking in the composite region was not of primary concern and therefore was not evaluated.)

3. The observed cracking in the high-hydrogen specimens was primarily delayed in nature. In other words, the cracks generally initiated shortly after application of the load and extended with time, accompanied by steady and/or intermittent hydrogen bubble evolution. The bubble evolution confirmed the association of hydrogen with delayed cracking.

4. Under similar welding conditions, the degree of cracking in specimens from Heat N was always less than in specimens from Heat P.

5. Cracking in the true heat-affected zone in both heats of HY-80 steel appeared to be nucleated by sulfide inclusions.

6. Most of the cracks, both at the fusion boundary and in the true heat-affected zone, appeared to propagate along light-etching bands of the base metal.

7. In the specimens welded under high-hydrogen welding conditions with the plate rolling direction oriented

parallel to the direction of the principal stress, the cracks were generally shorter and less likely to be nucleated within the fusion boundary than were those in specimens welded with the rolling direction transverse to the stress direction.

8. Cold cracks associated with the unmixed zone, partially-melted zone, and true heat-affected zone were predominantly intergranular.

The Role of Hydrogen. It should be noted that in this investigation, cracking in the true heat-affected zone did not occur in either Heat N or Heat P when welding was performed under low-hydrogen conditions. (The few fusion boundary cracks observed in Heat P will be discussed below.) These results conclusively confirm the fact that the amount of hydrogen present is a major factor influencing the degree of delayed cracking.

The absence of both cold cracking and bubble evolution in the specimens welded under low-hydrogen conditions implies that the low-hydrogen welding procedure was adequate in preventing the introduction of a significant amount of hydrogen. However, it must be pointed out that the specimens in this investigation were held under load for a maximum of only 12 hours. whereas, delayed cold cracking has been known to occur weeks

and even months after welding. Thus, it remains to be determined whether or not a specimen welded under the low-hydrogen procedure would develop cracks in this type of test if held for more extended periods.

With all of the cold-cracking-test specimens that were welded under high-hydrogen conditions, bubble evolution was observed at such sites as inclusions, grain boundaries, and cracks. Evolution at inclusions and grain boundaries usually appeared as single bubbles evolving with rapid regularity. Bubble evolution along the length of growing cracks occurred usually with regularity but also as intermittent bursts of a multitude of small bubbles.

The intermittent bursts of bubbles from near a crack-tip can be explained by the Troiano model for hydrogen-embrittlement.[56] According to this model, nascent hydrogen in the matrix of the embrittled metal diffuses to regions of triaxial stress associated with a stress riser. When the hydrogen concentration in the stressed region reaches a critical amount, atomic bonds break, causing either the formation of a new crack or the extension of an existing crack. Figure 45 is a schematic illustration of how the Troiano model can be used to explain the intermittent bursts of bubble evolution observed in this investigation. As is apparent in Figure 45, the bursts of bubbles at the tip of a crack correspond to the release of the built-up hydrogen as the crack extends.

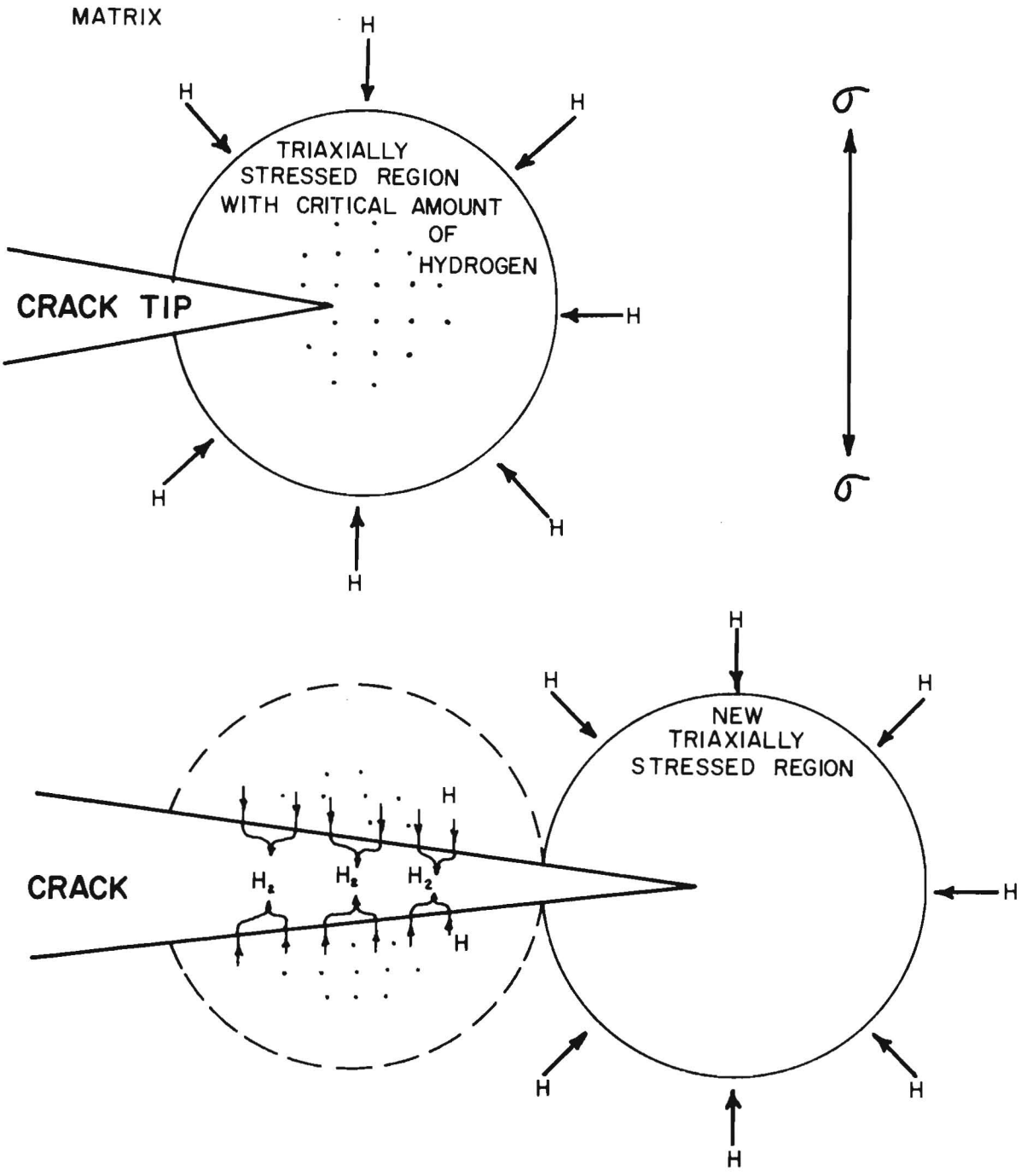

Figure 45 Schematic Illustration of the Probable Mechanism Producing the Intermittent Bursts of Hydrogen Observed During Delayed Cracking.

The Nucleation of Heat-Affected-Zone Cracks by Sulfide Inclusions. Table IX indicates that true-heat-affected-zone cracking, although occurring in both heats of HY-80 steel, was less extensive in Heat N than in Heat P. In both heats of HY-80 steel, elongated sulfide inclusions, in combination with dissolved hydrogen, appeared to be associated with cracking in the true-heat-affected zone. Typical examples of this association of sulfides and true-heat-affected-zone cracking are shown unetched in Figure 46. The fact that Heat N had less elongated sulfides than Heat P would account for the fewer cracks nucleated in Heat N.

Figure 47A shows an excellent example of cold-crack nucleation by a typical elongated sulfide in the heat-affected zone of a bead weld in a specimen from Heat P. Figure 47B is an over-enlargement of the same sulfide made for general viewing only. In this specimen, the principal stress direction was transverse to the banding. Note in Figure 47 that the cracks were nucleated at the acute edge of the inclusion where the stress concentration was undoubtedly higher. Although the cracks did not propagate beyond the extent shown in Figure 47, hydrogen bubble evolution was observed to continue for several hours in a periodic fashion from a site along the inclusion-matrix interface near the acute edge of the inclusion. The site of bubble evolution was probably a separation of the

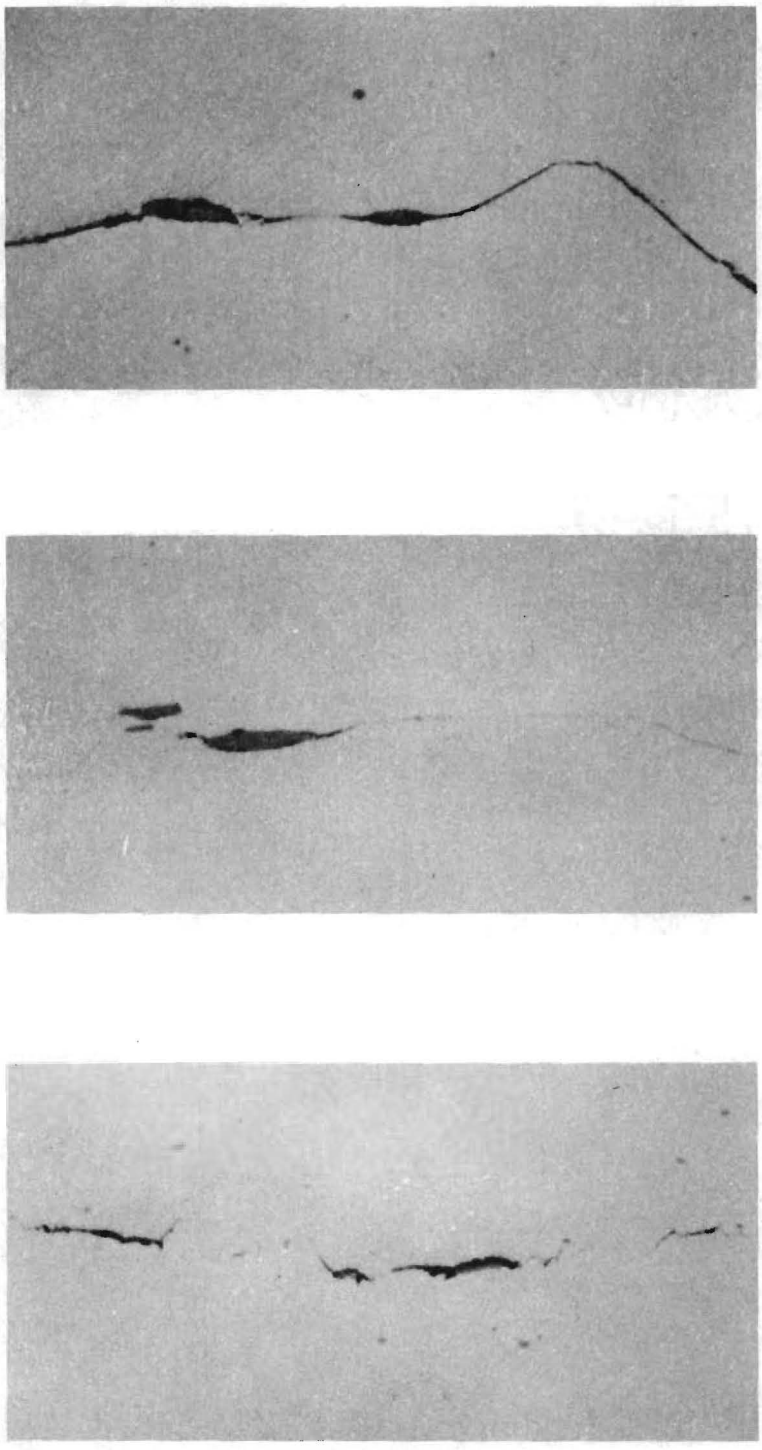

Figure 46 Examples of Sulfide Inclusions Along Cracks in the Heat-Affected Zone of a Cold-Crack-Test Specimen Welded Under High-Hydrogen Conditions. Polished and Unetched, 1000X.

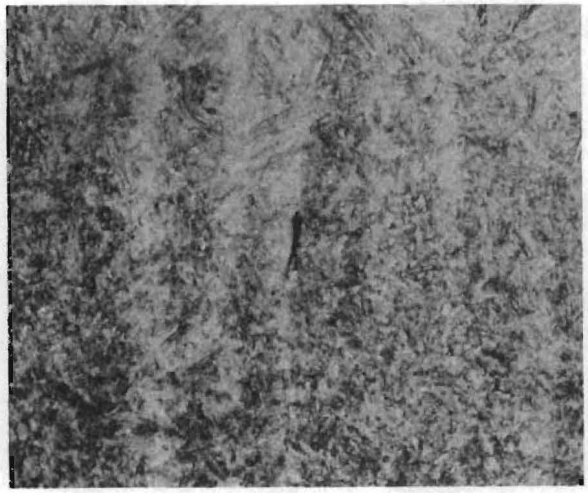

A.

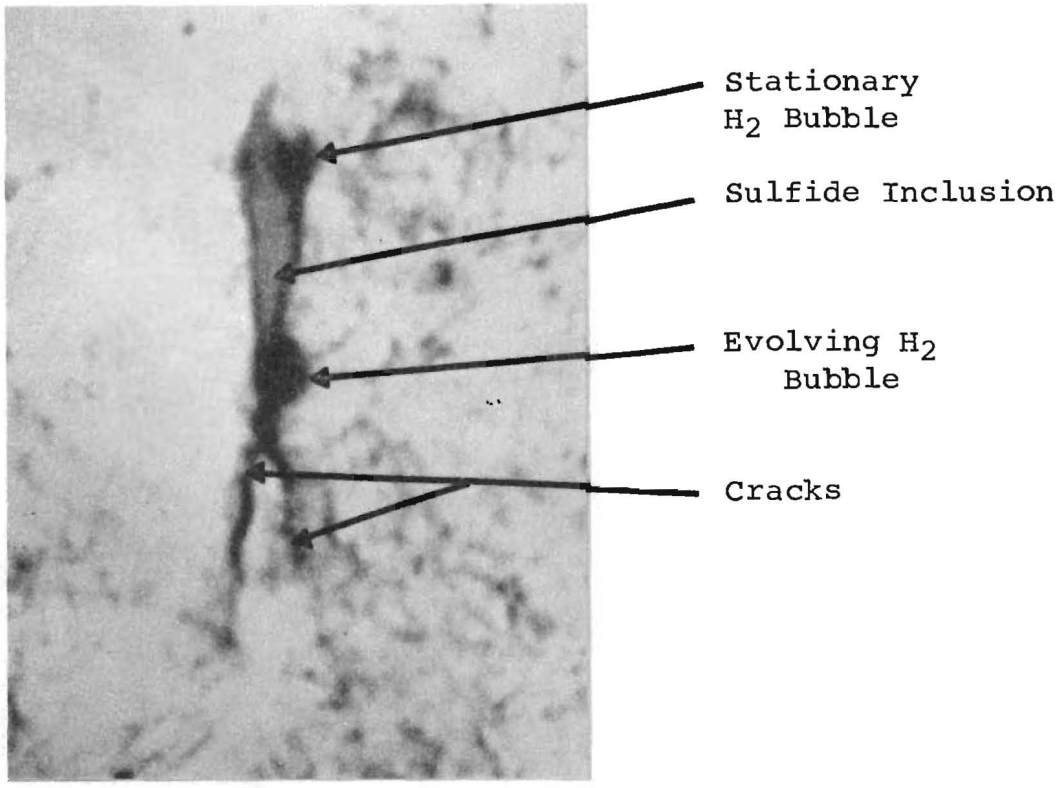

B.

Figure 47 Example of Crack-Nucleation by a Sulfide Inclusion in a Bead Weld in Heat No. 72P305. Nital Etchant. A. View of an Inclusion in the Heat-Affected Zone, 250X. B. An Over-Enlargement of the Same Inclusion, Approximately 2100X.

inclusion-matrix interface. Such a separation could be a result of the loss of cohesion due to a hydrogen-sulfur reaction at the inclusion-matrix interface.

The recognition that sulfide inclusions can cause crack formation is by no means novel. For example, Randall, et al.[57] showed that a difference in hot-cracking sensitivity between two similar heats of a constructional alloy steel could only be accounted for by a difference in the size and distribution of the sulfide inclusions. Similarly, Masubuchi and Martin[23] were concerned with the effect of sulfides on the high temperature properties of HY-80 steel. On the other hand, Berry and Allen[58] mentioned that inclusions (and segregational effects such as banding) can be a very important cause of cold-cracking in the heat-affected zones of welds in low-alloy steels.

In addition, the fact that an increase in the volume fraction of sulfides can cause a corresponding decrease in the notch toughness of heat-treated steels has been clearly shown by Hodge et al.[59] Similarly, Wei[60] has shown that an increase in the sulfur content causes a decrease in the K_{Ic} in ultrahigh-strength steels. Spitzig[61] has presented more detailed description of the role of the sulfur content in the fracture toughness of ultrahigh-strength steel.

With the obvious importance of sulfides in the fracture of heat-treated steels, it is rather surprising that almost all of the published research on the problem of cracking in HY-80 steels seems to have completely underestimated the role of sulfides in the initiation of cold cracking in the heat-affected zone of welds. In HY-80 steel, sulfide inclusions in combination with hydrogen would probably be especially effective crack initiators in the heat-affected zone because they could be surrounded by a microstructure of untempered martensite.

The results of this investigation suggest that the size and shape of the sulfides can influence the nucleation of cold cracks in different heats of HY-80 steel even though the volume fraction of the sulfides in the heats is about the same. It can be argued that the amount of hydrogen necessary to cause a sulfide inclusion to become a crack initiator is a function of how effective the inclusion is as a stress riser. Large, thin ellipsoidal sulfide inclusions would be extremely effective in nucleating cracks in the heat-affected zone of welds in HY-80 steel. Furthermore, such large, flat sulfide inclusions would be more effective than globular inclusions in pinning moving grain boundaries in the true heat-affected zone during welding. If prior-austenite grain boundaries become aligned with elongated sulfides, an especially effective crack

initiation site would result because hydrogen could arrive at the triaxially stressed region more readily via the grain boundary. In other words, the grain boundary could then serve as a "pipeline" tapping sources of hydrogen relatively far removed from the stress riser. Furthermore, the grain boundary could serve as a barrier to dislocations, which could then either dump hydrogen at the grain boundary or serve as "secondary pipelines" for hydrogen diffusion. In fact, the probable ease of hydrogen diffusion along grain boundaries may account for the predominance of intergranular cold cracks.

The newer quenched and tempered steels being developed have very low sulfur contents (0.003 to 0.009%) and apparently improved weldability.[62] Such steels probably have a lower susceptibility to cold cracking than HY-80 steel because of a lower volume-fraction of sulfides. However, even with such low sulfur contents, the nature of the sulfides in some heats could be deleterious. For example, Randall et al.[48] have reported that in a heat of ultrahigh-strength steel, with a sulfur content of 0.007 percent, the stringered nature of the sulfide inclusions was responsible for the heat having poorer bend-ductility than another heat of the same material in which the sulfides were not in a stringered form. Similar stringered sulfide distributions could occur in the newer quenched and tempered steels. Consequently, if the sulfide distribution

is not otherwise controlled, certain heats of the new steels could be susceptible to cold cracking in the presence of hydrogen in spite of their low sulfur contents.

Another factor that could influence the role of sulfides is that in the inner-regions of the heat-affected zone, nearer to the fusion boundary, the cohesion of the inclusion-matrix interface of sulfides may be significantly lower due to the very high temperatures attained. Such an occurrence has been suggested by Boniszewski and Baker[47] who noted that sulfide inclusions in the heat-affected zone of a weld in a ferritic steel were easy to extract, whereas sulfides in the unaffected base metal were difficult to extract. A substantial change in the cohesion of the inclusion-matrix interface of sulfides near the fusion boundary could allow the welding stresses to pull the matrix away from the inclusion providing a void sufficient in size to become a hydrogen trap thereby resulting in a more effective crack initiator. Boniszewski and Moreton[63] have proposed that hydrogen traps resulting from the separation of inclusions from the matrix during plastic deformation may retard hydrogen diffusion from steel at room temperature.

The Influence of Banding on Heat-Affected-Zone Cracking. The orientation of the bands in the specimen with respect to the principal stress direction had a considerable effect on the degree of cold cracking in the true heat-affected zone. After repolishing and etching with the two-stage procedure, all true heat-affected zone cracks in the specimens in which the banding was transverse to the stress direction were observed to be within light-etching alloy-rich bands, as exemplified in Figure 48. Although several of the longer cracks had crossed over to adjacent parallel light-etching bands, the cross-over locations were generally at ends of dark-etching bands or where the dark-etching bands were relatively narrow. However, the cracks in Heat N also generally appeared to be shorter than in Heat P indicating that cracks did not propagate as readily in Heat N. The reason for the low propensity for crack propagation in Heat N is not obvious but could be related to the somewhat lower strength of Heat N (see Table IV) which, in turn, would result in a less-sharp crack-tip in specimens from Heat N.

On the other hand, in the specimens in which the bands were parallel to the stress direction, true heat-affected-zone cracking was virtually eliminated. Heat N had no cracks and Heat P had two cracks. Figure 49A is a photomicrograph made during testing which shows one of the cracks in Heat P

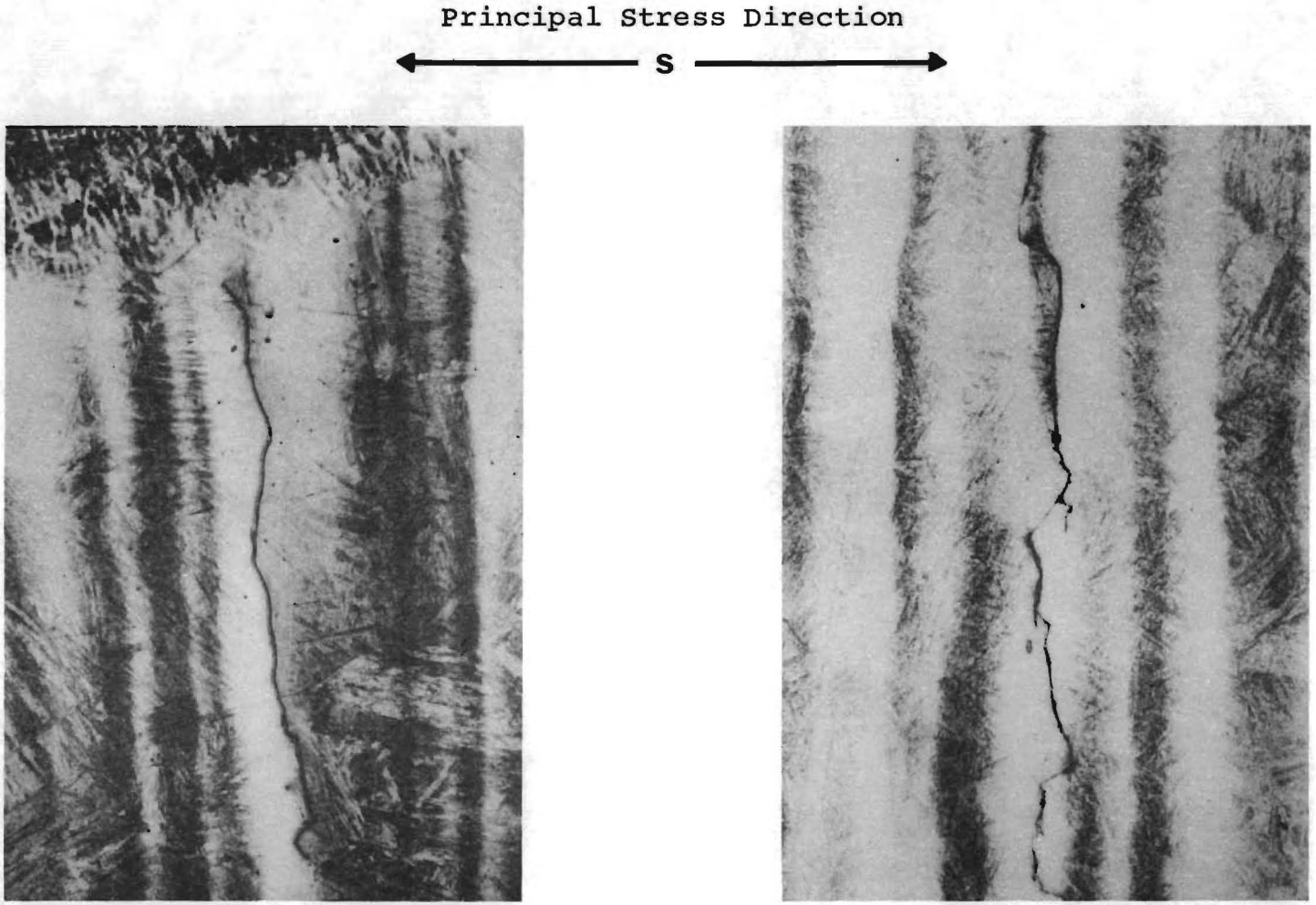

Figure 48 Examples of True Heat-Affected Zone Cracks Along Light-Etching Bands in the Cold-Cracking Test Specimen From Heat No. 72P305 Welded Under High-Hydrogen Conditions. Nital and Sodium Bisulfite Procedure, 250X.

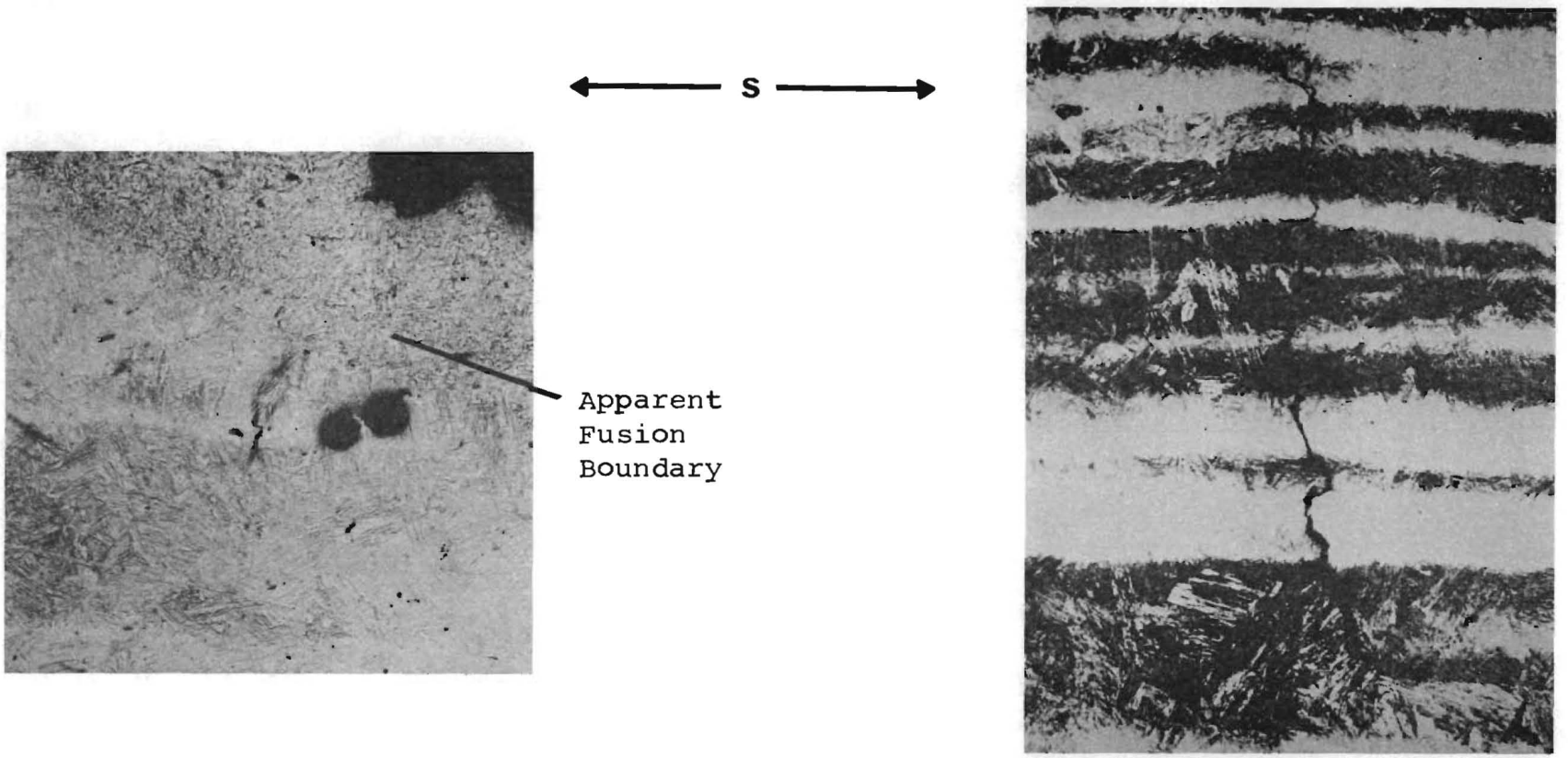

Figure 49 Examples of True Heat-Affected Zone Cracks in a Cold-Cracking Test Specimen From Heat No. 72P305. The Banding Was Parallel to the Stress Direction. A. A Crack Soon After Nucleation in a Light-Etching Band (the Black Specks are Dirt on the Oil Film). Nital Etchant, 250X. B. A Crack With Propagation Stopped in Dark-Etching Bands. Nital and Sodium Bisulfite Procedure, 500X.

soon after being nucleated in a light-etching band. The other crack in Heat P is shown in Figure 49B after repolishing and etching with the two-stage procedure. Note in Figure 49B that both ends of the crack were arrested in a dark-etching band. This observation suggests that cracks become severely blunted upon entering alloy-lean bands which are probably relatively tough. Also, the low incidence of cracking in specimens with the parallel banding-to-stress orientation is in agreement with the observation that elongated sulfides are the primary cause of crack nucleation. With the parallel orientation, it is expected that elongated sulfides, being parallel to the stress direction, are less effective as stress risers and thus crack nucleation is considerably reduced or essentially eliminated.

Cracking Associated With the Fusion Boundary. As shown in Table IX, the specimens from both Heat N and Heat P which were welded under high-hydrogen conditions, and with the planes of banding transverse to the stress direction, exhibited some degree of cold cracking associated with the fusion boundary. The type of crack which was generally predominant was the type that was observed to nucleate at or near the apparent fusion boundary and developed into a macrocrack by propagating into the heat-affected zone preferentially along the light-etching bands. One example of the development of

this type of cracking, in a specimen from Heat P, is shown in Figure 50 by a sequence of photomicrographs at 50X. A second example, also in a specimen from Heat P, is shown in Figure 51. The largest crack in Figure 51 developed after the fusion boundary crack linked with a crack that nucleated in the true heat-affected zone. An example of the development of cracks from the fusion boundary in a specimen from Heat N is shown in Figure 52. Note that Figures 50, 51 and 52 all indicate that the cracking was delayed in nature and accompanied by the evolution of hydrogen bubbles which appear as solid black circles on the photomicrographs.

In a specimen from Heat P welded under high-hydrogen conditions but with the bands parallel to the principal stress direction, a few small fusion boundary cracks were observed during testing. However, repolishing the specimen for further examination resulted in the removal of these cracks which indicates the crack had been very shallow. The shallow nature of the cracks suggests that crack propagation across alloy-lean bands at the fusion boundary is relatively difficult. As discussed above, a similar observation was noted for the propagation of true heat-affected-zone cracks. A specimen from Heat N which was welded under high-hydrogen conditions and with the parallel banding-to-stress orientation exhibited no cracking at the fusion boundary.

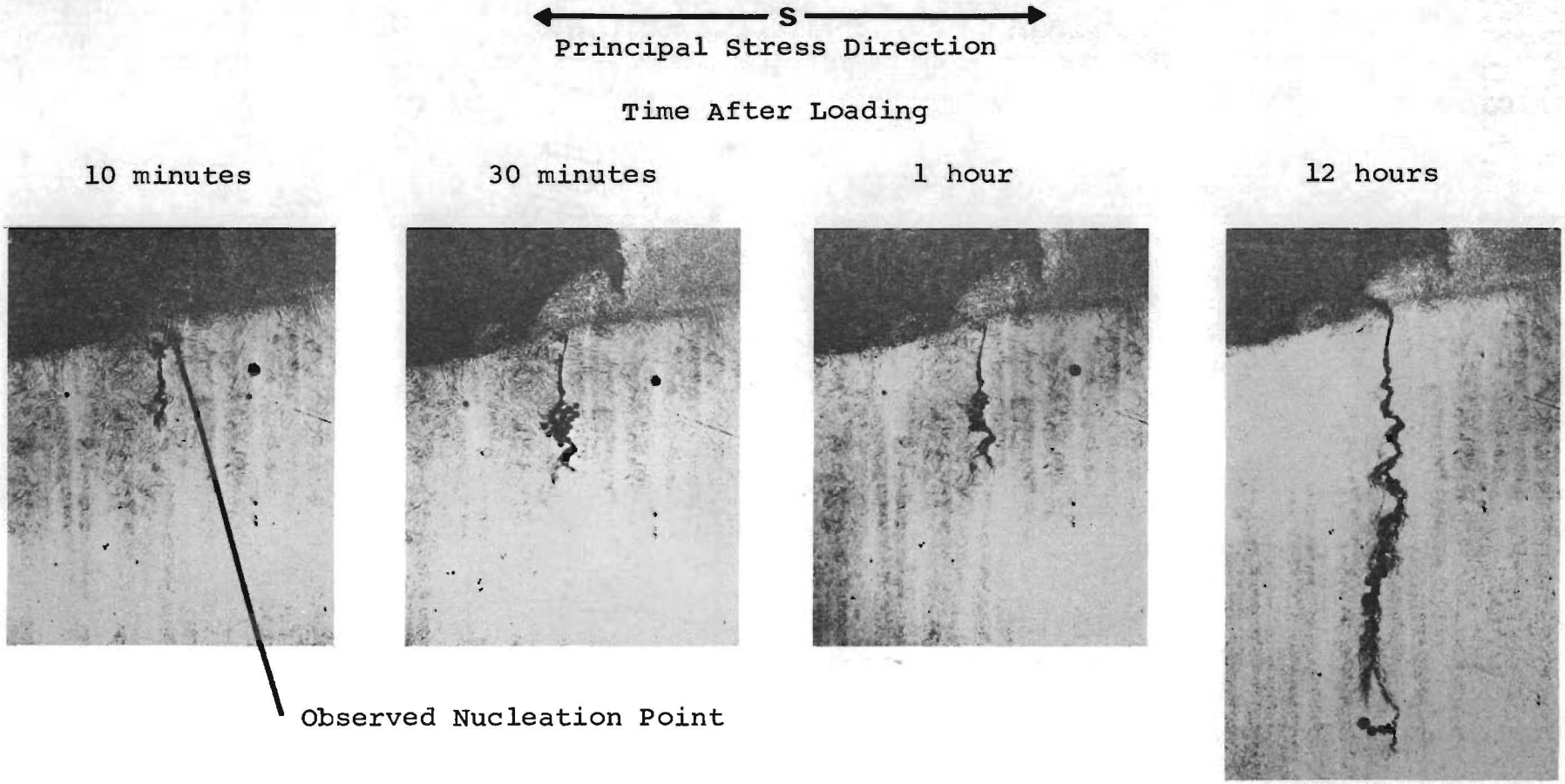

Figure 50 An Example of Delayed Cracking Nucleated at the Fusion Boundary in a Cold-Cracking-Test Specimen From Heat No. 72P305. The Black Area at the Upper Left Corner of the Photomicrographs is a Region Pulled Out During Separation of the Welded Specimens. Nital Etchant, 50X.

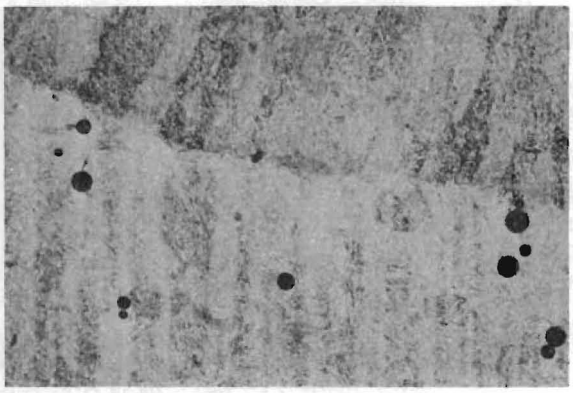

5 minutes

1 hour

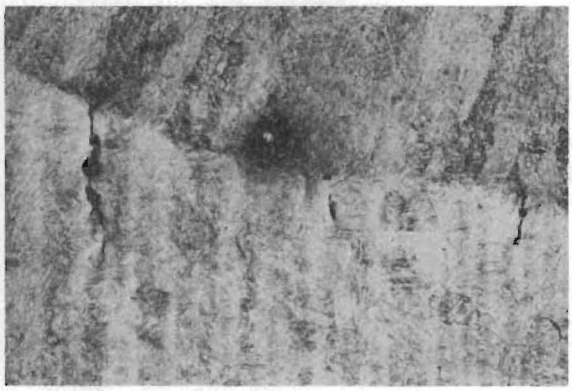

3 hours

6 hours

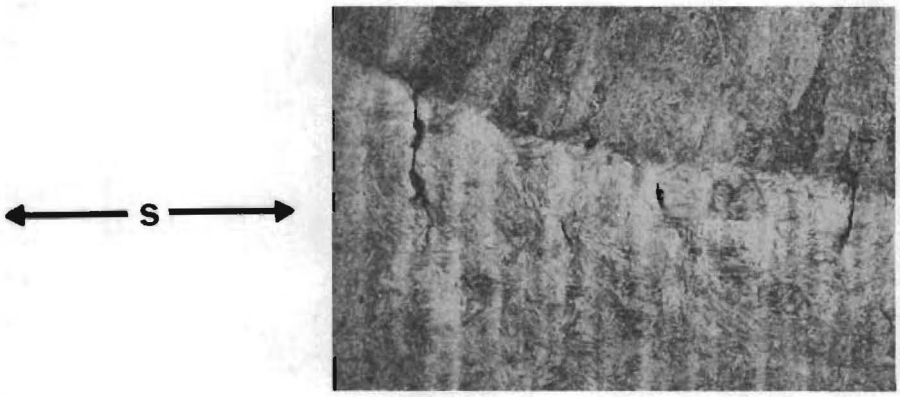

12 hours

Figure 51 Examples of Delayed Cracking Nucleated at the Fusion Boundary in a Cold-Cracking-Test Specimen From Heat No. 72P305. The Composite Region is at the Top in the Photomicrographs. Nital Etchant, 50X.

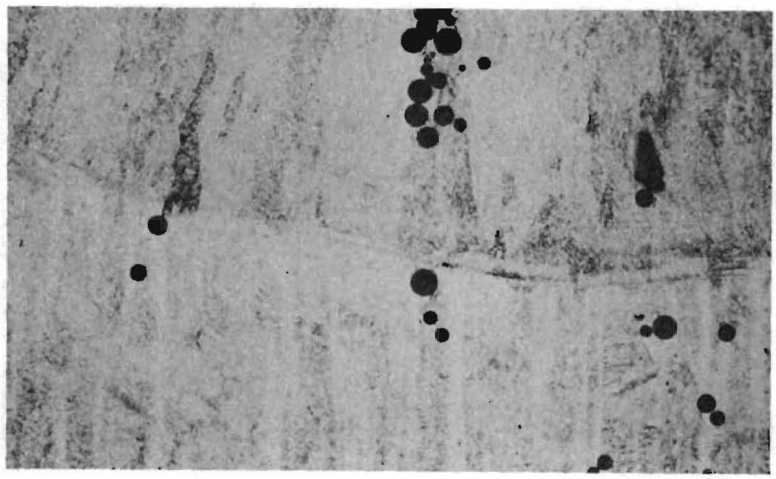

10 minutes

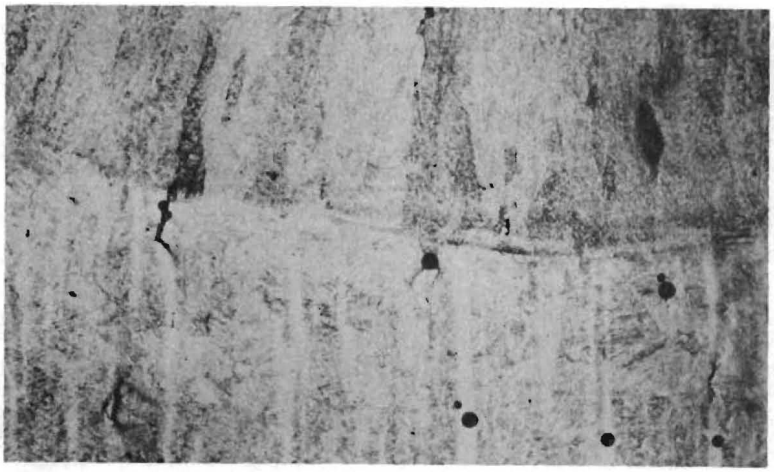

8 hours

Figure 52 Examples of Delayed Cracking in the Weld Metal, at the Fusion Boundary and in the Heat-Affected Zone of a Cold-Cracking-Test Specimen from Heat No. N51755. Nital Etchant, 50X.

It should be mentioned that a factor contributing to the lower incidence of cracking with the parallel banding-to-stress orientation is the low depth-to-width ratio of bead welds which in this investigation was nearly 1 to 6. This low depth-to-width ratio means that the number of bands intersecting the fusion boundary would be greater with the transverse banding orientation, hence, more opportunities for crack initiation sites to be present at the fusion boundary.

The examination of specimens after repolishing and etching with the two-stage procedure revealed that the cracking tentatively identified as fusion boundary cracking was indeed associated with both the unmelted zone and the partially-melted zone. Specific examples are shown in Figure 53. The nucleation of such cracks will be discussed in greater detail in the following subsection.

In a specimen from Heat P welded under low-hydrogen conditions and with a transverse banding-to-stress orientation, three locations exhibiting apparent hot cracking were also found. Two of these locations, both associated with alloy-rich bands, are shown in Figure 54. The cracks shown in Figure 54A are entirely within the unmixed zone and are clearly at substructure boundaries. The morphology of the cracks shown in Figure 54A are indicative of hot-cracking and not cold-cracking. The crack shown in Figure 54B has a striking resemblance to the

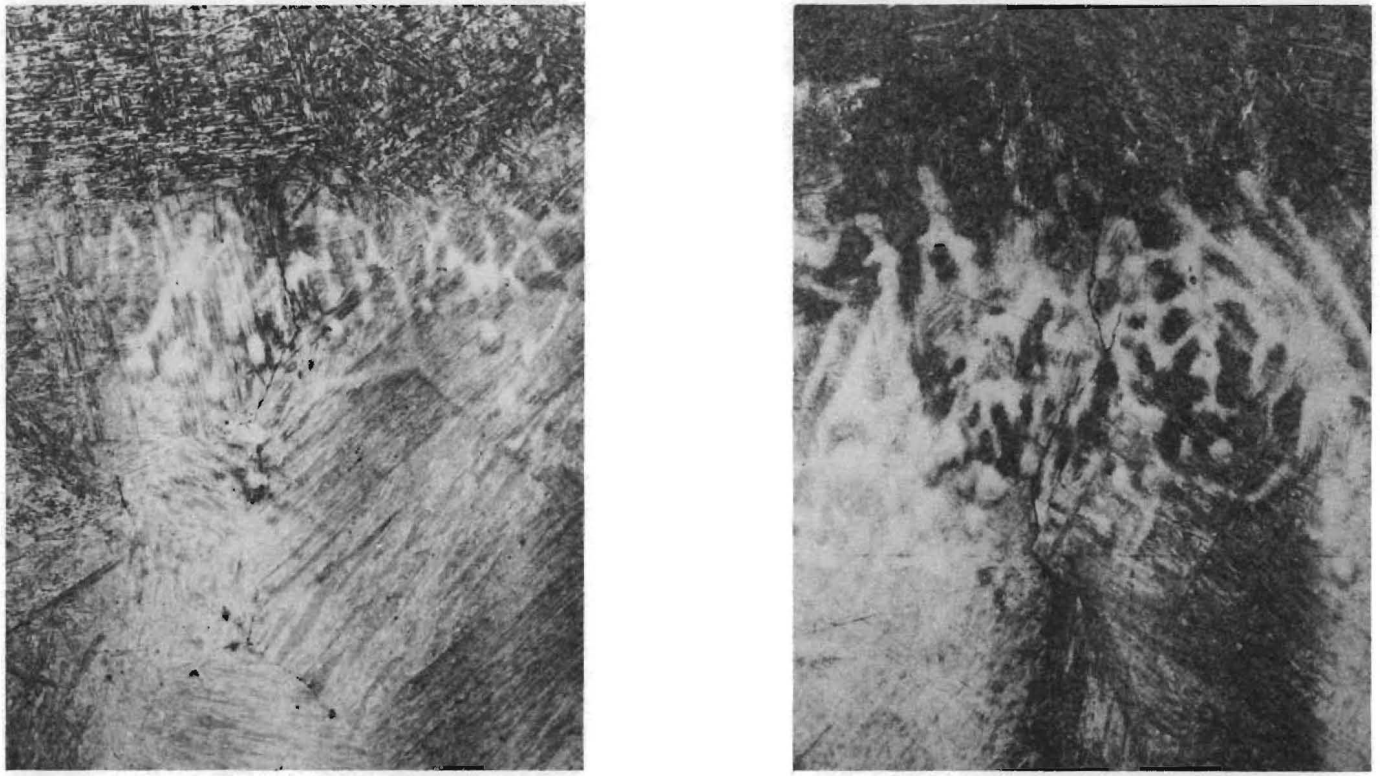

Figure 53. Examples of Cold Cracking Primarily Within the Unmixed and Partially-Melted Zones in a Cold-Cracking Test Specimen From Heat No. 72P305 With the Banding Transverse to the Stress Direction. Welded Under High-Hydrogen Conditions. Nital and Sodium Bisulfite Procedure, 1000X.

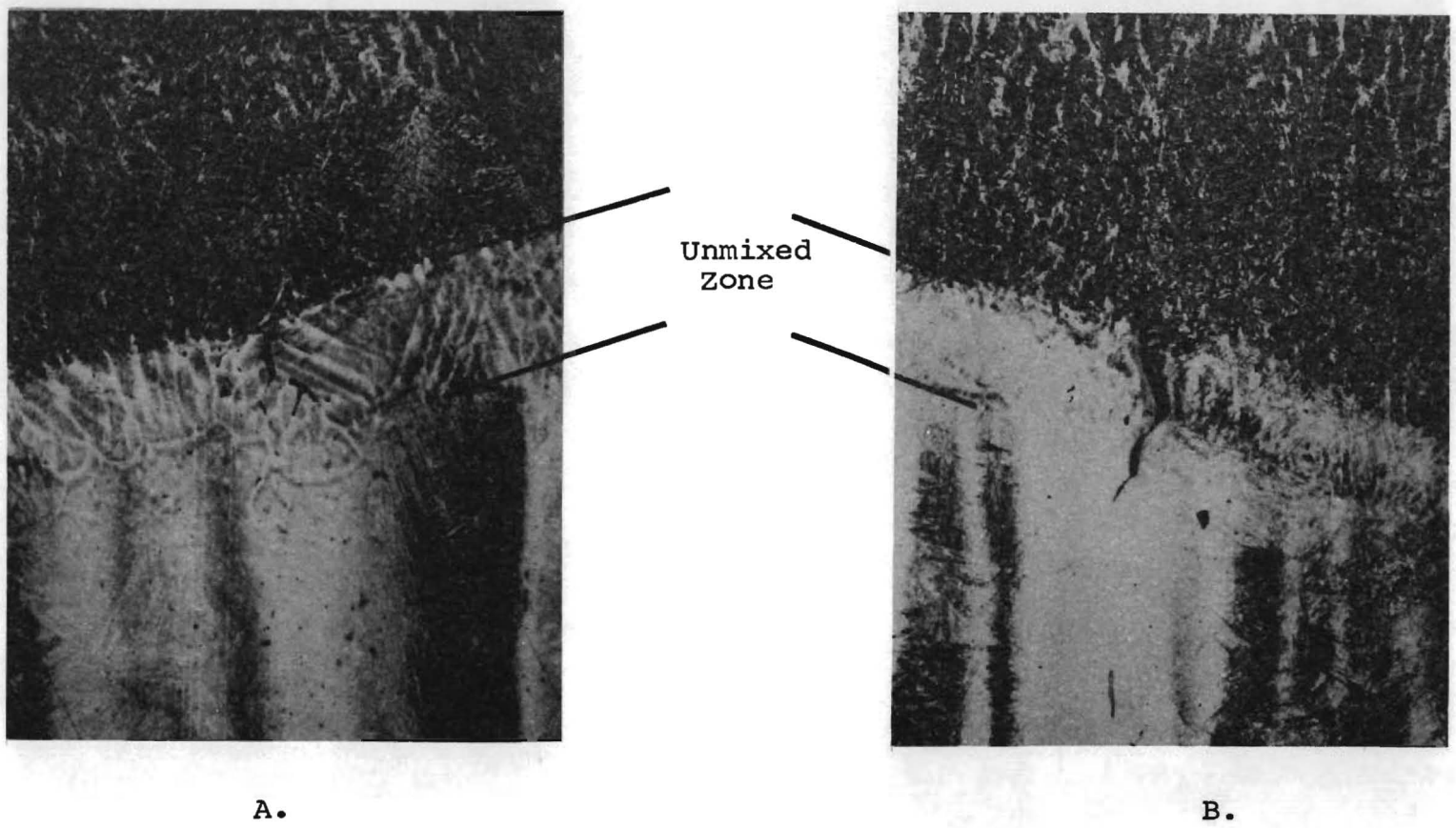

Figure 54 Hot-Cracks in the Unmixed Zone in a Cold-Cracking-Test Specimen From Heat No. 72P305 With the Banding Transverse to the Stress Direction Welded Under Low-Hydrogen Conditions. Nital and Sodium Bisulfite Procedure, 500X. A. Cracks at Substructure Boundaries. B. A Crack Similar to the Hot-Crack Shown in Figure 44.

hot crack that occurred in the Varestraint Test specimen, see Figure 44. Therefore, it is concluded that the cracks shown in Figure 54 are indeed hot cracks that occurred primarily within the unmixed zone during or shortly after welding and confirms the hot-cracking tendency of unmixed weld metal in Heat P. The fact that these cracks did not propagate significantly even though the specimen was held 12 hours under a load near the yield stress is undoubtedly the result of the low-hydrogen content of this specimen.

On the basis of these observations, it is concluded that hot-microcracking can occur in HY-80 steel but is probably limited to segregated regions in relatively rich-analysis heats. Furthermore, such microcracks could propagate at lower temperatures only if sufficient hydrogen is present. Therefore, hot-microcracking plays only a minor role in the overall cracking problem in HY-80 steels.

Nucleation of Cold Cracks in the Partially-Melted Zone. From the photomicrographs of cold cracking associated with the unmixed and partially-melted zones shown in Figure 53, the specific nucleation point of the cracks is not apparent. However, careful examination of the partially-melted zone in the specimen from Heat P, welded under high hydrogen conditions, revealed crack-embryos for which the nucleation point was quite obvious. For example, Figure 55A shows a crack-embryo associated

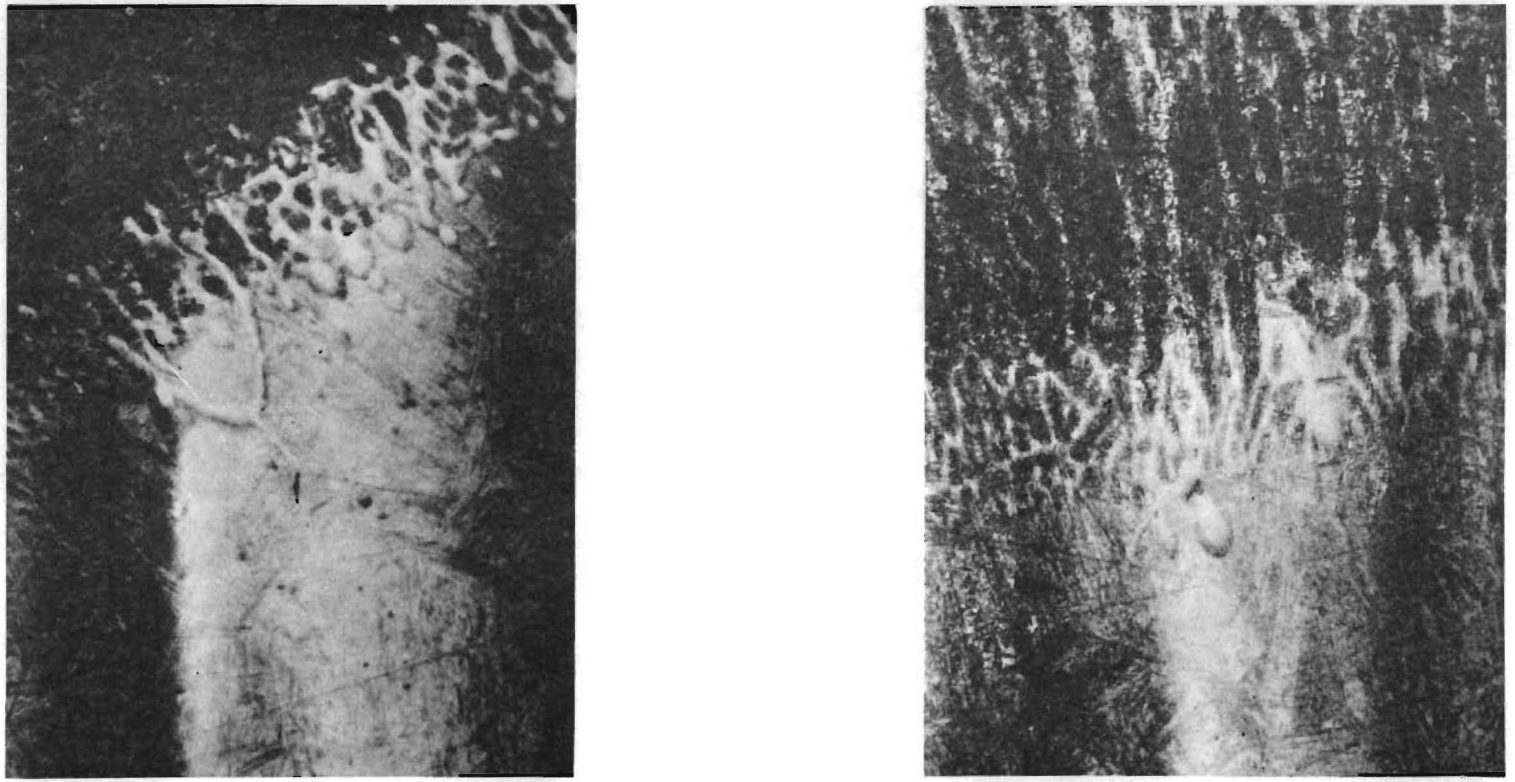

A. B.

Figure 55 Examples of Crack-Embryo in the Partially-Melted Zone of a Specimen From Heat No. 72P305 With the Banding Transverse to the Stress Direction Welded Under High Hydrogen Conditions. Nital and Sodium Bisulfite Procedure, 500X. A. Crack Nucleated at a Liquated Grain Boundary. B. Crack Nucleated at the Matrix-Inclusion Interface of a Sulfide in a Constitutionally Liquated Region.

with a liquated grain boundary. On the other hand, Figure 55B shows a crack nucleated by a very small sulfide which precipitated in a constitutionally liquated region. These two examples in Figure 55 prove conclusively that the phenomena contributing to partial melting, discussed in earlier subsections, can indeed be sources of cracking. Also, it is interesting to note that both of the cracks shown in Figure 55 occurred within alloy-rich bands, again emphasizing the role of solute segregation in the base metal.

A factor that aids a region of localized melting in eventually becoming a site for crack nucleation is the large difference in hydrogen solubility between liquid iron and either delta-iron or austenite. Because liquid iron can dissolve approximately three to four times more nascent hydrogen than the solid, the liquated grain boundaries, with hydrogen present, can serve as "pipelines" along which hydrogen can readily diffuse from the weld metal into the heat-affected zone. In addition, alloy-rich liquated regions probably solidify directly to austenite, which has a somewhat higher solubility for hydrogen than does ferrite. Therefore, the liquated boundaries, even after cooling to ambient temperatures, could be locations of high hydrogen concentration. In such cases, any rift, inclusion-matrix interface and/or stress riser in the vicinity of the liquated regions has a very immediate source of hydrogen which can catalyze crack propagation.

A Mechanism for Crack Nucleation in the Unmixed Zone. Crack nucleation in the unmixed zone may be largely a result of the redistribution of solute during solidification of the unmixed zone. This statement is based on the fact that almost every one of the usual alloying elements and impurity elements in steels such as HY-80 steel will segregate to grain boundaries and subgrain boundaries during solidification. Furthermore, each of these elements, with the exception of cobalt and aluminum, would lower the M_s temperature.[64] Therefore, the M_s at subgrain boundaries and/or solidification grain boundaries is undoubtedly lower than at the core of the subgrains. Upon cooling, transformation to martensite would first take place in the core of the subgrains. However, if the difference in the M_s between the boundary and the core is great enough, transformation would be "blocked" by austenite at the boundaries which is unable to transform until a lower temperature is reached. In fact, the boundaries may still be austenite at room temperature but comprise a very small volume fraction. The result of the interference with transformation is a structure which is finer in the unmixed zone than in either the partially-melted zone or the composite region.

Figure 56 shows evidence that this mechanism is a valid one. Note in this figure that in the unmixed zone, most of the platelets of low-temperature transformation product

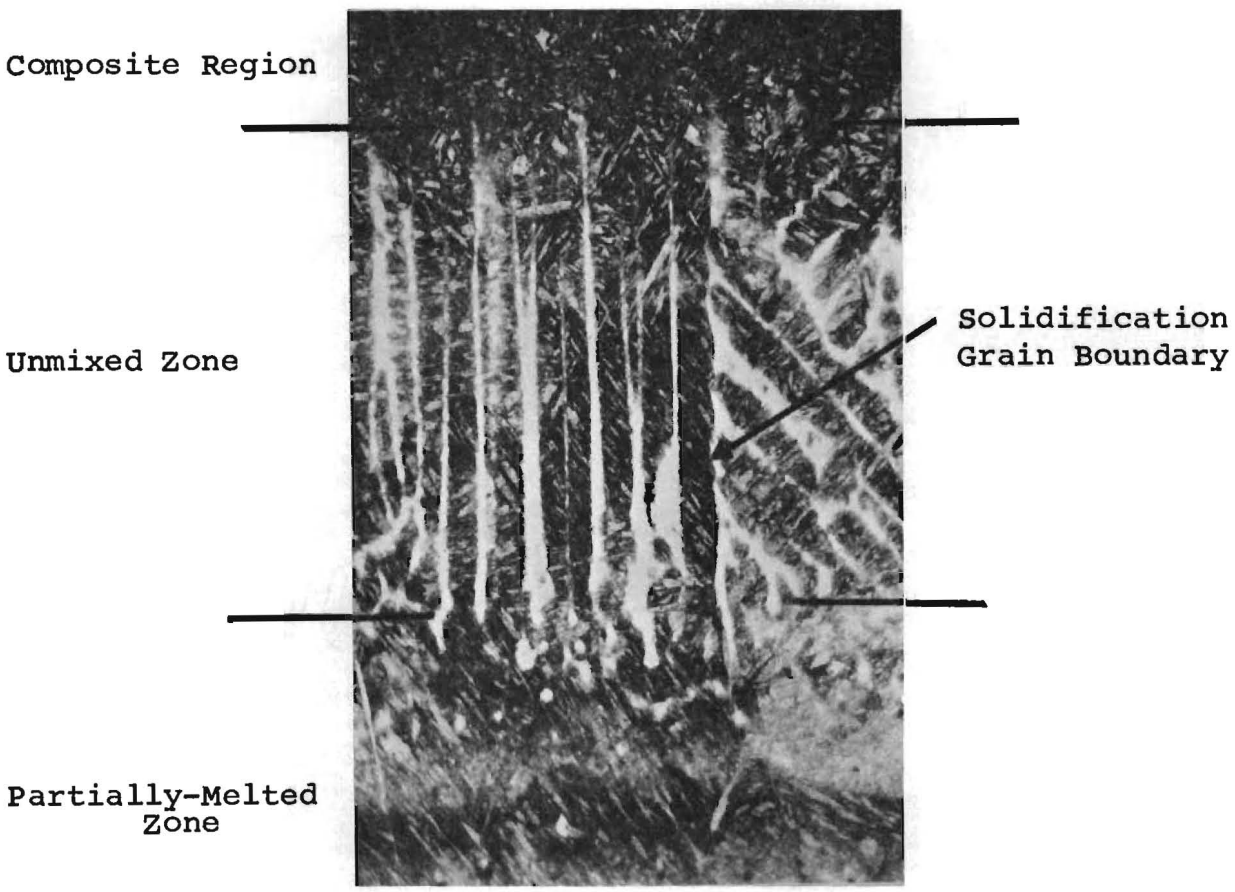

Figure 56 A View of the Unmixed Zone on a Transverse Section of a Bead Weld in a Specimen From Heat No. 72P305. Note the Predominance of Platelets of Low-Temperature Transformation Product Which are not Continuous Across Adjacent Cells. Nital and Sodium Bisulfite Procedure, 500X.

do not extend across subgrain boundaries or solidification grain boundaries. On the other hand, in the outer regions of the partially-melted zone, the products appear to have been less inhibited during transformation. In the composite region, the lower alloy content allowed for the formation of a significant amount of high-temperature transformation products.

It is not difficult to imagine that during cooling of a weld, the relatively early transformation of the composite region will force much of the dissolved hydrogen into the adjacent unmixed zone where it becomes further concentrated at late-transforming subgrain boundaries and solidification grain boundaries. Such locations would then be ideal sites for crack nucleation.

Also, the crack-susceptibility of the unmixed zone may well be influenced by the extent and configuration of the delta-ferrite region. It is envisioned that during solidification, the extent and configuration of the delta-ferrite region is influenced by the microsegregation arising from the solidification process. For example, Figure 57 is an idealized illustration of several adjacent cellular subgrains extending into liquid metal. For a low-alloy steel, it is expected that at the tip of the cells, which subsequently become the core of the cells, liquid solidifies directly to delta-ferrite. However, depending upon the type and amount of solute that

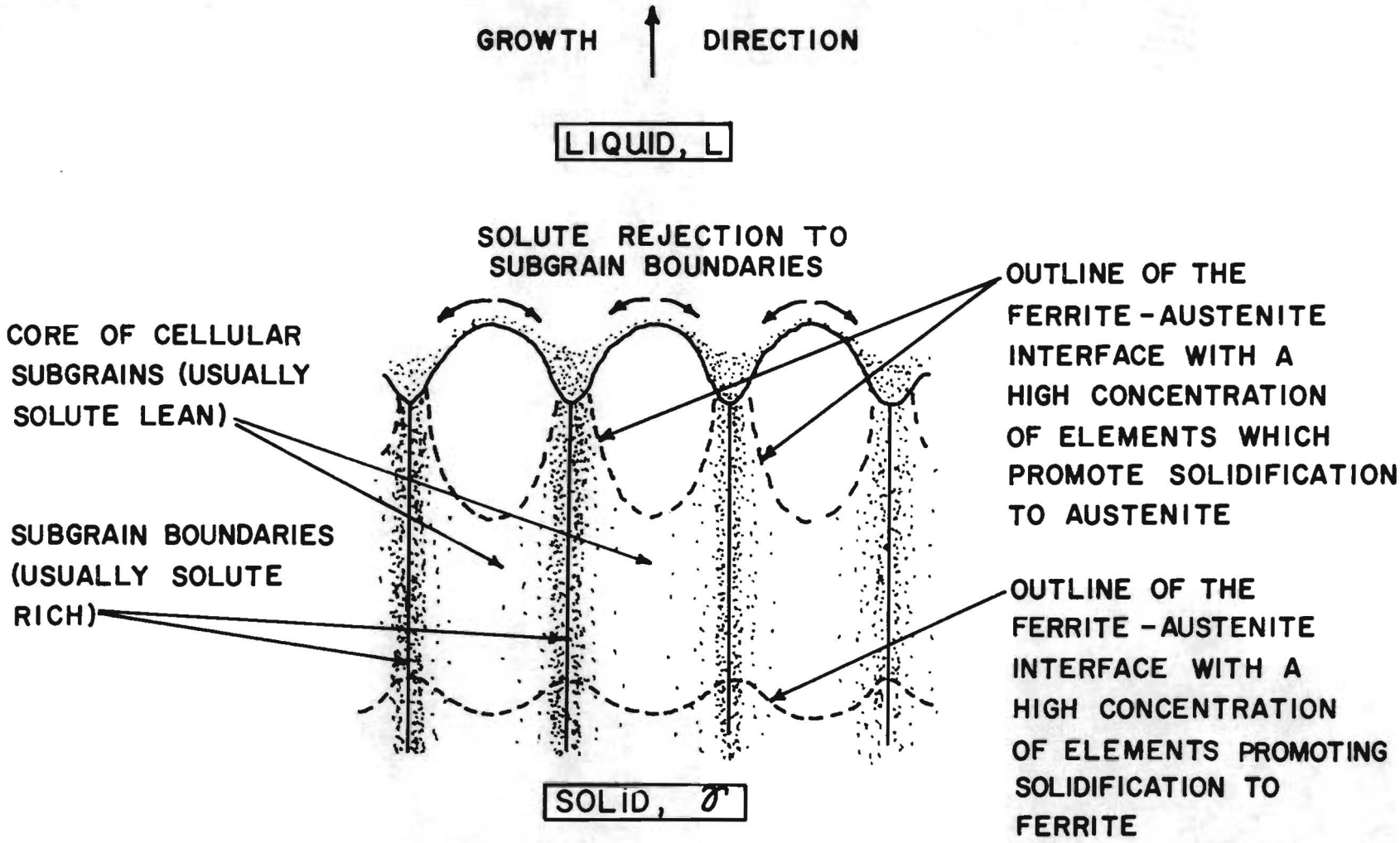
GROWTH
DIRECTION
LIQUID, L
SOLUTE REJECTION TO SUBGRAIN BOUNDARIES
CORE OF CELLULAR SUBGRAINS (USUALLY SOLUTE LEAN)
SUBGRAIN BOUNDARIES (USUALLY SOLUTE RICH)
OUTLINE OF THE FERRITE-AUSTENITE INTERFACE WITH A HIGH CONCENTRATION OF ELEMENTS WHICH PROMOTE SOLIDIFICATION TO AUSTENITE
OUTLINE OF THE FERRITE-AUSTENITE INTERFACE WITH A HIGH CONCENTRATION OF ELEMENTS PROMOTING SOLIDIFICATION TO FERRITE
SOLID, δ

Figure 57 Schematic Illustration of the Extent of the Delta-Ferrite Region Under a High Concentration of Elements Promoting Solidification to Austenite and Under a High Concentration of Elements Promoting Solidification to Ferrite.

becomes concentrated between the cell stalks, the liquid along the cell boundaries can solidify directly to austenite. In other words, the type and concentration of the solutes can determine whether only a portion of the cell-tip is delta-ferrite. Therefore, the solutes, which tend to be either ferrite-stabilizers or austenite-stabilizers, determine the extent and configuration of the delta-ferrite region. If conditions are such that the elements that promote solidification directly to austenite become sufficiently concentrated in the liquid between the stalks of the growing subgrains, the subgrain boundaries will solidify directly to austenite and not delta-ferrite. This situation is schematically shown in Figure 57.

Probably the only available approximation of the role of solutes in the solidification of HY-80 steel can be obtained by inspection of the iron-base binary diagram for each of the usual elements in this steel. Such a procedure was described in an excellent review by Borland.[9] From inspection of the binary diagrams, it can be assumed that high concentrations of carbon, manganese, nickel, and sulfur would tend to promote solidification directly to austenite. All other elements in HY-80 steel produce a binary with iron in which the dilute liquid solidifies directly to ferrite. The possibility of austenite at the subgrain boundaries is important

because austenite has a greater ability to dissolve hydrogen than does ferrite. Therefore, the conditions that produce austenite subgrain boundaries can thereby produce significant partitioning of the hydrogen in the solidified unmixed zone. Also, the stresses resulting from the transformation of delta-ferrite to austenite could account for the hot cracking at subgrain boundaries and solidification grain boundaries shown in Figure 53A.

Also, it should be noted that both the effect of subgrain boundaries (and solidification grain boundaries) on the low-temperature transformations and the effect of alloys on the local transformations of delta-ferrite would be greater with higher alloy contents (particularly with the solutes; carbon manganese, nickel, and sulfur). This would account for the observation in this investigation that fusion boundary cracks consistently occurred at locations where alloy-rich bands intersected the fusion boundary because such locations would be even richer in those elements. In fact, in the rich-analysis heats of HY-80 steel, the crack-susceptibility of such locations would be extremely high.

Cracking in the Cruciform Test

A preliminary metallographic examination of the sample taken from a cruciform test specimen revealed the presence of one macrocrack under fillet weld C. Under commonly-used

super-picral etchant, this crack appeared to be almost exclusively within the heat-affected zone immediately adjacent to the fusion boundary. This location of the cracking is typical for cruciform tests of low-alloy steels.

However, when the sample was repolished and etched with either ammonium persulfate etchant or the two-stage nital and sodium bisulfite procedure, much of the intergranular crack-path was observed to pass through the unmixed zone and the partially-melted zone. For example, Figure 58A shows a typical digression of the crack-path into the unmixed zone. Figure 58B shows typical crack branches into the unmixed zone.

Therefore, these results indicate that it is inaccurate to assume that cracking in the cruciform test is primarily heat-affected-zone cracking. On the contrary, the evidence indicates that cruciform cracking is significantly associated with both the unmixed zone and partially-melted zone of the fillet weld. Furthermore, this observation can explain the fact that Heat P showed a higher crack susceptibility than Heat N in both the Varestraint tests conducted by Bell[55] (autogenous welds) and the cruciform tests conducted by Rathbone and Gross[22] (heterogeneous welds).

The fact that cracking in the cruciform tests can be associated with the unmixed and partially-melted zone does not necessarily detract from the usefulness of the cruciform test

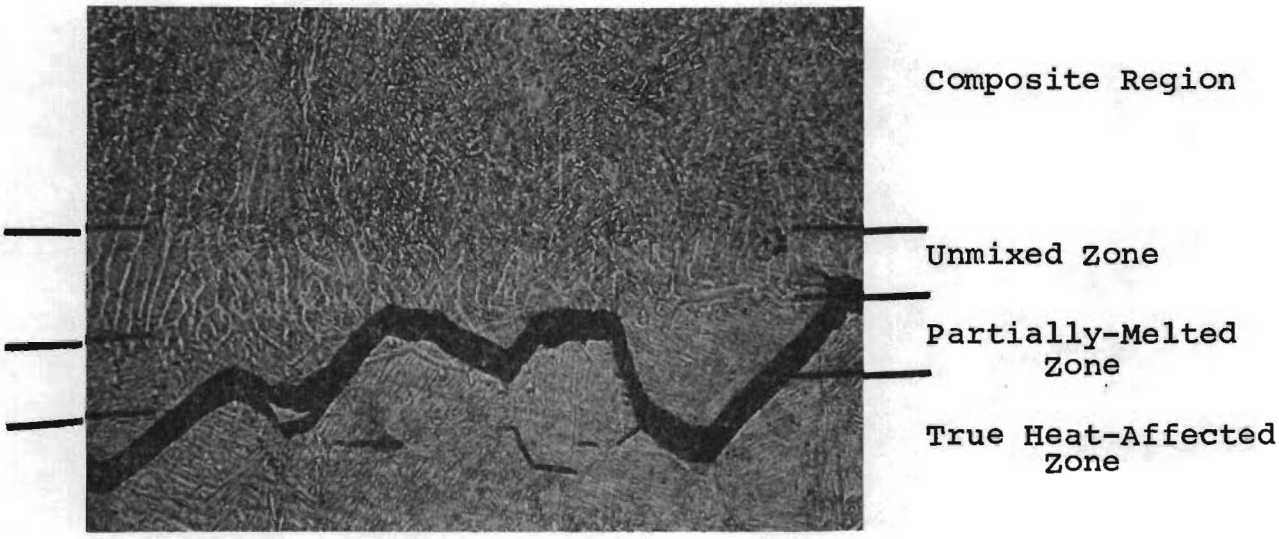

A.

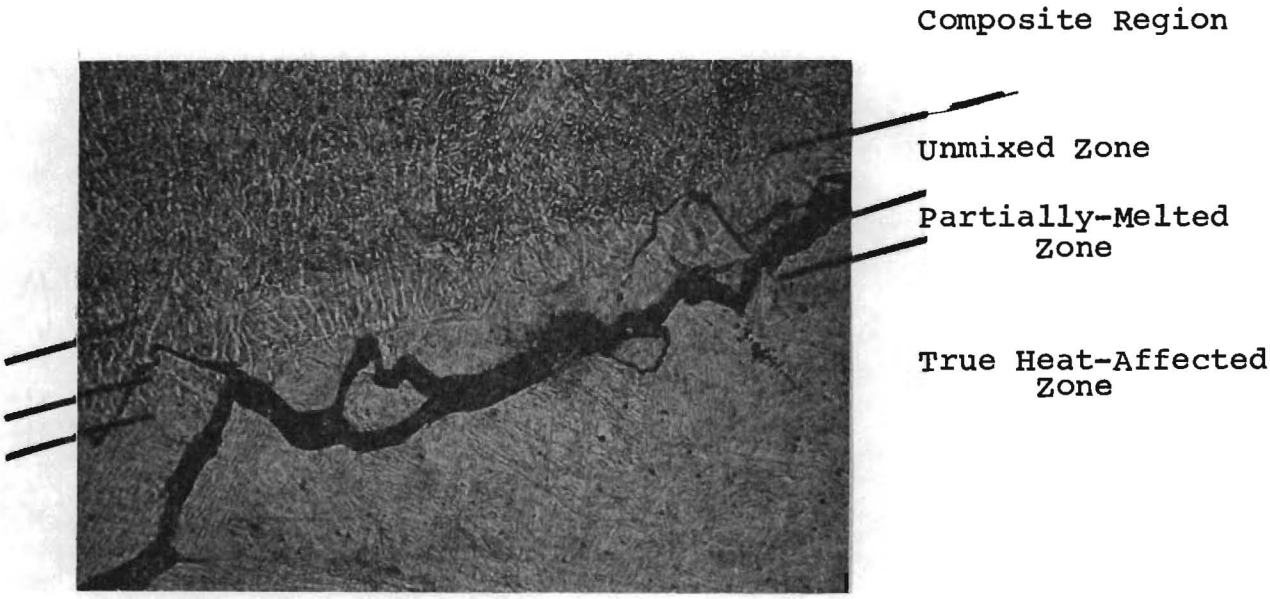

B.

Figure 58 Views Along the Macrocrack Under Fillet Weld C on a Transverse Section of a Cruciform Test Specimen of HY-80 Steel. Ammonium Persulfate Etchant, 250X. A. A Digression of the Crack-Path into the Unmixed Zone. B. Crack-Branches into the Unmixed and Partially-Melted Zones.

in evaluating base-metal weldability. However, comparisons should be avoided between cruciform test results and results of tests in which only the true heat-affected zone is tested.

A New Approach to the Understanding of Cold Cracking in Welds

From the results of this investigation, a new approach to the understanding of cold cracking of welds in quenched-and-tempered low-alloy steels can be formulated. This approach incorporates the following basic premises, the details of which have been discussed above:

1. In heterogeneous welds, the junction between the composite region and the true heat-affected zone is not simply a "fusion line" but, in fact, a complex region consisting of two distinct narrow zones which can be called the unmixed zone and the partially-melted zone. The various phenomena that occur within these zones can contribute significantly to the nucleation of cracks. However, the more common metallographic procedures presently in use do not reveal these zones.
2. In the heat-affected zone, the microstructure primarily affects the propagation of cracks which are chiefly nucleated either by sulfide inclusions or by conditions resulting from sulfide inclusions. However, the nature of the inhomogenieties in the

base metal, produced when the ingot solidifies, greatly influences both crack-nucleation and crack-propagation. In other words, the weldability of plates from a given ingot of low-alloy steel is to some degree "cast into the steel" and normal variations in the processing of the ingot alter it very little. The factors influencing the weldability appear to be:

a) the degree of segregation that occurs during the solidification of the ingot and becomes manifested as banding in the final product;

b) the size, shape, and distribution of the sulfide inclusions.

It is very important to note that the nominal composition obtained by a usual check analysis reveals no information about either of these two factors.

3. Hydrogen is the catalyst for the initiation as well as the propagation of cold cracks. Although, under certain conditions, a small amount of hot-microcracking may occur in welds in low-alloy steels, the presence of dissolved hydrogen is essential for the propagation of these microcracks in the cold condition.

Applying these premises to the observations and results of previous investigations into the problem of cracking in HY-80 steel results in a surprisingly coherent picture.

For example, the influence of banding and elongated sulfide inclusions can explain some of the observations of Griffin[24] who reported a type of heat-affected-zone cracking which was associated with a weakness of the material in the direction perpendicular to the plane of rolling. Also, Masubuchi and Martin[23] stated that the results of metallographic examinations of weldments showed that microcracks in fillet welds tended to be parallel to the surface of the plate. However, Masubuchi and Martin also reported that there did not appear to be any relation between the location of the bands and the location of cracks in the heat-affected zone of welds in HY-80 steel in that some of the cracks they observed were in line with bands and others were not. With regard to this observation, it should be pointed out that a crack generally follows a direction transverse to the principal stress direction. For example, it has been observed in this investigation that cracks can nucleate in alloy-rich bands and extend transverse to the banding because of the dictates of the imposed stress. Furthermore, the location of a crack in a random section is not as significant as its point of nucleation and the actual nucleation point of a crack in usual

metallographic sections is evident only fortuitously. In addition, Masubuchi and Martin did not have the benefit of an etchant such as the two-stage nital and sodium bisulfite procedure used in this investigation which clearly delineates banding in metallographic samples of HY-80 steel.

By equating low sulfur content with low sulfide content the approach of this investigation can account for the relationship between low sulfur content in HY-80 steel and low crack-susceptibility as documented by Rathbone and Gross,[22] Masubuchi and Martin,[23] and Emmanuel et al.[25] (also, in the investigation by Interrante and Stout,[25] vacuum-melted crack-resistant heats of HY-80 steel had low sulfur contents). But even more important than volume fraction, differences in the nature of the sulfides may explain some of the scatter in the correlation between crack susceptibility of heats of HY-80 steel and the sulfur and nickel contents which was shown in the study by Rathbone and Gross.[22] Furthermore, the mechanisms shown in the present investigation, such as constitutional liquation, grain boundary wetting, etc., clearly account for the possible segregation of sulfur in a manner consistent with the arguments of Duvall and Owczarski[3] who rejected the hypothesis that in welds, sulfur segregates at elevated temperatures by either equilibrium segregation or by a grain boundary "sweeping" action.

The recognition of constitutional liquation of sulfide inclusions in HY-80 steel can account for the triangular and lenticular sulfides observed by Ledman et al.[20] above the nil-ductility temperature in Gleeble tests of heats of HY-80 steel. Investigation of sulfide inclusions in as-polished samples or those etched with Norens etchant did not reveal what was probably constitutional liquation of sulfide inclusions. Similarly, constitutional liquation would also account for the changes in sulfide distribution in Gleeble specimens noted by Emmanuel et al.[25]

The presence of an unmixed zone and a partially-melted zone can clearly account for the particular location of microcracking (just below the apparent fusion boundary) documented by Masubuchi and Martin[23] and Emmanuel et al.[25] Furthermore, the unmixed zone may be an important common factor in explaining why the relative behavior of two heats of HY-80 steel was the same in both the cold-cracking tests conducted by Rathbone and Gross[22] and the autogenous-weld-metal hot-cracking tests conducted by Bell.[55]

Also, the hypothesis that crack nucleation at the fusion boundary is related to the redistribution of solute during the solidification of the unmixed zone and that carbon, manganese, nickel, and sulfur are particularly detrimental is consistent with both the results of Rathbone and Gross[22]

(who found a correlation between cracking and the nickel and sulfur contents) and Interrante and Stout[27] (who showed a relationship with the carbon equivalent of the base metal). Furthermore, the results of this investigation further suggest that the nominal concentrations would not be as indicative of crack-susceptibility as would the average concentration within alloy-rich bands (as could be obtained by electron-beam microanalysis).

The higher effective segregating effects associated with the solidification of the unmixed zone and the partially-melted zone, described in this study, can account for the rapid increase in crack-susceptibility with relatively small increases in alloy content (within the specified ranges) of such elements as sulfur, nickel, carbon, and manganese.[22,27]

With respect to the influence of hydrogen on cold cracking, the results of this investigation are consistent with the results of Interrante and Stout[27] who showed that the susceptibility to delayed cracking in HY-80 steel was proportional to the hydrogen content of the welding atmosphere.

Although the results of this investigation have also shown that microcracks can initiate without the presence of hydrogen, such microcracks probably occur only in HY-80 steels having a composition near the high end of the specified

range. In other words, the two-stage cracking hypothesis (hot microcracking, cold propagation[22,27]) cannot be applied to all heats of HY-80 steel. Therefore, contrary to the hypothesis of Emmanuel et al.,[25] hydrogen is an extremely important factor in the initiation of cold cracking in leaner heats of HY-80 steel.

In summary, this investigation has indicated that the phenomena associated with an unmixed zone and a partially-melted zone can account for the uniqueness of the fusion boundary as a crack initiation site in low alloy steels. Also, it has been found that the distribution of nonmetallics can explain the difference in crack susceptibility between similar heats of HY-80 steel of similar composition. Finally, it has been confirmed that hydrogen is essential for the propagation of cold cracks in HY-80 steel.

CONCLUSIONS

1. The following conclusions pertain to the metallographic examinations of the as-received HY-80 steel plate used in this investigation:
   a. Heat N and Heat P both had a similar microstructure consisting of low-temperature transformation products and both appeared to be equally banded.
   b. Although both Heat N and Heat P had about the same volume fraction of sulfides, the sulfides in Heat P were predominantly larger and very elongated, whereas the sulfides in Heat N were predominantly globular.
2. The following conclusions pertain to the metallographic examination of heterogeneous bead welds in low-alloy steels:
   a. Information about the solidification substructure of a weld can be obtained by metallographic examination only if certain etching procedures are used in preparing the sample.
   b. A two-stage nital and sodium bisulfite etching procedure is an excellent procedure for revealing solidification structure at the fusion boundary of welds in HY-80 steels.

c. The two-stage procedure reveals that at the fusion boundary of bead welds there exists a zone of partial melting and a zone of melted base metal (the unmixed zone) which does not mix significantly with the bulk of the weld metal and therefore etches to a different appearance.

3. The following conclusions pertain to the electron-beam microanalyses of the fusion boundary of bead welds in HY-80 steel:

   a. A significant portion of the weld metal adjacent to the weld interface has a chromium and manganese composition identical to that of the base metal, therefore, the region has been identified as an unmixed zone.

   b. It is possible for folds of melted but unmixed base metal to be washed into the bulk weld metal.

4. The following conclusions pertain to terminology applied to heterogeneous welds:

   a. Five new terms should be used in describing heterogeneous welds. They are the composite region, the unmixed zone, the weld interface, the partially-melted zone, and the true heat-affected zone. The present AWS terminology is not sufficiently descriptive of heterogeneous welds.

5. The following conclusions pertain to partial melting that occurs adjacent to the weld pool during welding:
   a. Constitutional liquation of large sulfide inclusions and small unidentified inclusions occurs in the base metal near the weld interface.
   b. In addition to super-solidus melting, grain boundary liquation occurs by the intersection of migrating grain boundaries with regions of constitutional liquation which thereby wet the grain boundaries.
   c. Sulfides at the weld interface can result in the formation of microvoids.
   d. Sulfides that dissolve in the unmixed zone can precipitate as small globules at subgrain and solidification grain boundaries during the solidification of the unmixed zone.
6. The following conclusions pertain to Varestraint tests of the weld metal produced in HY-80 steel with E11018G electrodes:
   a. Hot-cracking in the composite region bead welds deposited with E11018G electrodes is extremely irregular and is not readily evaluated quantitatively.
   b. The difference in weldability between the two heats of HY-80 steel did not influence the

hot-cracking behavior of the composite region of the weld metal produced in the Varestraint test.

7. The following conclusions pertain to cold-cracking tests of HY-80 steel:

   a. The cold-cracking test procedure used in this investigation is an excellent method for investigating the nucleation and propagation of cold cracks in low-alloy steels.

   b. Hydrogen is necessary for the propagation of cracks and appears to be the catalyst for the nucleation of the cracking.

   c. Hot-microcracking in the unmixed zone at alloy-rich locations is a valid but probably infrequent mechanism of crack-nucleation in rich-analysis heats of HY-80 steel. However, the presence of hydrogen is required for the propagation of such microcracks.

   d. Cold cracking occurs preferentially in alloy-rich bands in the true heat-affected zone and adjacent to the weld interface.

   e. In this investigation, cold cracking in the true heat-affected zone was almost exclusively nucleated by elongated sulfide inclusions.

f. Cold-cracking in the partially-melted zone can be nucleated by liquated grain boundaries and by small precipitated sulfides in constitutionally liquated regions.

g. A mechanism involving the lower M_S temperature of subgrain and solidification grain boundaries as well as the segregation of carbon, manganese, nickel, and sulfur may explain the development of crack-susceptible sites in the unmixed zone.

8. The following conclusions pertain to the observed location of the cracks in the sample from the Cruciform test specimen:

a. A considerable length of the crack under fillet weld C traversed the unmixed zone and the partially-melted zone, indicating that it is inaccurate to assume that cracking in the cruciform test is simply heat-affected-zone cracking.

b. The existence and nature of the unmixed zone and the partially-melted zone may provide an explanation for the correlation between the cold-cracking susceptibility as measured by the curciform test and the hot-cracking susceptibility as measured by the Varestraint Test.

ACKNOWLEDGMENTS

The author wishes to acknowledge the expert guidance of his advisor, Dr. Warren F. Savage. In addition, the suggestions and assistance of fellow students and various members of the faculty of the Department of Materials Engineering is appreciated. Dr. Carl D. Lundin gave particularly helpful suggestions concerning metallographic techniques.

Also, the author extends his gratitude to the U. S. Steel Applied Research Laboratory and its personnel, especially Dr. W. D. Doty and Dr. W. J. Murphy, for their generous support. The electron beam microanalyses performed by Dr. R. Natesh is also appreciated.

Finally, the author would like to thank Mr. Timothy Miller for drawing the graphs and the illustrations and Mrs. Jack Dillon for typing the manuscript.

LITERATURE CITED

1. Udin, H., Funk, E. R., and Wulff, J., Welding for Engineers, John Wiley and Sons, Inc., New York, N. Y. (1954).

2. Linnert, G. E., "Alloying During Welding," Metals Engineering Quarterly, 1(3), 39 to 56 (1961).

3. Owczarski, W. A., Duvall, D. S., and Sullivan, C. P., "A Model for Heat-Affected-Zone Cracking in Nickel-Base Super-Alloys," Welding Journal, 45(4), Research Suppl., 145-s to 155-s (1966).

4. Pepe, J. J. and Savage, W. F., "Effects of Constitutional Liquation in 18Ni Maraging Steel Weldments," Welding Journal, 49(9), Research Suppl., 411-s to 422-s (1967).

5. Welding Handbook, 5th Edition, Section 1, American Welding Society, New York, N. Y. (1964).

6. Brown, P. R. and Adams, C. M., Jr., "Fusion-Zone Structures and Properties in Aluminum Alloys," Welding Journal, 39(12), Research Suppl., 520-s to 524-s (1960).

7. Calvo, F. A., Bentley, K. P., and Baker, R. G., "Growth Substructures in Weld Metal," Acta Met., 8(12), 898 to 900 (1960).

8. Chalmers, B., Principles of Solidification, John Wiley and Sons, Inc., New York, N. Y. (1964).

9. Borland, J. C., "Suggested Explanation of Hot Cracking in Mild and Low Alloy Steel Welds," British Welding Journal, 8(11), 526 to 540 (1961).

10. Savage, W. F., Lundin, C. D., and Aronson, A. H., "Weld Metal Solidification Mechanics," Welding Journal, 44(4), Research Suppl., 175-s to 181-s (1965).

11. Wada, T., "Solidification Processes of Weld Metal," Transactions of National Research Institute for Metals, 8(4), 136 to 143 (1966).

(Continued)

12. Hurle, D. T. J., "Mechanisms of Growth of Metal Single Crystals from the Melt," Progress in Materials Science, 10, Pergamon Press (1962).

13. Brice, J. C., The Growth of Crystals from the Melt, North Holland Publishing Co., Distributed by John Wiley and Sons, Inc., New York, N. Y. (1965).

14. Winegard, W. C., An Introduction to the Solidification of Metals, The Institute of Metals, London (1964).

15. Pfann, W. G., Zone Melting, 2nd Edition, John Wiley and Sons, Inc., New York, N. Y. (1966).

16. Rutter, J. W. and Chalmers, B., "A Prismatic Substructure Formed During Solidification of Metals," Canadian Journal of Physics, 31(1), 15 to 39 (1953).

17. Savage, W. F. and Aronson, A. H., "Preferred Orientation in the Weld Fusion Zone," Welding Journal, 45(2), Research Suppl., 85-s to 89-s (1966).

18. Savage, W. F. and Chase, R. J., Jr., "An Investigation of the Solidification Mechanics of Fusion Welds in Face-Centered Cubic Metals" (to be published in the Welding Journal).

19. "Mechanical Properties of HY-80 Armor Plate Steel," Publication ADVCO 01079, U. S. Steel Corporation, Pittsburgh, Pa. (1961).

20. Ledman, J. L., Lundin, C. D., and Savage, W. F., "Study of the Transformational Characteristics and the Weldability of HY-80 Steel," Rensselaer Polytechnic Institute Final Report, Contract 78813, January (1963).

21. Doty, W. D. and Grotke, G. E., "Some Observations on the Weldability of Quenched and Tempered High-Yield-Strength Alloy Steels," Conference Proceedings, U. S. Navy Bureau of Ships, Washington, D. C., 34 to 67, March 21 and 22, 1960.

22. Rathbone, A. M. and Gross, J. H., "Factors Influencing Heat-Affected-Zone Cracking of HY-80 Steel Weldments," Technical Report 56.02-001(4), U. S. Steel Corp., Applied Res. Lab., Monroeville, Pa., June (1962).

(Continued)

23. Masubuchi, K. and Martin, D. C., "The Mechanism of Cracking in HY-80 Steel Weldments," Welding Journal, 41(8), Research Suppl., 375-s to 384-s (1962).

24. Griffin, R. J., "Cold Cracking in the Heat-Affected Zone of HY-80 Welded Joints," Bureau Ships Journal, 5, 9 to 17 (1959).

25. Emmanuel, G. N., Young, D. E., and Spahr, G. L., "The Metallurgy of Heat-Affected Zones in HY-80 High Strength Steel," Metals Engineering Quarterly, 1(3), 82 to 97 (1961).

26. Sibley, C. R., "Welding of HY-80 Steel With the Gas-Shielded Metal Arc Process," Welding Journal, 42(5), Research Suppl., 219-s to 232-s (1963).

27. Interrante, C. G. and Stout, R. D., "Delayed Cracking in Steel Weldments," Welding Journal, 43(4), Research Suppl., 145-s to 160-s (1964).

28. Duvall, D. S. and Owczarski, W. A., "Technical Note: Behavior of Solute at Mobile Heat-Affected Zone Grain Boundaries," Welding Journal, 45(8), Research Suppl., 356-s to 384-s (1966).

29. "The TM. 74 Photometallurgical Microscope," Notice 1680A—Nachet France, Eric Sobotka Co., Inc., Farmingdale, New York.

30. Savage, W. F. and Lundin, C. D., "The Varestraint Test," Welding Journal, 44(10), Research Suppl., 433-s to 442-s (1965).

31. Savage, W. F. and Lundin, C. D., "Application of Varestraint Technique to the Study of Weldability," Welding Journal, 45(11), Research Suppl., 497-s to 503-s (1966).

32. Granjon, H. P., 1961 Adams Lecture: "Studies on Cracking of and Transformation in Steels During Welding," Welding Journal, 41(1), Research Suppl., 1-s to 11-s (1962).

33. Poteat, L. E. and Warner, W. L., "The Cruciform Test for Plate-Cracking Susceptibility," Welding Journal, 39(2), Research Suppl., 70-s to 76-s (1960).

(Continued)

34. Winterton, K. and Nolan, M. J., "Factors Affecting Severity of Cruciform Test for Hardened-Zone Cracking," Welding Journal, 39(2), Research Suppl., 77-s to 82-s (1960).

35. Salmon Cox, P. H. and Charles, J. A., "Further Observations on the Analysis and Distribution of Non-Metallic Inclusions in a 0.2 Percent Steel Ingot," Journal of Iron and Steel Institute, 203(5), 493 to 499 (1965).

36. Yeo, R. B. G., "The Effect of Oxygen in Resulfurized Steels," Part I, Journal of Metals, 19(6), 29 to 32, Part II, ibid, 19(7), 23 to 27 (1967).

37. VanVlack, L. H., Riegger, O. K., Warrick, R. J., and Dahl, J. M., "Sulfide Inclusions in Steel," Transactions of the Met. Soc. of AIME, 221(4), 220 to 228 (1961).

38. McGannon, H. E., Editor, The Making, Shaping, and Treating of Steel, 8th Edition, U. S. Steel Corp., Pittsburgh, Pa. (1964).

39. Heine, R. W. and Rosenthal, P. C., Principles of Metal Casting, McGraw-Hill, Inc., New York, N. Y. (1955).

40. Derge, G., Editor, Basic Open Hearth Steelmaking, The American Institute of Mining, Metallurgical, and Petroleum Engineers, New York, N. Y. (1964).

41. Baeyertz, M., Nonmetallic Inclusions in Steel, American Society for Metals, Cleveland, Ohio (1947).

42. Wilner, A. R. and Salive, M. L., David Taylor Model Basin, (DTMB) Report 1605, January (1965).

43. Private Communication, Krysiak, K. F., Air Reduction Co., to C. D. Lundin, Rensselaer Polytechnic Institute, February 28, 1966.

44. Wilcox, W. R., "Incomplete Liquid Mixing in Crystal Growth From the Melt," Journal of Appl. Physics, 35(3), 636 to 643 (1964).

45. Savage, W. F., Lundin, C. D., and Matthews, S. J., "Weld Metal-Base Metal Interactions in Heterogeneous Gas Metal Arc Welds" (to be published in the Welding Journal).

(Continued)

46. Aronson, A. H., "Constitutional Liquation in the Iron-Iron Carbide System," Masters Thesis, Rensselaer Polytechnic Institute, Troy, N. Y., May 1963.

47. Boniszewski, R. and Baker, R. G., "Burning and Hot Testing in the Weld Heat-Affected Zone of Ferritic Steel," Journal of the Iron and Steel Institute, 202(11), 921 to 928 (1964).

48. Randall, M. D., Monroe, R. D., and Rieppel, P. J., "Causes of Microcracking and Microporosity in Ultra-High Strength Steel Weld Metal," Welding Journal, 41(5), Research Suppl., 193-s to 206-s (1962).

49. Kammer, P. A., Masubuchi, K., and Monroe, R. D., "Cracking in High-Strength Steel Weldments," Defense Metals Information Report 197, Battelle Memorial Institute, Columbus, Ohio, February 7, 1964.

50. Savage, W. F., Lundin, C. D., and Miller, T., "An Investigation of Microsegregation in 70Cu-30Ni Welds" (to be published in the Welding Journal).

51. Brammer, I. S. and Honeycombe, R. W. K., "Formation of Sulfides at Grain Boundaries in Some Pure Iron Alloys," Journal of the Iron and Steel Institute, 202(4), 335 to 342 (1964).

52. Benz, M. G. and Elliott, J. F., "The Austenite Solidus and Revised Iron-Carbon Diagram," Transactions of the Met. Soc. of AIME, 221(4), 323 to 331 (1961).

53. Lyman, T., Editor, Metals Handbook, 1948 Edition, The American Society for Metals, Cleveland, Ohio (1948) page 451.

54. Herres, S. A., "Practical Importance of Hydrogen in Metal-Arc Welding of Steel," Transactions of the American Society for Metals, 39, 162 to 189 (1947).

55. Bell, J. R., "A Study of the Relationship of Micro-segregation to Cracking in Constructional Alloy Steels," Masters Thesis, Rensselaer Polytechnic Institute, Troy, New York (1966).

(Continued)

56. Elsea, A. R. and Fletcher, E. E., "Hydrogen-Induced Delayed Brittle Failures of High Strength Steels," Defense Metals Information Center Report 199, Battelle Memorial Institute, Columbus, Ohio, January 20, 1964.

57. Randall, M. D., Monroe, R. D., and Nichols, H. J., "Study of the Causes of Cracking in Submerged-Arc Welds in Constructional Alloy Steels," Welding Journal, 40(9), Research Suppl., 385-s to 392-s (1961).

58. Berry, J. T. and Allen, R. C., "A Study of Cracking in Low Alloy Steel Welded Joints," Welding Journal, 39(3), Research Suppl., 105-s to 116-s (1960).

59. Hodge, J. M., Frazier, R. H., and Boulger, F. W., "The Effects of Sulfur on the Notch Toughness of Heat-Treated Steels," Transactions of the Met. Soc. of AIME, 215(10), 745 to 753 (1959).

60. Wei, R. P., "Fracture Toughness Testing in Alloy Development," ASTM Special Technical Publication, No. 381, 279 to 289 (1965).

61. Spitzig, W. A., "Correlations Between Fractographic Features and Plane-Strain Fracture Toughness in an Ultrahigh-Strength Steel" (to be presented at the ASTM Symposium on Electron Microfractography in San Francisco, California, June 1968).

62. Rathbone, A. M., Connor, L. P., and Gross, J. H., "Weldability of a High-Toughness Alloy Plate Steel With a Minimum Yield Strength of 140 KSI," Welding Journal, 43(12), Research Suppl., 551-s to 563-s (1964).

63. Boneszewski, T. and Moreton, J., "Effect of Micro-Voids and Manganese Sulphide Inclusions in Steel on Hydrogen Evolution and Embrittlement," British Welding Journal, 14(6), 321 to 336 (1967).

64. Reed-Hill, R. E., Physical Metallurgy Principles, D. Van Nostrand Company, Inc., New York, N. Y. (1964) p. 500.